Study of a lunar satellite navigation system

-Project Report-

by

GEMMA SAURA CARRETERO

A dissertation submitted to the Department of Aerospace Engineering,
ETSEIAT – Universitat Politècnica de Catalunya,
in partial fulfillment of the requirements for the degree of
Aeronautical Engineer

Tutor: Dr. Elena Fantino

September 2012

Escola Tècnica Superior d'Enginyeries
Industrial i Aeronàutica de Terrassa

Enginyeria Superior Aeronàutica

Escola Tècnica Superior d'Enginyeries
Industrial i Aeronàutica de Terrassa
UNIVERSITAT POLITÈCNICA DE CATALUNYA

This page is intentionally left blank

Acknowledgments

En primer lugar, me gustaría expresar mi más sincero agradecimiento a todas las personas que me han ayudado directa o indirectamente durante la realización de este proyecto. De ese grupo de personas, me gustaría agradecer especialmente a mi tutora la Dra. Elena Fantino. Ella me ha enseñado que la perfección no es una opción y que frases como “no lo sé” o “no es importante” no deben pasar por la cabeza de un ingeniero. Sus enseñanzas durante el último año me han ayudado a entender y apreciar un método de trabajo que era totalmente desconocido para mi. Su esfuerzo y su capacidad de trabajo me han obligado a nunca dejar de pedir más de mi misma, esforzarme por evitar mis malas costumbres y mejorar mis virtudes. Gracias, Elena.

No hay que olvidar que este proyecto es el final de un viaje que ha durado cinco años. Ha sido un viaje duro y, a veces, interminable. Pero fue el viaje que elegí y junto a mis compañeros de clase ha sido una experiencia inolvidable. Juntos nos hemos apoyado, aguantado y animado durante cinco años. Os doy las gracias a todos vosotros y espero veros en un futuro. También agradecer a todos los docentes que han contribuido a aumentar mis conocimientos. Nunca me ha gustado estudiar pero aprender es lo más bonito del mundo, así que gracias por dejarme aprender de vosotros.

Por último, no me puedo olvidar de los que siempre han estado ahí: mi familia. Su apoyo durante los momento difíciles ha sido indispensable. Su orgullo por mis éxitos y su cariño hacen que los momentos de alegría sean aún más especiales. Me gustaría acabar acordándome de mi abuelo. Ojalá estuvieras aquí para compartir conmigo este momento pero, estés donde estés, sé que estarás orgulloso de mi.

Gracias a todos.

Abstract

The objective of the present study is to hold a preliminary analysis and design of a lunar global satellite navigation system able to provide accurate positional information to operators on the surface or in low lunar orbits. The outcome is a set of indications concerning the implications inherent in such a system. This set of indications consists in the main objectives, requirements and constraints needed during the definition and implementation of an infrastructure for global precise positioning on the lunar surface.

In any preliminary mission analysis it is important to determine the design drivers. In our case, the main drivers are the orbital height, the number of satellites in the constellation, the orbital inclination and the number of orbital planes. These four parameters are the main characteristics that define the constellation performance, therefore their final selection is crucial for the mission success. In our case, two constraints have been applied in order to determine the constellation: (1) no more than three orbital planes and (2) no more than 18 satellites. The constellation selection process has been carried out with the help of computer simulation. Thanks to it, we were able to choose the constellation whose parameters combination resulted in the best performance. The final constellation has a height of 6500 km, three orbital planes, 15 satellites and an inclination of 90°.

In order to maintain the correct performance of the constellation, a station-keeping strategy has been developed. Computer simulation of the chosen constellation allowed us to quantify the perturbation effects on the satellites and to identify which perturbation is the primary source of orbital deviations. Central body gravitation, third body-perturbations and solar radiation pressure have been computed for a period of one year with the result of a propellant (also known as Δv) budget of 1 km/s.

Payload selection is an important step in the design process. The characterization of its mass, power and thermal requirements, and components influences the design of all the other subsystems. Relativistic effects on time are taken into account because the accuracy of the system depends on clock errors. The study concludes that, although relativistic effects on time are less significant on the constellation than on the terrestrial GPS system, they still need to be corrected.

This study also undertakes a preliminary design of the satellite subsystems. Power and mass budget are made and a preliminary analysis of the propulsion, thermal and communications subsystems are also carried out. The proposed preliminary satellite

design consists in a 1000kg-1600W class platform which will transmit in the L-band (to the lunar surface) and in the X-band (to the Earth). If the station-keeping is carried out by a bipropellant thruster, the propellant budget needed is 225 kg. However, some indications for electrical propulsion for the station-keeping maneuvers are also provided. The thermal environment is the biggest challenge of the mission because of the Earth eclipses[1]. They can last more than 5 hours which leads to the temperature getting as low as -35°C. During lunar[2] eclipses, secondary batteries can produce around 1300 W which will probably not be sufficient to maintain the spacecraft temperature within operational limits during Earth eclipses, so an extra set of batteries will be needed.

Keywords: *System's engineering, Moon, global satellite navigation system, orbital perturbations, atomic clocks, eclipse, constellation.*

[1] Earth eclipses refer to the shadow caused by the Earth on the spacecraft; the Earth is between the spacecraft and the Sun.

[2] Lunar eclipses refer to the shadow caused by the Moon on the spacecraft; the Moon is between the spacecraft and the Sun.

Aim

The aim of this project is to define a set of indications regarding the implications inherent in the design and implementation of a satellite constellation for global precise positioning on the lunar surface and low lunar orbits. This study is also a compilation of a feasibility and preliminary analysis of the most important design elements.

Introduction

The main purpose of this report is to develop a Systems approach to a specific aerospace engineering problem consisting in the creation of a lunar global satellite navigation system (LGSNS). The present study constitutes a preliminary analysis of the objectives, the requirements and the constraints of such a system. The study also focuses on mission analysis aspects such as the choice of the most suitable constellation to accomplish the mission objectives and specific issues concerning the design of the spacecraft subsystems.

Systems Engineering is based in what is called Systems Theory. Systems Theory is a transdisciplinary approach to the study of a complex problem; rather than reducing a problem to a collection of parts, it focuses on the interrelationship between the parts which connect them into a whole, also known as a System. This kind of work methodology is basic for aerospace engineering because spacecraft are complicated, and efficient designs require the optimisation and integration of the many subsystems. Systems engineers must be able to envision how a change to one subsystem will affect all the others[1].

Some Systems Engineering Elements are: requirements analysis, requirements allocation, functional analysis, specification development, top-level architecture development, subsystem design and analysis, interface definition and control, trade-off and alternative evaluation, life cycle costing, reliability, maintenance and availability, test and evaluation, training, documentation, production and operations.

This study focuses on some of these elements. Some of them, such as requirements analysis or subsystem design, have already been mentioned. However some others, such as trade-off evaluation, are also going to be analysed. Concerning subsystem design and analysis, a basic and very preliminary evaluation is going to be carried out for the main spacecraft's subsystems; power, propulsion, thermal control and communications. An elementary mass budget and the characterization of the payload are also an important part of this study. The rest of elements such as reliability, availability or redundancy are very difficult to approach during a preliminary design and, therefore, they are out of the scope of this study.

Basic references concerning mission and subsystem design are [1] and [59]. Another important reference for this subject is *"Space Vehicle Design"* by M.D. Griffin and J.R. French.

Justification

"That's one small step for a man, one giant leap for mankind"

These were Neil Armstrong's first words just after stepping onto the Moon's surface on July 20th, 1969. The events that led to this precise moment in history began in 1961 when the USA's President John F. Kennedy proposed the national goal of "landing a man on the Moon and returning him safely to the Earth". With that goal in mind, the Apollo program was born.

The Apollo program had a huge popular and governmental support and its success enhanced people's interest in space. It achievement was possible because of the experience gained with the Mercury and Gemini programs, Apollo's predecessors. Mercury's goal was to place American astronauts into orbit for as long as one day whereas the Gemini program had the objective of developing the necessary procedures to travel and land on the Moon with the upcoming Apollo program. Gemini carried out long-duration spaceflights, perfected extra-vehicular activity and orbital maneuvers necessary to achieve rendezvous and docking.

It is easy to believe that Neil Armstrong's steps on the Moon paved the way to the many different programs that followed after Apollo ended. As a matter of fact, the International Space Station and the STS Space Shuttle program are the most notable examples of how the interest in exploring whatever is outside our own planet never ends. A few years ago, when the end of STS program was approaching, the interest in returning to the Moon began to grow once again. The creation of the Constellation Program and the development of the Orion spacecraft, a new and superior multi-purpose crew vehicle, the Ares launch vehicle and the Lunar Surface Access Module (LSAM) had the clear objective of making the Moon a more accessible place. However, on October 11th 2010 the Obama Administration cancelled the Constellation Program and, with it, the Ares launch vehicle development. The Orion's objective was directed away from the Moon toward some Near-Earth objects (asteroids) mission and possible human landing on Mars.

Still, the decision of changing the Moon for an asteroid as a first step toward a Mars landing has not been well received by the scientific community [2]. Scientist all around the world believe that although it is true that humans have already been to the Moon, it doesn't mean that our satellite has nothing more to offer. In fact, after all the experience gained with the International Space Station concerning how to maintain a

permanent base in space, an enduring lunar scientific base is considered the logical next step. It would allow developing new technology back on Earth and it could be the perfect “pit-stop” in a future Mars mission. The lack of any suitable asteroid near the Earth that would allow a proper landing on it and the few experiments that can be done on its surface makes the idea of the ”asteroid pit-stop” even less interesting.

While waiting for a re-consideration from the USA Administration about the fundings and the mission objectives of the near future space programs, NASA and ESA specialists are still working on a Lunar Base concept [3], [4], [5], [6]. Studies of infrastructure solutions, surface operations, automated surface infrastructure elements, simulation of a power distribution network and others have already been carried out.

It is understandable that any future manned mission to Mars should pass by the Moon before reaching the red planet even if the USA government thinks differently. Furthermore, other space agencies could play an active role in returning the man to the Moon. In not so many years, the CNSA (China National Space Administration) has increased its presence and influence in space. In particular, it has established its interest in our satellite with the Chinese Lunar Exploration Program. The program has 4 phases that will lead to a manned lunar landing. Chang’e 1 and Chang’e 2 were launched in 2007 and 2010, respectively, and their objective was to orbit the Moon.

With the above reasons, in order to maintain a permanent base on the Moon, some kind of surface navigation information would be needed. Such a system would also be necessary in order to extend and make more effective the surface exploration of our natural satellite and to collect more accurate information of the landing process. Besides, it is known that in the Apollo mission astronauts had difficulties in navigating on the lunar surface due to a lack of familiar landmarks, loss of aerial perspective and the fact that the sense of balance is affected by ambiguous perception of depth. Spatial disorientation limited astronauts’ capabilities and it exposed them to serious risks. Hence, the idea of developing technologies to improve the spatial-orientation skills of astronauts operating on the lunar surface is completely pertinent. Moreover, it would also be able to position satellites on low lunar orbits.

This study constitutes a preliminary analysis of a LGSNSsimilar to the terrestrial global positioning systems. The Lunar Global positioning system presented in this report would be able to satisfy the needs related to any kind of Moon’s surface mission or low lunar orbit.

Scope

As mentioned in the introduction, this report is a Systems Engineering study of a LGSNS. The report is structured in seven parts:

- state of the art (*Chapter one*),
- mission design (*Chapter two*),
- top-level architecture design (*Chapters three* and *four*),
- spacecraft design (*Chapter five* and *six*) and,
- conclusions (*Chapter seven*)

Chapter one presents information about the current and future global navigation satellite systems (GNSS) in Earth orbit. It also presents the only lunar navigation system that has been developed: the Lunar Astronaut Spatial Orientation and Information System or LASOIS[7].

The objective of *Chapter two* is to define the mission by determining its main objectives and requirements. The requirements are going to be classified on different levels: top-level, functional, performance and critical. The identification of trade-offs and the evaluation of alternative design options by the creation of a list of mission constraints and drivers will complete the first section of *Chapter two*. A functional analysis of the mission will also be carried out by the elaboration of the Functional Flow Block Diagram (FFBD), the Functional Allocation Matrix (FAM) and the Interface Matrix (N^2) of the mission. Finally, in *Appendix A*, a Technology Readiness Level (TRL) evaluation will be elaborated. The definition of the concepts of functional analysis and TRL can be found in [1] and [8].

Chapters three and *four* have the aim of defining the top-level architecture design of the LGSNS. To do this, simulations of different configurations of satellite constellations are carried out. Once the most suitable satellite constellation is selected, a simulation of its orbital propagation is also made. The orbit propagation simulation helps to indentify the relative importance of the several orbital perturbations: third body-perturbations, central body gravity and solar radiation pressure (SRP). Coverage and performance data of the chosen constellation can also be obtained from simulation's results. A study concerning the eclipse periods of the final satellite constellation is executed. The station-keeping strategy is very important, so an estimation of the propellant budget needed for station-keeping is mandatory for a preliminary design. Finally, a presentation of the different space environment hazards of a lunar orbit is given.

Spacecraft design is carried out in *Chapters five* and *six*. *Chapter five* focuses on the payload design, hence it includes a presentation of the components of the navigation payload, a study of the relativistic effects on time and an estimation of the power needed by the payload, its mass and its thermal limits. *Chapter six* presents the subsystems preliminary design. Preliminary power and mass budgets are going to be elaborated based on historical data and approximate estimation formulas and rules of thumb. Solar array and battery sizing are mandatory to elaborate a preliminary design of the power subsystem. Concerning the propulsion subsystem, a propellant budget is estimated. Finally, thermal control and communications subsystems are also studied. Concerning the former, the extreme thermal conditions (hot and cold case) are identified and, in the latter, the sizing of the radio-link and a possible option for the ground segment on the lunar surface are carried out.

To complete this report, in *Appendix B*, we present a cost budget based on a parametric model that applies the Cost Estimation Relationship (CER) equations[1].

Table of contents

List of tables

List of Figures

Chapter one.

State of the art of the satellite navigation systems

In this chapter we describe all the satellite navigation systems of the Earth's history from the very first attempt with the Transit system up to all the new navigation systems that are being developed (Galileo, BeiDou, etc). A lunar navigation system is also describes.

References from this section are [7], [9], [10], [11], [12], [13] and [14].

1.1. Terrestrial satellite navigation systems

Historically, navigation has always been present in our culture, but the capability to know the exact position with the first navigation techniques was difficult since they were not precise enough. During the 16th century, when the first world tour was made, it was possible to estimate the ship's velocity, the direction and the latitude but not the longitude. It was not until 200 years later that sailors were able to estimate their longitude. 250 years have passed since then, and we are capable to estimate position, velocity and time with great precision and without difficulty thanks to the development of satellite navigation systems.

1.1.1. Transit system

Transit was the first satellite navigation system: launched between 1961 and 1962, it became operational in 1964. In order to achieve a reasonable global coverage, a constellation of, at least, five satellites was needed in low polar orbit at an altitude of about 1100 km [3].While the system was operational, at least ten satellites were kept in orbit.

The Transit satellites (Figure 1.1) broadcast two UHF (150MHz and 400MHz) carrier signals that provided precise time hacks, together with the satellite's orbital elements

[3] TRANSIT was a global navigation system but its coverage was not continuous. In order to achieve a reasonable coverage, an altitude of 1100 km was selected.

and orbit perturbation variables. With this information, a ground receiver was able to calculate the location of the satellite at any time. The critical information that allowed the receiver to compute the satellite's location was a unique frequency curve caused by the Doppler effect. However, in the best cases, the user had only one satellite visible and the time required to process a position determination was about 100 minutes.

Since the system was based on the Doppler effect, it was used to position stationary or almost stationary users (in particular, the Navy used it to position submarines). Trying to locate a moving receiver would have caused mismatches with the idealized Doppler curves and degraded the position accuracy. The typical positioning error was 25 meters, but it was possible to achieve a five meters error for static users by accumulating measurements over several days.

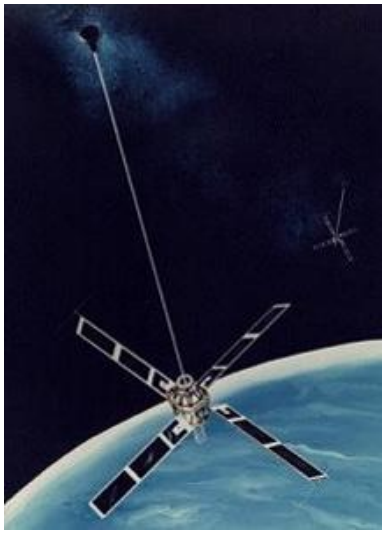

Figure 1.1 Transit art concept

1.1.2. Global Positioning System

The Global Positioning System or GPS (Figure 1.2) supplies continuous location and time information under all weather conditions. Data is provided by four or more satellites simultaneously and it is maintained by the USA government and is freely accessible by anyone with a compatible receiver.

The GPS project was developed in 1973 to overcome the limitations of the Transit system. It was created by the USA Department of Defence and was originally run with 24 satellites. It became fully operational in 1994. Nowadays the constellation is formed by 30 satellites instead of the 24 initially planned. The satellites are positioned in 6 circular Medium Earth Orbit (MEO) planes at 26000 km altitude. The orbits have an eccentricity

of less than 0.02 and an inclination of 55 degrees. Their orbital period is half a sidereal day (11h 58min).

The main objective of the GPS constellation is to guarantee that four satellites are always visible, no matter the location of the receiver. It consists of three segments: the spatial segment, described above, the control segment and the user segment. The control segment, or ground segment, consists of a web of ground stations which allow to monitor the satellite state and to update navigation parameters. The user segment is each and everyone of us who has a GPS receiver.

Figure 1.2 GPS art concept

1.1.3. Galileo

Galileo is a satellite navigation system currently being built by ESA. The aim of Galileo is to provide a high-precision positioning system upon which European nations can rely on independently from the Russian GLONASS, the American GPS and the Chinese BeiDou-2 systems. It will be a free service and it is intended to provide horizontal and vertical position measurements with one meter accuracy and better positioning services at high latitudes than any other existing system.

The fully deployed Galileo system consists of 30 satellites in a Walker constellation (27 operational + three active spares), positioned in three circular MEO planes at 23222 km altitude, and inclined by 56 degrees to the equator. Each plane will contain nine operational satellites, equally spaced 40° apart, plus one spare satellite to replace any of the operational satellites in case of failure.

The first two Galileo In-Orbit Validation satellites were launched on October 21th, 2011. Two more are scheduled for launch in 2012. Figure 1.3 shows an art concept of a Galileo spacecraft.

Figure 1.3 Galileo art concept

1.1.4. Global Navigation Satellite System

Global Navigation Satellite System or GLONASS (Figure 1.4) is a radio-based satellite navigation system operated for the Russian government by the Russian Aerospace Defence Forces. At present, it is the only alternative to the GPS since there is no other navigation system in operation with global coverage and similar accuracy. Galileo and BeiDou-2 are still in progress.

The development of GLONASS began in 1976 and the constellation was completed in 1995 but, due to the financially difficult period between 1989 and 1999, the space program's funding was cut by 80% and Russia found itself unable to maintain it. However, in the early 2000s the restoration of the system became a top government priority and funding was substantially increased. By 2010 GLONASS achieved full coverage of Russia and in 2011 all the 24 satellites were restored enabling full global coverage.

The fully deployed constellation consists of 24 satellites divided in three planes (eight satellites each) with an inclination of 64.8 degrees. Their orbits are circular and are located at an altitude of 19100 km (MEO). Their period is of 11h and 15min. GLONASS was designed to provide an accuracy of 65 meters, but nowadays it performs better; in the civil signal the accuracy is 20 meters and in the military signal ten meters.

Figure 1.4 GLONASS art concept

1.1.5. Compass Navigation Satellite System

Compass Navigation Satellite System or BeiDou-2 will be a global satellite navigation system consisting of 35 satellites. It became operational with the coverage of China in 2011 with ten satellites in use and it is planned to offer services to customers in the Asia-Pacific region by 2012. The global coverage should be achieved by 2020.

The constellation will include five geostationary satellites for backward compatibility with BeiDou-1 (the previous Chinese positioning program). There will also be 27 satellites in MEO orbit and three in an inclined geostationary orbit. It will offer complete coverage of the globe with an accuracy of ten meters, it will synchronize clocks with an accuracy of ten nanoseconds and it will be able to measure speeds within 0.2 m/s. In Figure 1.5 can be seen an art concept of a BeiDou-2 satellite.

Figure 1.5 BeiDou-2 art concept

1.2. Lunar navigation systems: LASOIS

LASOIS (Lunar Astronaut Spatial Orientation and Information System) is an integrated sensor network that incorporates data from multiple types of sensors: orbital satellite sensors (1), on-suit sensors (2) and ground-based sensors (3). LASOIS is being developed by the Ohio State University and is a system designed to provide astronauts with continuous navigation updates. LASOIS is the only advanced study on navigation on the lunar surface since the Apollo programme.

Navigation data is produced by the combination of the measurements done by the three types of sensors. A characterization of each type of sensor follows:

1) Orbital sensors, such as LROC (Lunar Reconnaissance Orbiter Camera), capture high-resolution images from extensive lunar surface regions.
2) On-suit sensors include an Inertial Measurement Unit (IMU) mounted on the heel of the astronaut boot, one step sensor mounted on the bottom of the same boot that has the IMU, and a pair of stereo vision sensors.

The IMU measures both acceleration and angular velocity of the astronaut, whereas the step sensor gives step pressure information and counts the number of strides of the astronaut. Finally, the stereo vision sensors capture stereo images of the landing site.

3) The ground-based sensor network can be extended to include multiple beacon transmitters on the ground as well as receivers mounted on the astronauts' suits. Beacon-based sensing can provide astronauts with absolute position information at a lower frequency than that used by the IMU and vision sensors.

Figure 1.6 shows a diagram of how LASOIS works.

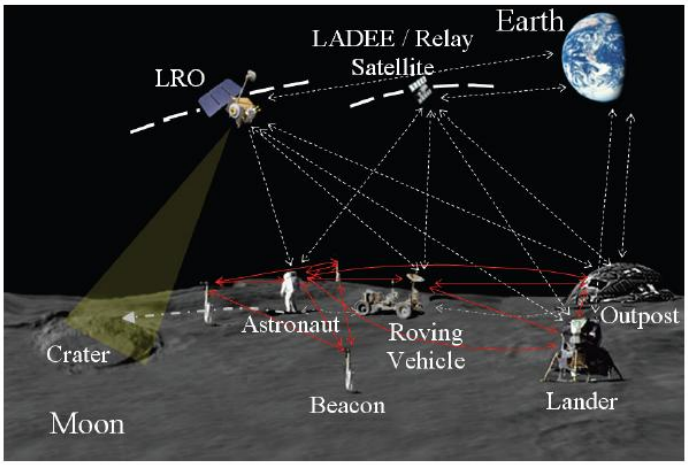

Figure 1.6 LASOIS diagram[11]

Chapter two.

Lunar satellite navigation system: Mission design

In this chapter we present the mission objectives, requirements and constraints for the design of a lunar mission for satellite navigation. Mission objectives are divided in two categories: primary and secondary. Requirements are also divided in categories: top-level, functional, performance and critical. Performance requirements are going to be justified in the following chapters of this report. Nevertheless, they are summarized here to provide an overview of the final constellation.

Mission design drivers are presented and a trade-off study is carried out in order to identify the main design parameters and their impact on the design. Finally, a Functional Flow Block Diagram (FFBD), a Functional Allocation Matrix (FAM) and an Interfaces Matrix (N^2 diagram) will be illustrated as a final overview of the lunar global satellite navigation system.

It will also be made a Technology Readiness Level evaluation. Because the evaluation needs the global picture of the mission technology, it can be found in *Appendix A* after all the technical development of the spacecraft.

The general reference for this chapter is [1]. The references used to justify the performance requirements are going to be provided in the corresponding chapters.

2.1. Mission Objectives

The first step in analyzing and designing a space mission is to define the mission objectives, i.e., the broad goals that the system must achieve to be productive. We draw these qualitative mission objectives largely from the mission statement or aim. There are two kinds of objectives: primary and secondary. The primary objectives are related to the scientific or technological purpose of the mission, whereas the secondary objectives are typically non-technical but rather social and political issues. However, they are equally important to satisfy.

2.1.1. Primary Objectives

- To create a lunar global satellite navigation system.
- To provide accurate position data to a spacecraft orbiting around the Moon in a low orbit or about to land on it or to astronauts/operators on the lunar surface.

The LGSNS mission pursues the goal of creating a global satellite navigation system on the Moon. The aim of the mission is to be able to locate a user on the lunar surface or in a low lunar orbit at any time with good accuracy. This mission should be supported by public funding and as any other mission, the cost of the space segment (satellite constellation) should be maintained as low as possible. Thus, the primary objectives focus on the creation of the satellite constellation and on the ability to provide accurate position data in the lunar surface or in low lunar orbit.

2.1.2. Secondary Objectives

- To promote the construction of a permanent lunar scientific base.
- To provide scientists with precise topographic data of the lunar surface.
- To encourage the exploration of Mars by transfer of technology.

In addition to the primary objectives, the LGSNS mission aims at promoting the construction of an international permanent lunar base. This would bring the additional advantage of developing technology that would encourage and help the preparation to the manned exploration of Mars. Another secondary objective of the mission is to provide precise topographic data of the lunar surface. The satellite constellation would provide with very accurate information of the Moon's topography by measuring the surface height. This information would improve the knowledge of the Moon and it would help the scientists with their research.

2.2. Requirements and Constraints

Having defined the mission objectives, we need to transform them into a preliminary set of numerical requirements and constraints on the mission's performance and operation. These requirements and constraints will largely establish the operational concepts that will meet the objectives. Thus, we must develop requirements which truly reflect the

mission objectives and be ready to trade them as we more clearly define the space system.

Top-level requirements are the basic objectives and constraints. Functional requirements are engineering specifications that identify what characteristics are required, whereas performance requirements quantify the functions that are required. Finally, critical requirements are those requirements that dominate the overall design and that are mandatory to the realization of the mission objectives. They are not negotiable.

2.2.1. Top-Level Requirements

- The LGSNS shall be able to locate any user at any time on the lunar surface and in a low lunar orbit (i.e., with an orbital height lower than 600 km).
- The mission shall provide service during a minimum of ten years.
- The LGSNS shall be able to process its own positioning data through ground stations on the lunar surface.
- At least, one control station shall be placed on Earth.
- The mission shall be mainly supported by public funding.
- The LGSNS shall be an international cooperation.

These requirements are fundamental to the success of the mission. The main requirements focus on the localization of users on the lunar surface or in low lunar orbit and the ability to process navigation data. However, these are not the only important requirements; funding and organization are a key factor to a successful mission. If the whole pack of requirements is respected, the correct performance of the satellite constellation is assured. It also guarantees global scientific benefits for each party involved in the mission, which is why an international cooperation is preferred.

Earth control station will be part of the ground segment and it will focus its operations in satellite maintenance and station-keeping instead of the creation of the navigation message.

Due to the high cost and effort, this mission will be feasible in every aspect if it lasts over a long enough period of time. Based on previous experiences concerning GNSS, this period should be between 10 and 15 years. Since it is the first attempt at a GNSS at the Moon, the mission lifetime should be long enough to gain experience but not too long to

hamper changes or improvements in the mission concept. In other words, the opportunity to upgrade the constellation should be not restricted by its lifetime.

2.2.2. Functional Requirements

- LGSNS shall have three segments: space, ground and user.
- The space segment shall consist of a satellite constellation around the Moon.
- Each of the LGSNS satellites will broadcast navigation time signals together with navigation data signals which will contain the clock and ephemeris correction data essential for navigation.
- The ground segment will consist of a control centre and a global network of transmitting and receiving stations on the Moon.
- The orbital elements of all the satellites shall be maintained against perturbations.
- There shall be a spare satellite in each orbital plane to ensure that in case of failure the constellation can be repaired quickly by moving the spare to replace the failed satellite.
- The satellite bus shall have a propulsion system to maintain the orbit against perturbations.
- The LGSNS shall operate in a Middle Moon Orbit (MMO, from 545 km to 9752 km).

Global navigation coverage can be achieved by a satellite constellation which constitutes the navigation system. This system usually has three segments: space, ground and user. The constellation itself is known as the space segment. The ground segment consists of a control centre and a network of stations on the Moon whereas the user segment consists of a receiver able to read and process the navigation data transmitted by the satellite.

The satellite constellation is the main element of the mission, so its characteristics need to be well defined. In order to maintain the accuracy of the system above a given value, it is important to keep the orbital elements constant against perturbations. Their variation margins will be defined in the next section: *Performance Requirements*. The constellation needs to operate in a MMO where the individual satellite visibility is higher and the perturbation effects are lower. Finally, one spare satellite in each orbital plane would increase the reliability of the entire system.

2.2.3. Performance Requirements

The justification to the payload performance requirements can be found in *Chapter five*, orbit and constellation requirements are justified in *Chapters three* and *four* and, finally, bus and communication requirements are explained in *Chapter six*.

2.2.3.1. Payload

- The payload shall be able to correct relativistic errors in order to achieve an accuracy better than ±1m.
- The payload shall consist of four different units: a clock unit, a signal generation unit, a frequency generation unit and an amplifier unit.
- Clocks shall be of atomic type and there shall be more than one type of clocks in order to increase reliability.
- The payload mass shall represent no more than 25% of the satellite dry mass, according to historical data.
- The payload power shall represent no more than 60% of the total supplied power, according to historical data.
- The payload shall be able to perform inter-satellite link (ILS) and AutoNav functions (definitions of these concepts can be found in *Chapter five*).

2.2.3.2. Orbit and constellation

- The average geometric dilution of precision or GDOP (definition provided in *Chapter three*) obtained by the satellite constellation shall be less than seven both in latitude and longitude.
- The orbital radius shall not exceed 9000 km.
- The number of satellites of the constellation shall be between 12 and 18.
- There shall not be more than three orbital planes.
- The propellant budget for station-keeping shall correspond to a maximum total velocity variation of 1 km/s per year.
- Right ascension of the ascending node (RAAN) and inclination variation shall not exceed 3° and 1°, respectively.

2.2.3.3. Bus

- The end of life (EOL) power needed to fully operate the spacecraft shall not exceed 1600 W.
- The loaded mass of the satellite shall be between 950 and 1100 kg.
- The bus shall include photovoltaic arrays as main power source.
- The bus shall accommodate batteries capable to accumulate sufficient energy to power all the subsystems when solar arrays are not operative and to sustain peak loads.
- The bus shall accommodate and protect the payload as far as volume and mass are concerned in a lunar orbit space environment.
- Solar arrays shall be completely directional in order to reduce their area.
- In order to maintain a constant temperature during orbit shadow time, an emissivity variation device, such as a louvre (a definition can be found in *"Satellite Thermal Control Engineering"* by Philippe Poinas, ESA-ESTEC), shall be included.
- During lunar eclipses, active thermal control shall be used to make sure that the temperature of the several components stays within the prescribed limits.
- During Earth eclipses, an extra set of batteries shall be used.

2.2.3.4. Communications

- The satellite shall have at least two antennas: one with a transmission frequency of 1575.42 MHz (L-band) and the other with a transmission frequency of 8.4 GHz (X-band).
- The minimum power guaranteed in reception on the lunar surface shall be -155.5 dBW, according to GPS data.
- The transmission beamwidth shall be 20°.
- The energy per bit to noise rate with the Earth's communication link shall be 24.6 dB in order to guarantee a good link quality.
- The download data rate shall be 50 bps.

2.2.4. Critical Requirements

- The LGSNS mission shall be feasible technically and economically.

- To maintain GDOP under an average value of seven, station-keeping shall be planned every six months in order to maintain the orbital elements within the limits.
- Maneuvers shall be carried out during orbital periods when the satellite does not feel third body-perturbations effects.
- The Payload's Mission Data Unit shall be able to maintain an accuracy of less than one meter using relativistic corrections.
- Payload's thermal limits shall be always fulfilled for a good performance.

Positioning is the base of this mission and its heritage implies that state-of-the-art technology is ready to fulfil the mission objectives. However, the main difficulties of the missions are related to the satellite constellation and the payload.

For a LGSNS, being able to maintain the accuracy at its maximum is very important and for this reason the station-keeping strategy and maneuver planning become especially important. Station-keeping sets one or more orbital parameters back to some reference value by means of one or more orbital maneuvers. Orbital elements define the DOP of the system. The time of application of the correction maneuvers is also extremely important because third body-perturbations can change the final value of the semimajor axis. Further explanation of this phenomenon can be found in *Chapter four*.

Corrections in payload measurements are also necessary and important to maintain the system's accuracy. The LGSNS payload suffers from relativistic time errors which need to be corrected before sending the navigation signal to the receiver. Earth eclipses also represent a challenge in spacecraft design because of their duration (up to five hours) and the temperatures which the spacecraft reaches.

2.2.5 Constraints

- The total space segment cost shall be between 630 and 880 $M.
- The inclination shall be defined in order to achieve global lunar surface coverage.
- The unit launch cost shall be between 250 and 350 $M
- All the flight units shall be launched in no more than 9 launches in order to maintain the mission economically feasible.
- The launcher shall be already flight proven and it shall be of the Atlas V family since it allows to launch two satellites at the same time.

- Every step in the mission design, manufacturing and operations has to respect international cooperation agreements and policies.

Most of the constraints are always related with cost issues and launch segment characteristics. In the case of the LGSNS mission, the cost is a very important constraint. It is known that the cost of launching anything to the Moon is $110000 per kilogram (see *Appendix B*) so, sending two satellites in a single launch (2500-3000 kg, considering the Earth-Moon transfer orbit stage) would cost 275-330 $M. Regarding the total cost of the space segment, a parametric cost analysis has been done and its result is 630.45 $M $\pm$ 248.88 $M. This cost estimation is the very first estimation of the mission's cost. Hence, it would be wise to understand its results as the minimum expected cost for the mission.

2.3. Mission design drivers

Mission drivers define the mission parameters that affect performance, risk and cost. Table 2.1 shows the mission drivers of the LGSNS.

Driver	Design Issues	Design Impact
Height	Orbital dynamics, single satellite visibility, constellation's dilution of precision (DOP) and communications, cost	Gravity effects increase when height decreases which means that station-keeping would be needed to be done more often. Single satellite visibility decreases with height thus, to obtain global coverage in a low orbit, more satellites would be needed. Communications are also affected by height. Higher satellites take more time to transmit data to the surface.
Nº of satellites	Cost, Constellation's DOP and complexity.	More satellites means higher cost, but it also means better DOP.
Inclination	Orbital dynamics, single satellite visibility, constellation's DOP and communications.	Satellites in polar orbits offer better global visibility. However, polar orbits suffer from higher temperature gradients which increase the complexity of the spacecraft.

Nº of planes	Cost, constellation complexity.	As with the number of satellites, more planes means higher cost.

Table 2.1 Mission design drives and their design issues and impacts

2.4. Trade-off analysis

Trade-off analysis is the essence of mission and systems design. In the real world, the requirements, constraints and available resources never match perfectly so the system designer has to find the best compromise between all the factors. There are two main trades-off in the LGSNS mission: (1) Height/Number of satellites/Number of planes and (2) Payload performance/Cost.

2.4.1. Height/Number of satellites/Number of planes

The main trade-off of the mission is the relation between height, number of satellites and number of planes. These values define the coverage achieved by the satellite constellation.

On the one hand, increasing the number of satellites and planes result in an increase of the system DOP or, which is the same, the accuracy. In any case, increasing the number of satellites is a better option than increasing the number of planes because the last option is more expensive and increases the complexity of the constellation a lot. However, on the other hand, higher orbit means better single satellite coverage which results in the need for fewer satellites to fulfil global coverage.

The cost is also a very important point to take into account. The cheapest combination of height, satellites and planes with a good accuracy will shape the final constellation configuration.

2.4.2. Payload performance/Cost

Payload accuracy depends highly on its atomic clocks. More accurate atomic clock as passive hydrogen masers are more expensive than cesium or rubidium clocks which are

cheaper but less accurate. Depending on the precision that we want in the LGSNS, the cost of the whole system will vary.

If the payload is also capable of AutoNav function and inter-satellite link, its cost will also be higher. Finally, relativistic corrections also increase the payload cost. However, for a reliable and precise navigation system they are indispensable.

2.5. Functional Analysis

In order to define the functions required to produce the mission, we need to perform the functional decomposition of the objectives. The functional flow block diagram (FFBD) is a key tool because it visualises relations between elements of the system. It is applicable at all levels and can be used to relate: major mission and system elements, interaction of major subsystems within the system and relationships between the major assemblies within a subsystem.

After preparing the FFBD which provides us with a big list of functions, we can elaborate the functional allocation matrix (FAM). The FAM references the functions to those elements that provide each function. Finally, from the subsystem list of the FAM, we can build an N^2 diagram or interface matrix. With this last matrix, we can relate every function defined in the FFBD with all the subsystems needed to perform them. It helps us visualize the interfaces between subsystems.

2.5.1. Functional Flow Block Diagram

Figure 2.1 represents the FFBD of the LGSNS mission. It is an example of the functions that would be needed during the entire duration of the mission. However, issues such as production and launch are only mentioned here and they are not going to be elaborated in further detail in the following chapters because these issues are very difficult to approach during a preliminary design and, therefore, they are out of the scope of this study. Only aspects of constellation's creation and preliminary spacecraft design are going to be developed in the following chapters.

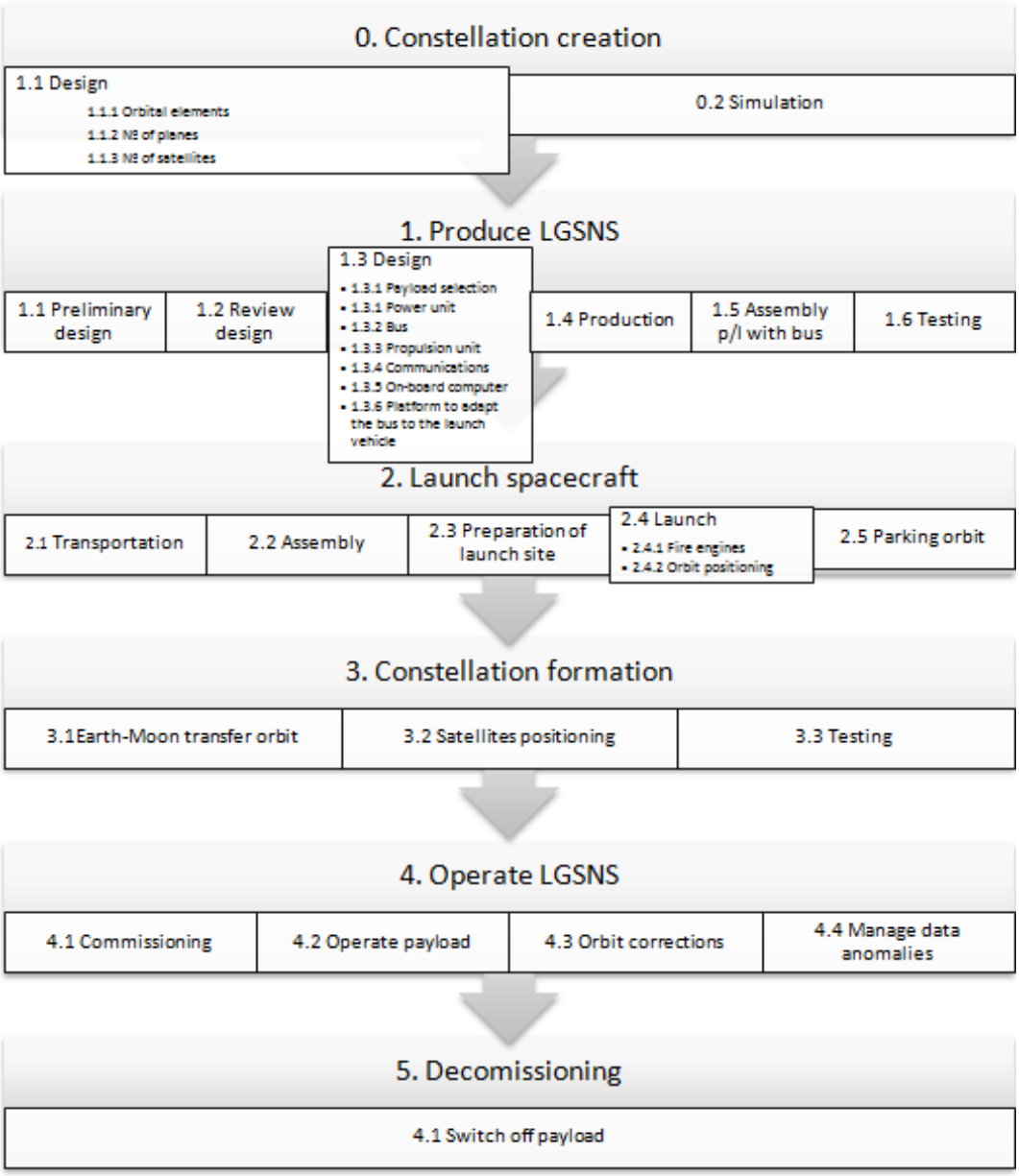

Figure 2.1 FFBD of the mission

2.5.2. Functional Allocation Matrix

Table 2.2 shows the FAM of the mission. In this case, unlike in the case of the construction of the FFBD, only aspects of constellation formation, operation and decommissioning are going to be represented because they are the functions with the largest number of subsystems relations.

Element o segment / Function	Propulsion	Attitude	Power	Payload	Processing facility	Telemetry and telecommand	On-board data handling
0. Constellation formation	**X**	**X**	**X**	**X**	**X**	**X**	**X**
0.1 Earth-Moon transfer orbit	X		X			X	
0.2 Satellites positioning	X	X	X			X	
0.3 Testing				X	X	X	X
1. Operate LGSNS	**X**	**X**	**X**	**X**	**X**	**X**	**X**
1.1 Commissioning			X	X		X	
1.2 Operate payload			X	X		X	
1.3 Orbit corrections	X	X	X			X	
1.4 Manage data anomalies						X	X

2. Decomissioning	**X**			**X**		**X**	
2.1 Switch off payload				X		X	

Table 2.2 FAM of the mission

2.5.3. Interface Matrix

Finally, Table 2.3 presents the N^2 diagram. As in the case of the FAM, only aspects of constellation formation, operation and decommissioning are taken into account.

	Propulsion	**Attitude**	**Power**	**Payload**	**Processing facility**	**TT&C**	**On-board data handling**
Propulsion		x	X			x	
Attitude	Satellite positioning, orbit corrections		X			x	
Power	Earth-Moon transfer orbit, satellites positioning, orbit corrections	Satellites positioning, orbit corrections		x		x	x

Payload			Comissioning, operate payload		x	x	x
Processing facility				Testing			
TT&C	Earth-Moon transfer orbit, satellites positioning, orbit corrections	Satellites positioning, orbit corrections	Earth-Moon transfer orbit, satellites positioning, comissioning, operate payload, orbit correction	Testing, comissioning, operate payload, switch-off payload			x
On-board Data handling				Testing		Testing, manage data anomalies	

Table 2.3 N^2 diagram of the mission

Chapter three.

Constellation selection

In this chapter the final constellation chosen for our mission will be presented but, before talking about the constellation selection process and presenting the selected constellation, we shall introduce the concepts used through the entire process of creating a GNSS satellite constellation: issues like what it is, how it works, how much accurate a GNSS is, are going to be explained in this chapter. Differences between a GNSS on the Earth and on the Moon are also going to be discussed.

3.1. What is a GNSS? How does it work?

Basically, a GNSS is a navigation system that offers information at regular intervals in the form of analogue signals about longitude, latitude, height and time to a receiver on the surface which uses them to compute its position. Any GNSS will include a minimum of four satellites to offer proper information to the receiver. The fourth measurement helps the receiver determine its own position by taking into account the clock error, that is always present. The other three satellites are used to triangulate the position of the receiver. To understand how triangulation works imagine a beacon emitting an omnidirectional signal. One could receive this signal, and having precise knowledge of the time of emission and reception, construct a sphere around the beacon, with its radius being the light-time trip. The receiver then would be located anywhere on the surface of the sphere. If we add now a second beacon, and construct an analogous sphere, we have a second condition on the possible position of the receiver. Then the receiver can only be located in the intersection of two spheres, that is, a circle. Adding a third beacon, the receiver's possible localizations is reduces to two points, and one of them is always a point under the Earth's surface[15].

Why time is important to the determination of position? GNSS does not send distances but information about where the receiver is. If the receiver is moving, distance measurements would be wrong because the receiver would have changed its location by the time the calculation of its position ends. It is because of this that receivers calculate the time taken by the signal to cover the distance between them. With this aim, the

time when the signal leaves the satellite needs to be known. As the satellite positions are known (by the process of orbit determination), it becomes straightforward for the receiver to compute the time taken by the signal to reach it. However, this travelling time is based on the comparison between the received signal and the reference signal generated by the receiver and both are affected by clock errors; therefore, the measured range is not the real one and is called *pseudorange* [8].

Pseudorange measurements $R_R^S(t)$ are defined as

$$R_R^S(t) = c \cdot (t_R - t^S) = \rho(t) + c \cdot \Delta\delta + e, \tag{3.1}$$

where c is the speed of light in vacuum, e represents the original measurement noise plus model errors and any non-modeled effects, t_R is the receiver's estimate of time, t^S is the time of transmission, assumed to be perfect because the receiver can compute it with a high degree of accuracy using the satellite atomic clock correction in the navigation message; $\Delta\delta$ is the receiver clock offset and ρ is the geometric range between the receiver at signal reception time and the satellite at signal transmission time, in other words, the true distance between satellite and receiver

$$\rho(t) = \sqrt{(X(t)^S - X_R)^2 + (Y(t)^S - Y_R)^2 + (Z(t)^S - Z_R)^2}. \tag{3.2}$$

The receiver must simultaneously solve Eq. 3.2 for every measurement that it receives. To determine the receiver coordinates, it is necessary to estimate the receiver's initial position in order to linearize the pseudorange equations. The linearization is needed because ρ is a nonlinear function of the receiver and satellite coordinates. After the linearization, corrections to the initial estimates are applied to obtain the receiver's actual coordinates and clock offset. The model becomes

$$\boldsymbol{\Delta R_R^S} = [A] \cdot \boldsymbol{\Delta x} + \boldsymbol{e}, \tag{3.3}$$

where $\boldsymbol{\Delta R_R^S}$ is the n-elements vector of the differences between the corrected pseudorange measurements and the linearized values, $\boldsymbol{\Delta x}$ designates the four-elements vector of unknown parameters (receiver position and clock offset), *[A]* is an (n x 4) matrix of partial derivatives of the pseudoranges with respect to the unknown parameters and, finally, $\boldsymbol{e}$ is an n-elements vector of errors. There are n equations because a GNSS receiver computes its three-dimensional coordinates and its clock offset from four or more simultaneous pseudorange measurements. The number of equations depends on how many satellites are in sight from the receiver[16], [17], [18].

3.2. Sources of errors

The main differences between a GNSS on the Earth and on the Moon are due to the different types of errors that the system has to deal with.

Environment errors are not the same in the two cases. On the Earth, there are more environment effects than on the Moon. Ionospheric and tropospheric errors are very important on our planet but the Moon does not have an atmosphere so these errors do not exist there.

Mutipath errors can happen on the Moon due to its topography but on Earth they are more common, not only because of the more variable landscape but also because of the many man-made constructions. This kind of error is caused by multiple reflections of the signals at the receiver or at the satellite due to multiple paths taken by the signal to reach the destination.

There are errors which affect a navigation system both on the Earth and on the Moon. These are[19], [20], [21]:

- Ephemeris errors: due to slight deviations in the orbital path of the satellites from their predicted trajectory. They can be eliminated by differential positioning.

- Clock errors (already mentioned):
    - Satellite clock error: can be modelled by the polynomial coefficients transmitted in the navigation message with respect to a reference time.
    - Receiver clock error: appear due to using a non-precise clock in the receiver which causes an offset and drift in the receiver clock and GNSS reference time. As already mentioned, this error is treated as an unknown in the pseudorange computations.

- Satellite geometry: affects the accuracy of the calculated GNSS positions. Dilution of precision or DOP is used to quantify this error. GDOP, which is a kind of DOP, refers to where the satellites are relatve to each other. A more detailed discussion on the DOP follows.

3.3. Measuring accuracy and precision: DOD

The DOP measures the accuracy of a GNSS. It evaluates the effect of satellite geometry on GNSS position determination and time accuracy. It is the ratio of the standard deviation of the position error to the standard deviation of the measurement errors, assuming all measurements errors are statistically independent, have a zero mean and have the same standard distribution. The smaller the values of DOP the better the accuracy of the system. The DOP takes different forms: geometrical (GDOP), positional (PDOP), horizontal (HDOP), vertical (VDOP) and time (TDOP).

As already said, a GNSS receiver computes its three-dimensional coordinates and its clock offset from four or more simultaneous pseudorange measurements. The accuracy of the measured pseudoranges and the fidelity of the model used to process them, determine the overall accuracy of the receiver coordinates.

To find the accuracy, we need to know how the pseudorange measurement and model errors affect the estimated parameters or, equivalently, $\boldsymbol{\Delta x}$. This is given by the law of propagation of error, i.e., the covariance law. If we assume that the measurement and model errors are the same for all observations, that they are uncorrelated and that they all have a particular standard deviation σ, the expression for the covariance $[C_{\Delta x}]$ of $\boldsymbol{\Delta x}$ can be simplified as

$$[C_{\Delta x}] = \left([\mathrm{A}]^{\mathrm{T}}[\mathrm{A}]\right)^{-1}\sigma^2 = [D]\sigma^2. \tag{3.4}$$

The diagonal elements of $[C_{\Delta x}]$ are the estimated receiver coordinate and clock offset variances, and the non-diagonal elements indicate the degree to which these estimates are correlated.

In order to be able to compute the components of $[C_{\Delta x}]$ we need a value for σ. If we assume that measurement errors and model errors components are all independent, we can RSS (Root-Sum-Squares) these errors to obtain a single value for σ (known as UERE or User Equivalent Range Error). With this value a measure of the overall quality of the least-squares solution can be found by taking the square root of the sum of the diagonal elements (variances):

$$\sigma_G = \sqrt{D_{11} + D_{22} + D_{33} + D_{44}} \cdot \sigma = GDOP \cdot \sigma = \sqrt{\sigma_{East}^2 + \sigma_{North}^2 + \sigma_{Up}^2 + \sigma_{Time}^2}. \tag{3.5}$$

As it can be seen, the standard deviation, or UERE, is multiplied by a scaling factor equal to the square root of the trace of the matrix *D*. The elements of the matrix *D* are a

function of the receiver-satellite geometry only and because the scaling factor is typically greater than one, it amplifies the pseudorange error, or it dilutes the precision, of the position determination. This scaling factor is therefore usually called the geometric dilution of precision (GDOP).

With these variances, the different definitions of DOP can be found:

$$PDOP = \frac{\sigma_P}{\sigma} = \frac{\sqrt{\sigma_E^2 + \sigma_N^2 + \sigma_U^2}}{\sigma} = \sqrt{D_{11} + D_{22} + D_{33}}, \tag{3.6}$$

$$HDOP = \frac{\sigma_H}{\sigma} = \frac{\sqrt{\sigma_E^2 + \sigma_N^2}}{\sigma} = \sqrt{D_{11} + D_{22}}, \tag{3.7}$$

$$VDOP = \frac{\sigma_V}{\sigma} = \frac{\sqrt{\sigma_U^2}}{\sigma} = \sqrt{D_{33}}, \tag{3.8}$$

$$TDOP = \frac{\sigma_T}{\sigma} = \frac{\sqrt{\sigma_T^2}}{\sigma} = \sqrt{D_{44}}. \tag{3.9}$$

Note that $PDOP^2 = HDOP^2 + VDOP^2$ (3.10) and $GDOP^2 = PDOP^2 + TDOP^2$ (3.11).

If the tips of the receiver-satellite unit vector lie in a plane, the DOP factors are infinitely large. The solution cannot distinguish between an error in the receiver clock and an error in the receiver position. Conversely, when the satellites are spread out in the sky, DOP values are smaller which makes solution errors smaller too.

Since normally there are more than only four satellites in sight, receivers make use of a satellite selection algorithm to choose the four satellites that would produce the lowest DOP values. However, the more satellites used in the solution, the smaller the DOP values and hence the smaller the solution errors.

Usually VDOP values are larger than HDOP values. It happens because all the satellites from which the vertical position is obtained are above the receiver. The horizontal coordinates are more accurate due to the fact that the receiver gets signals from all sides. One way to improve the vertical coordinates is to have a much better accurate receiver clock so that the receiver only needs to estimate its position and not its clock offset[22].

A table of DOP values and their ratings is presented in Table 3.1,

DOP value	Rating
1	Ideal
1-2	Excellent
2-5	Good
5-10	Moderate
10-20	Fair
>20	Poor

Table 3.1 DOP value meanings

3.4. Constellation Selection

During the selection process ten different constellations have been considered and simulated: they are characterized by different values of height, inclination, number of satellites and number of planes (the design drivers). The simulation has been done with STK software and the aim was to find a constellation which could achieve global coverage of the lunar surface. For this reasons the main requirement for the selected constellation was that at least 4 satellites were always in sight. The spare satellite per orbital plane mentioned in the requirements is not taken into consideration during the constellation selection process. The main characteristics of the studied constellations are summarized in Table 3.2.

Constellation	Height [km]	Inclination [°]	Number of satellites	Number of planes
1	200	90	30	5
2	2000	90	6	2
3	2000	90	8	2
4	2000	90	12	3
5	2000	90	15	3
6.1	6500	90	15	3
6.2	6500	60	15	3
7	2000	90	18	3
8.1	4000	90	18	3
8.2	4000	60	18	3

Table 3.2 Possible constellations' characteristics

For further information on the constellations see *Annex C*.

Of these ten constellations only four meet the 4-satellite-in-sight requirement. They are the constellations labelled 6.1, 6.2, 8.1 and 8.2:

- Constellations 6.1 and 6.2 have an orbital height of 6500 km and consist of three planes with five satellites each. The only difference between these two constellations is the inclination of their orbital planes: the former has polar orbits whereas the latter is inclined 60 degrees to the equator.

- Also constellations 8.1 and 8.2 are made of polar orbits and of 60 degree-inclination orbits. The altitude is slightly lower, though, at 4000 km and they have one more satellite in each plane.

At first sight the best options are constellations 6.1 or 6.2 because they have a lower number of satellites. However, in order to decide which solution is the most suitable, a DOP study has been carried out for the four constellations. Constellations with 60 degree-inclination have lower performance because they exhibit two different peaks on their HDOP latitude value whereas polar constellations only presented one peak. For this reason, the final decision was between constellation 6.1 and 8.1. These constellations have very similar mean DOP values, however, constellation 8.1 presented higher peaks (GDOP peak value of 35 in latitude and 95 in longitude) than constellation 6.1 (GDOP peak value of 14 in latitude and 30 in longitude). Low DOP peak values added to the fact that constellation 6.1 has three satellites less than constellation 8.1 proves that the constellation with the best performance is **Constellation 6.1**.

Figures 3.1 and 3.2 show a 3D view and the ground track of Constellation 6.1. Figures 3.3, 3.4, 3.5 and 3.6 show different performance parameters by latitude and longitude of the selected constellation.

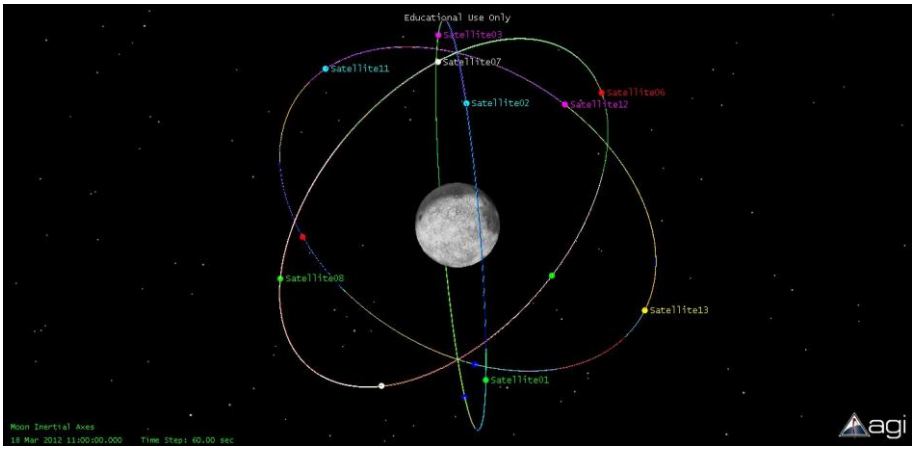

Figure 3.1 3D representation of the selected constellation

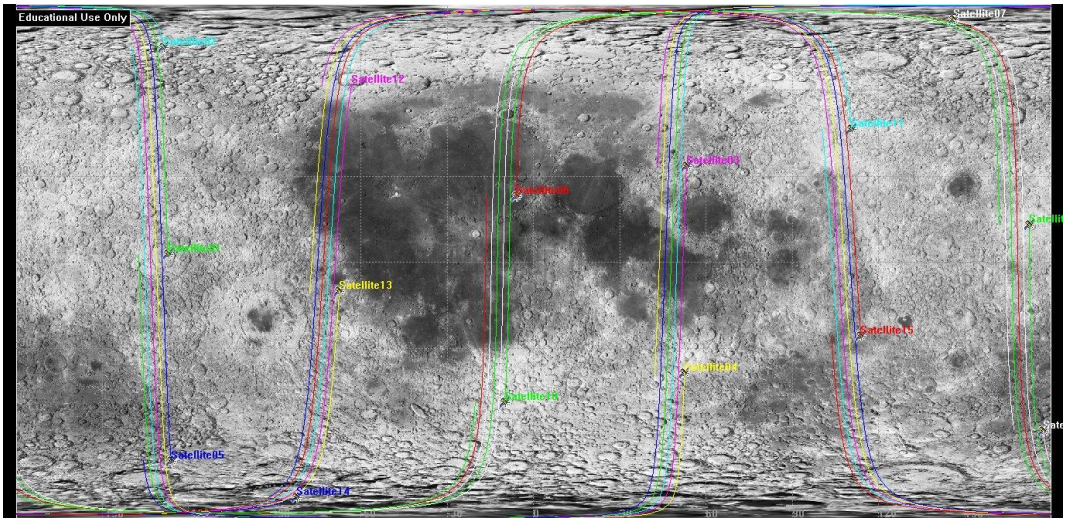

Figure 3.2 STK visualization of the satellites trace on the lunar surface

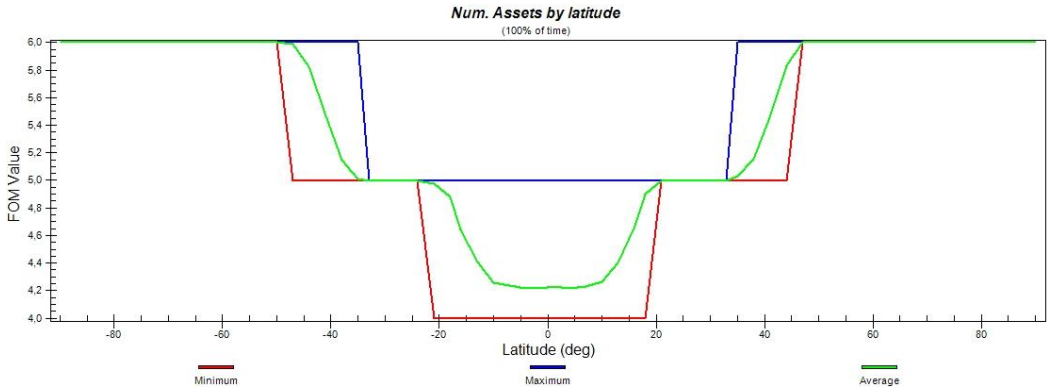

Figure 3.3 Number of satellites always in sight by latitude

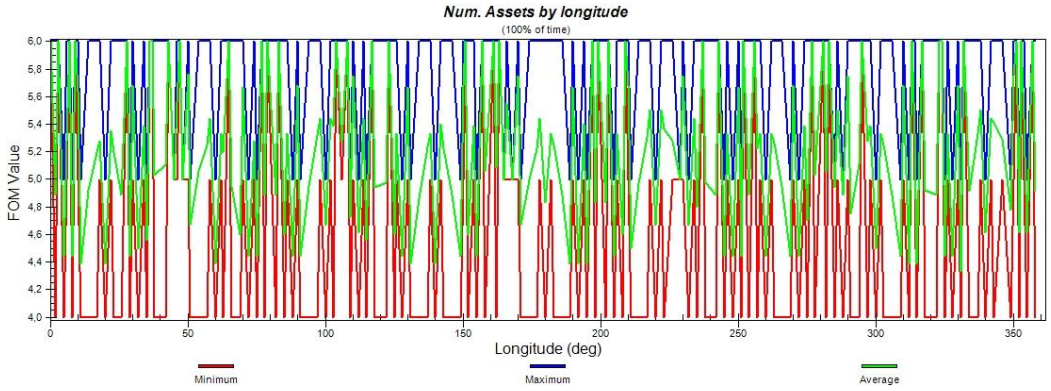

Figure 3.4 Number of satellites always in sight by logitude

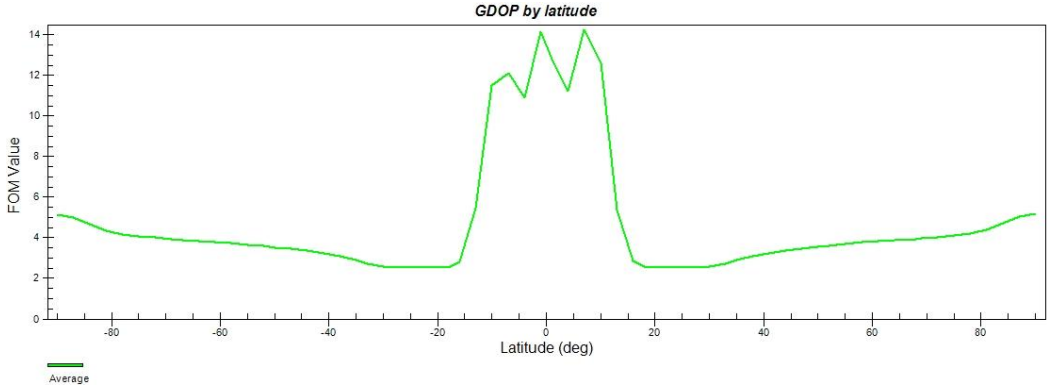

Figure 3.5 GDOP results by latitude

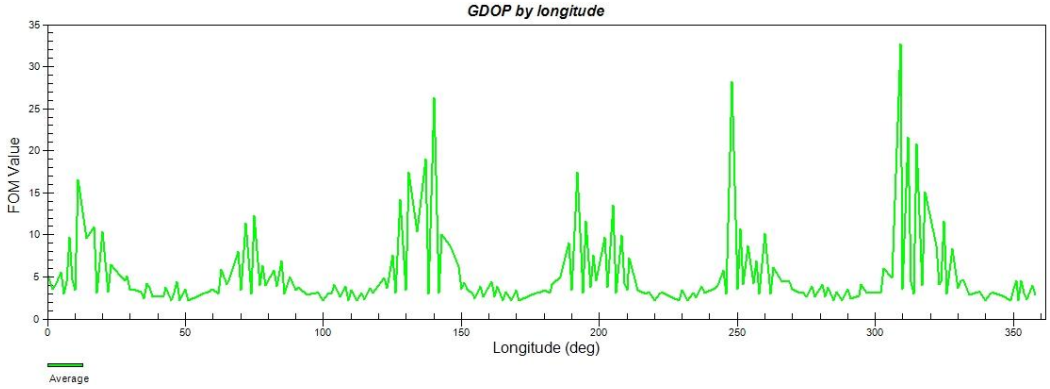

Figure 3.6 GDOP results by longitude

GDOP average value by latitude is around 5 but it is important to notice the increase in GDOP between -20° and 20°. If this fact is known, observations or experiments which need a high precision on surface position can avoid this latitude range. However the GDOP never exceeds the value of 20 in latitude, limit beyond which the measurements should be discarded. With GDOP average value by longitude something similar occurs: although its mean value is around 7 it exhibits peak values around 30.

These peak values have been reduced by imposing a smaller time step during the calculation. STK software has two ways of computing figures of merit: using a sampling method or using direct computations based on access intervals. The Coverage module uses algorithms based directly on the access intervals whenever possible to ensure accurate figure of merit values. For example, the Percentage Time Covered (used in the computation of the visible number of assets) is computed as the sum of the total time covered for each point divided by the duration of the coverage interval. This yields the same result as using a sampling method with an infinitely small sample time. However, DOP figure of merit uses a sampling method. In the sampling method, a sequence of times is determined or accumulated for each grid point to be used for sampling the figure of merit. An example of this method would be to evenly distribute 100 times across the coverage interval and compute the percentage of time covered for each point

as the number of times when the point is able to access an asset. The accuracy of the answer produced by sampling is dependent on the frequency of the sampling and the duration of the accesses between grid points and assets[23]. With this in mind, we selected the time step by means of a trade-off between the accuracy of the upcoming results and the computing time needed for them. The final selected time step was 50 seconds which is not small enough to avoid peak values induced by the calculation sampling method.

For further information about the DOPs of the other options and the final selection see *Annex C*.

3.5. Near-future possibilities

Once the constellation is chosen, it is important to discuss its near-future and long-term uses. As a matter of fact, if on the one hand a GNSS constellation will be completely necessary to a fully operative lunar permanent base, for the other objectives such as high precision scanning of the lunar surface, a complete navigation constellation is not needed. Hence, a study of an incomplete Constellation 6.1 has been done. Such incomplete constellation has three satellites in each of its three planes but, unlike the complete one, the satellites are not equidistant between them. The spacing between the satellites is the same as in the complete constellation: 72°. This fact allows global coverage of, approximately, half the lunar surface. The red colour in Figures 3.7 and 3.8 indicates the surface with four satellites always on sight. The covered area moves in time allowing the constellation to see the entire lunar surface during one day.

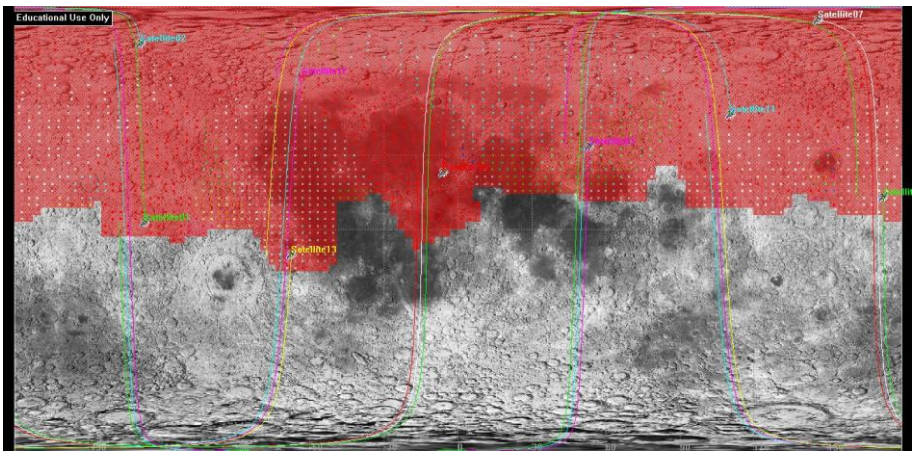

Figure 3.7 STK visualization of the incomplete constellation's satellites trace

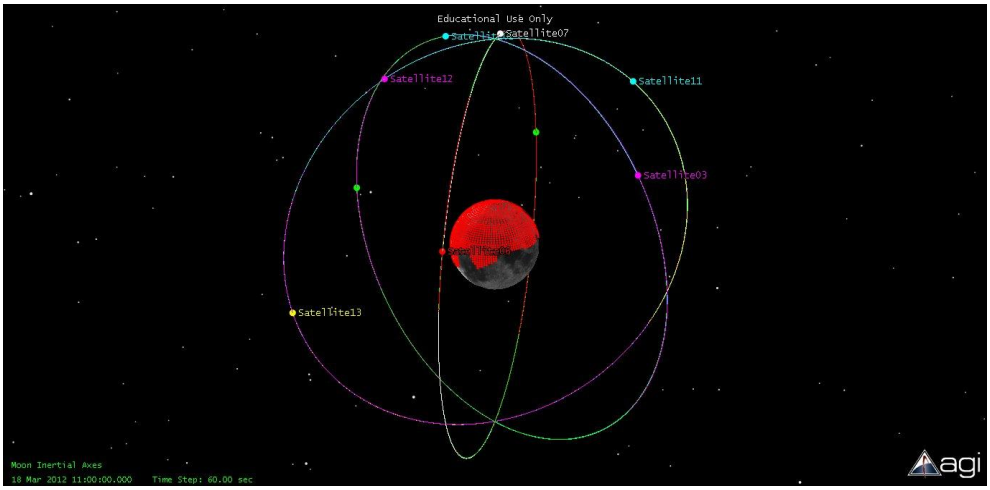

Figure 3.8 3D representation of the selected constellation. In red, the area with coverage

Important information about the incomplete constellation is coverage time and revisit time. Coverage time represents the % of time with four satellites always on sight, whereas revisit time represents time without coverage.

Figures 3.9, 3.10, 3.11 and 3.12 show the revisit time and coverage time of the uncompleted constellation by latitude and longitude.

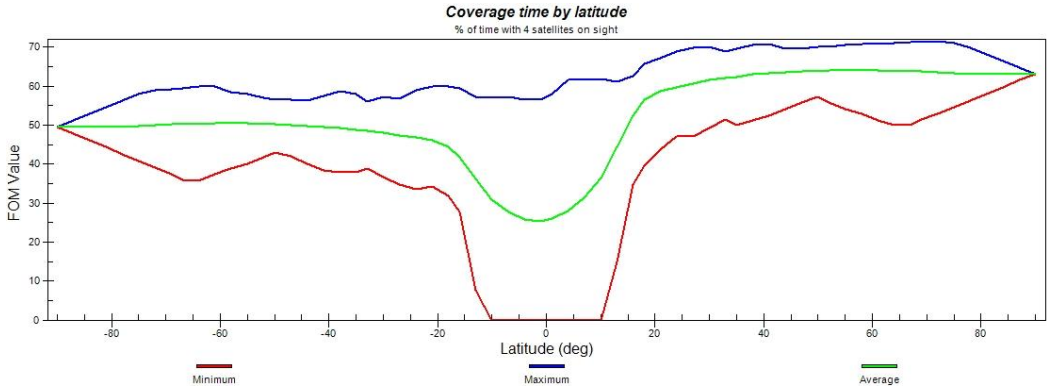

Figure 3.9 Coverage time of the incomplete constellation by latitude

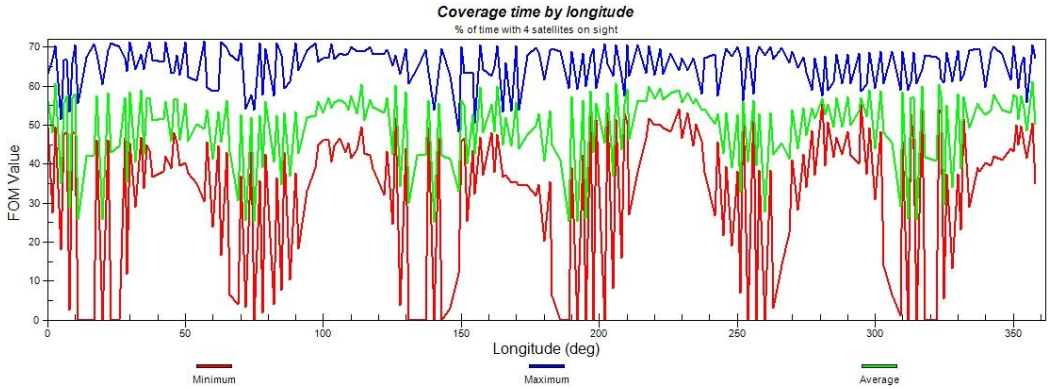

Figure 3.10 Coverage time of the incomplete constellation by longitude

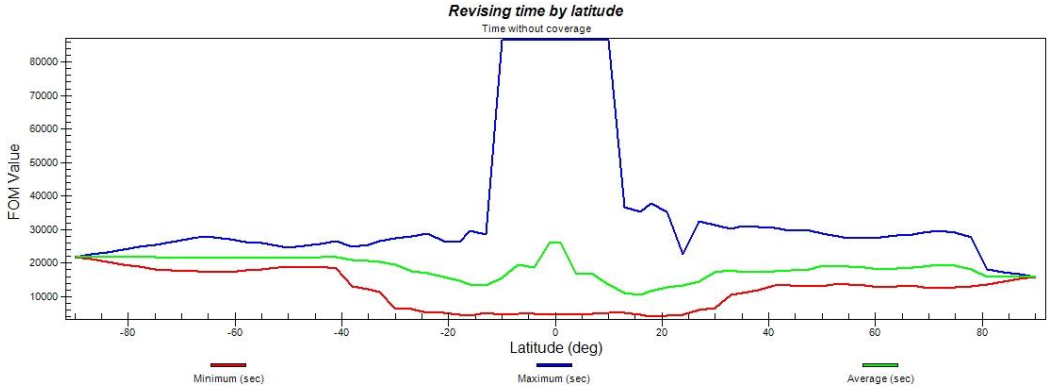

Figure 3.11 Revisit time of the incomplete constellation by latitude

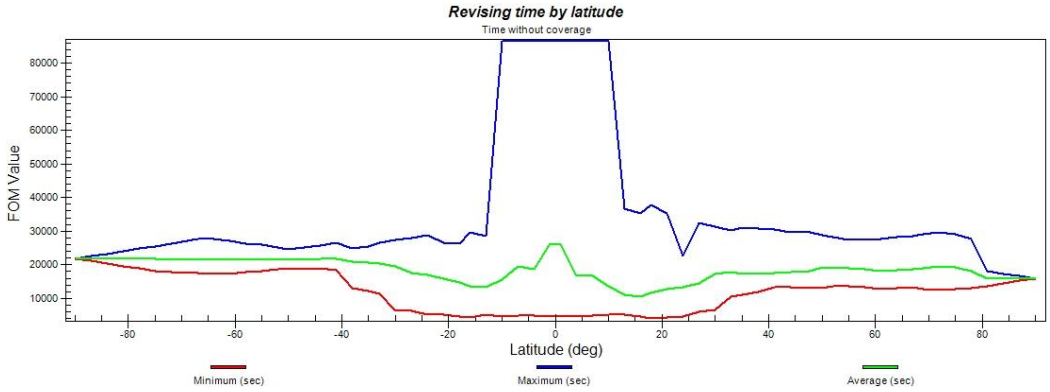

Figure 3.12 Revisit time of the incomplete constellation by longitude

The fact that this constellation does not perform a global coverage of the lunar surface does not necessarily mean that global coverage cannot be achieved. On Earth, receivers have an inaccurate clock because they need to be cheap in order to be sold to civilians but, on the Moon, receivers do not need to be cheap because its service would be restricted for scientific use and they would not have any commercial purposes. For this reason, they can be inertial receivers capable to calculate and maintain their own position during periods when satellite support is not possible. With this kind of receivers even an incomplete satellite navigation constellation would be able to perform global coverage over time through the entire surface. So, having more expensive receivers would allow to use an incomplete constellation which means that, in a short-middle time term (when the complete constellation is not needed because of the lack of a lunar base), a lot of money can be save.

Chapter four.

Orbital simulations

In this chapter we shall discuss the issue of orbital perturbations. The degradation that any orbit suffers after a long period of time is caused by a perturbing acceleration induced by several perturbations. For a satellite orbiting a planetary body, such acceleration $\boldsymbol{a}$ is the sum of the central body gravitational acceleration $\boldsymbol{a_{Central\ Body\ Gravity}}$ and the vector sum $\boldsymbol{a_{perturbation.}}$ of all other affects:

$$\boldsymbol{a} = \frac{d\boldsymbol{v}}{dt} = -\frac{\mu}{r^3}\boldsymbol{r} + \boldsymbol{a_{pert}} = \boldsymbol{a_{Central\ Body\ Gravity}} + \boldsymbol{a_{perturbation}}\,. \tag{4.1}$$

The effects on the chosen constellation are going to be simulated with STK software. This allows to foresee the evolution of the orbital elements and to set up a station-keeping strategy.

An eclipse simulation is also going to be held and the main space lunar environment hazards will be presented.

4.1. Perturbations

Unlike the Earth, the Moon does not have a significant atmosphere[24] which means that the small amount of the atmospheric gases does not constitute a relevant source of perturbation. Hence, atmospheric drag and lift can be neglected. The contribution of tidal effects can also be neglected because their magnitude on artificial satellites is very small. Finally, the Moon does not possess a global magnetic field such as that generated by a liquid metal core dynamo; as a consequence, magnetic interactions can also be neglected.

The only important orbital perturbations around the Moon are: the gravity due to the central body, third body gravitational-perturbations, solar radiation pressure and albedo and thermal radiation pressure of the central body. A brief description and simplified models to approach the computation of each of these perturbations are given in this chapter's section. They are only the base for what STK uses to compute the effect of perturbations during orbit propagation, therefore, they are not the complete STK model.

4.1.1. Central body gravity

The force ***F*** of a celestial body on an orbiting satellite when both are point masses is described by the well-known law of Newton:

$$\boldsymbol{F} = -G\frac{mM}{r^3}\boldsymbol{r} = -\mu\frac{m}{r^3}\boldsymbol{r}, \tag{4.2}$$

where *m* and *M* are, respectively, the masses of the satellite and the central body, ***r*** is the vector between both, and *G* is the gravitational constant. The unperturbed motion of the satellite can be described by means of

$$\frac{d\boldsymbol{r}}{dt} = \boldsymbol{v}, \tag{4.3}$$

$$\boldsymbol{a} = \frac{d\boldsymbol{v}}{dt} = -\frac{\mu}{r^3}\boldsymbol{r}, \tag{4.4}$$

where ***r*** represents the position, ***v*** the velocity and ***a*** the acceleration of the satellite with respect to the central body. The resulting motion is a Keplerian orbit: a circle, an ellipse, a parabola or a hyperbola, the occurrence of one type or the other depending on the value of the total mechanical energy. Now, a real body is neither a point mass nor a perfect sphere so, the gravitational potential *V* (and its gradients of any order) varies not only with the distance to the satellite, but more generally as a function of position. The acceleration is the first-order gradient of *V*,

$$\boldsymbol{a} = \nabla V. \tag{4.5}$$

For a point mass,

$$V = G\frac{M}{r}. \tag{4.6}$$

And, for *m* negligibly small compared to *M*, Eqs 4.5 and 4.6 are valid for a coordinate system whose origin is at the center of mass (CM) of *M*. The acceleration produced by several point masses M_i at distances r_i from *m* can be expressed as the gradient of the potential which is the sum of potentials V_i expressed by Eq. 4.6. If these particles form a continuous body of variable density ρ, their summation can be replaced by an integral over the volume of the body:

$$V = G\iiint \frac{\rho(x,y,z)}{r(x,y,z)}dxdydz. \tag{4.7}$$

In the case of a point mass, a specific component a_x of $\boldsymbol{a}$ is given by

$$a_x = \frac{\partial V}{\partial x} = -GM\frac{x}{r^3}, \tag{4.8}$$

whereas the second gradient yields

$$a_{xx} = \frac{\partial^2 V}{\partial x^2} = GM\left(-\frac{1}{r^3} + \frac{3(x^2+y^2+z^2)}{r^5}\right) = 0. \tag{4.9}$$

Which, summed to the remaining two diagonal elements of the second-order gravity gradient tensor, provides the equation of Laplace:

$$\nabla^2 V = \frac{\partial^2 V}{\partial x^2} + \frac{\partial^2 V}{\partial y^2} + \frac{\partial^2 V}{\partial z^2} = GM\left(-\frac{1}{r^3} + \frac{3(x^2+y^2+z^2)}{r^5}\right) = 0. \tag{4.10}$$

An equivalent result holds for any element of mass $\rho\, dxdydz$ in Eq. 4.7 and hence for the summation thereof.

The gravitational potential, solution of Eq. 4.10, is naturally represented in spherical harmonics (SH). For any mass distribution, in spherical polar coordinates $\rho(r,\lambda,\varphi)$ the potential *V* at the external point $P(r,\lambda,\varphi)$ can always be written as

$$V(P) = \sum_{i=0}^{\infty} r^i Y_i(\lambda,\varphi) + \sum_{j=0}^{\infty} \frac{1}{r^{j+1}} Z_j(\lambda,\varphi), \tag{4.11}$$

with Y_i and Z_i surface SHs (degree *i* and *j*, respectively), provided that ρ=0 in all points of a sphere *S* through *P* centered in *O*. Further manipulations allows to write

$$V(r,\varphi,\lambda) = \frac{\mu}{r}\sum_{n=0}^{\infty}\left(\frac{a}{r}\right)^n \sum_{m=0}^{\infty} P_n^m(\sin\varphi)\left(\tilde{C}_{nm}\cos m\lambda + \tilde{S}_{nm}\sin m\lambda\right), \tag{4.12}$$

where *a* is the mean radius of the celestial body, μ is the product of the universal gravitational constant and the mass of the celestial body, φ and λ are respectively, latitude and longitude, the quantities $\tilde{C}_{nm}$ and $\tilde{S}_{nm}$ are the fully normalized Stokes coefficients and, finally, $P_n^m(\sin\varphi)$ is the fully normalized ALF (Associated Legendre Function) of the first kind of degree *n* and order *m*[25].

It can be observed that all the orbital elements present oscillations which can be understood as a representation of the potential based on a reorganization of the classical spherical harmonics representation in the form presented by [26] in which the summations appear in the form of Fourier series, thus allowing a more direct analysis of

the "frequencies" that cause the observed oscillations. Figures from 4.3 to 4.22 are a graphic representation of these oscillations. There exist secular effects, those produced by J2 (zonal coefficient of degree 2) on Ω and ω are the main ones, long period effects (13.66 to 27.55 days[27]) and short periodic effects (period close to the period of the satellite). In general, each spherical harmonic term produces oscillations which appear in the evolution of the orbital elements. These oscillations decrease in amplitude as the degree and order of the SH increase (smaller and smaller strength). Note, however, that there may be resonances between terms; coupling of two terms which produce a short periodic oscillation and a long periodic one whose frequencies are close to the ratio of two integers. When this happens, the associated amplitudes in some parameter decrease considerably[28].

4.1.2. Third-body gravitational perturbations

The perturbed acceleration due to a third body can be expressed as

$$\boldsymbol{a_{TB}} = \mu' \left(\frac{\boldsymbol{\rho}}{\rho^3} - \frac{\boldsymbol{R}}{R^3} \right), \tag{4.13}$$

where $\boldsymbol{\rho} = \boldsymbol{R} - \boldsymbol{r}$, $\boldsymbol{R}$ is the distance between the Moon and the third perturbing body and $\boldsymbol{r}$ is the distance between the Moon and the satellite.

The Sun and the Earth constitute the only relevant contributors to this perturbation at the Moon[29]. Hence the perturbing acceleration will include the following two terms:

$$\boldsymbol{a_{TB,\oplus}} = \mu_\oplus \left(\frac{\boldsymbol{\rho}_\oplus}{\rho^3} - \frac{\boldsymbol{r}_{\subset\oplus}}{R^3} \right) \quad \text{and} \quad \boldsymbol{a_{TB,\odot}} = \mu_\odot \left(\frac{\boldsymbol{\rho}_\odot}{\rho^3} - \frac{\boldsymbol{r}_{\subset\odot}}{R^3} \right). \tag{4.14}$$

This perturbation does not produce secular or long-period variations in the semimajor axis; the only effects appear in the longitude of the ascending node and in the argument of pericenter. The long-periodic variation in eccentricity, inclination, Ω and ω are completely associated with the motions of the satellite's pericenter and the disturbing body. Finally, resonances appear when the rate of change of any of the arguments in the periodic terms vanishes [28].

4.1.3. Solar radiation pressure (SRP)

The pressure of the solar radiation produces a non-conservative perturbation, an acceleration resulting from the momentum exchange between the photons and the

satellite's surface. SRP depends on the distance from the Sun, the area-to-mass ratio and the reflectivity properties of the surface.

The pressure is simply the force divided by the incident area exposed to the Sun. This means that the pressure distribution is critical and it depends on the satellite's shape and composition. The force imparted is

$$\boldsymbol{F_{SR}} = -p_{SR} c_R A_{\odot} \boldsymbol{r}, \tag{4.15}$$

where p_{SR} is the pressure ($p_{SR} = \frac{J_s}{c}$), c_R is the surface reflectivity, $A_{\odot}$ is the front area exposed to the Sun and $\boldsymbol{r}$ is the vector to the Sun. The reflectivity indicates how the satellite reacts to the interaction with the photons and is a number in the range from zero to two: zero means that the surface is translucent, a value of one means that all the radiation is absorbed and a value of two indicates that all the radiation is specularly reflected.

Incorporating the mass allows to transform from force to acceleration:

$$\boldsymbol{a_{SRP}} = -p_{SR} c_R \frac{A}{m} \frac{\boldsymbol{r_{sat\odot}}}{|\boldsymbol{r_{sat\odot}}|}, \tag{4.16}$$

with *A/m* representing the area-to-mass ratio.

SRP only affects the satellite in the illuminated parts of its orbit: if the Earth or the Moon eclipse the satellite, the perturbation due to SRP is zero. SRP causes periodic variations in all the orbital elements and induce changes in pericenter height that can seriously affect the satellite's lifetime. Its effects are usually small for most satellites except for those with very low mass and large areas[28].

4.1.4. Thermal and albedo radiation pressure of the central body

Solar radiation that reflects off a celestial body is called albedo (ARP). The amount of reflected radiation by the Moon is about 7%[25] of the incoming solar radiation. The acceleration produced by ARP is modelled by taking into account that only the illuminated side of the Moon contributes to this effect.

A way to treat the problem with simplicity is by means of the radiative flux due to albedo:

$$J_a = a \cdot J_s \cdot F \cdot \cos\alpha, \tag{4.17}$$

where a is the planetary albedo coefficient (0.07 for the Moon), J_s is the solar flux, α is the angle in with the solar rays impact on the atmosphere and F is the view factor which can be compute as

$$F = \int_{A_2} \frac{\cos\phi_1 \cos\phi_2}{\pi R^2} dA_2. \tag{4.18}$$

This formula gives a view factor per dA_1. The angles and distances on the formula follow Figure 4.1:

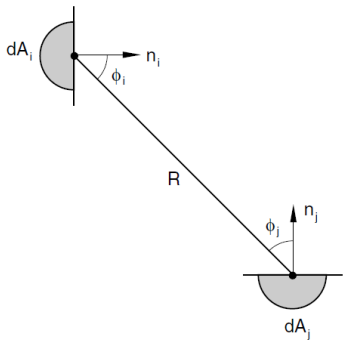

Figure 4.1 Representation of the view factor angles

The angle is defined between the area normal vector (n_i) and the vector of union between both areas of study. The distance R is the module of such vector.

Then, the radiation pressure becomes:

$$p_{AR} = \frac{J_a}{c}, \tag{4.19}$$

and a simplified relation for the acceleration due to albedo is

$$\boldsymbol{a_{ARP}} = -p_{AR} c_R \frac{A}{m} \frac{\boldsymbol{r_{sat\subset}}}{|\boldsymbol{r_{sat\subset}}|}. \tag{4.20}$$

Regarding the thermal radiation pressure, important differences in temperature exist between night (-153°C) and day (107°C) on the Moon due to the lack of greenhouse gases which do not mitigate the diurnal thermal gradients. Such temperature difference produces dramatically different emitted fluxes between day and night side. The radiative infrared flux (TRP) can be compute as

$$J_p = EIR \cdot F, \tag{4.21}$$

where EIR is the flux value and it is not constant over the lunar surface. It depends on the surface properties and on the lunar surface difference in temperatures. F is the view factor expressed in Eq 4.18. Therefore, the thermal lunar radiation pressure is obtained as:

$$p_{TR} = \frac{J_p}{c}, \tag{4.22}$$

and the perturbing acceleration of this effect can be computed as:

$$\boldsymbol{a_{TRP}} = -p_{tR} c_R \frac{A}{m} \frac{\boldsymbol{r_{sat\subset}}}{|\boldsymbol{r_{sat\subset}}|}. \tag{4.23}$$

4.2. Orbit propagation

The propagation of the orbits of the constellation has been carried out with STK using a Runge-Kutta-Fehlberg 7th order with 8th order error control integrator[23]. One satellite has been propagated for each orbital plane, resulting in three different orbits (with different RAAN: 0°, 120° and 240°). Their orbital characteristics are listed in Table 4.1.

Satellite	Radius [km]	Eccentricity	Inclination [°]	RAAN [°]	ω [°]	Argument of latitude [°]
Sat0	8238	0	90	0	0	288
Sat120	8238	0	90	120	0	24
Sat240	8238	0	90	240	0	120

Table 4.1 Orbits' parameters in Moon Inertial frame

Then, a number of simulation parameters have been specified. The epoch and the start and end time of the simulation are indicated in Table 4.2.

Epoch	18 Mar 2012 11:00:00.000 UTCG
Start time	18 Mar 2012 11:00:00.000 UTCG
Stop time	18 Mar 2013 11:00:00.000 UTCG

Table 4.2 Epoch, start and stop time of the STK simulation

Regarding the mass, the satellites were modelled taking into consideration the mass of a GPS and a Galileo satellite. The former have a mass of 700 kg, whereas the latter present different shapes depending on the release block, but their average mass is of 1500 kg. The final selected mass for our satellites is 1000 kg with a dry mass of 750 kg. The satellite area is 20 m^2 and the solar radiation pressure coefficient C_r is assumed equal to one.

The satellite elements presented in Table 4.1 are represented in what STK calls the Moon Inertial frame. However, STK gives the elements calculated during the propagation in another coordinate frame: J2000. Whereas the Moon Inertial frame is very close to the Mean Lunar Equator evaluated at J2000, J2000 frame represents the Mean Equator and Mean Equinox of the Earth at J2000 (JD 2451545.0 TDB – 1 Jan 2000 12:00:00.000 TDB). All the figures of this section are given in the J2000 frame instead of the Moon Inertial frame[23]. For a better understanding of the frame transformation see *Annex B*.

STK is able to simulate all the perturbations presented at the beginning of this section. The central gravity model uses an ASCII file containing the Central Body potential model coefficients of the model LP150Q[30]. For our simulation a 48 degree and order of potential coefficients have been selected to be included for the gravity computations. STK also takes into consideration solid-tides. In our case, only the permanent tide has been included in the computation. The permanent tide is the average attraction between the Earth (and Sun) and the lunar surface which causes small variations in the lunar topography[31]. Third body-perturbations are calculated with the influence of the Sun and the Earth.

The Solar Radiation Pressure model assumes a spherical spacecraft with a dual cone shadow model. The dual cone model uses the actual size and distance of the Sun to model regions of umbra, penumbra and sunlight (See Figure 4.2). The visible fraction of the solar disk is used to compute the acceleration during penumbra.

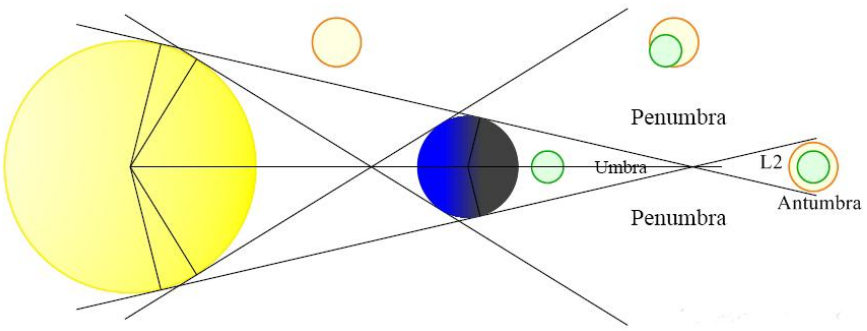

Figure 4.2 Sunlight, umbra and penumbra scheme

Finally, albedo and thermal radiation pressure of the Moon are also modeled. The coefficient of reflectivity of the satellite C_k is set equal to one.

The evolution of the orbital elements during the propagation can be found from Figure 4.3 to Figure 4.22. The figures represent the effect on the evolution of the orbital elements of the different perturbations, taken together and individually. The following combinations of effects have been analysed:

- Central body gravity + SRP + Third body-perturbation
- Central body gravity
- Central body gravity + SRP
- Central body gravity + Third body-perturbation

In this way it is possible to check which perturbation has the highest effects on the evolution of the orbital elements. We report here only the results from the evolution of the orbital elements of one of the orbital planes, i.e., that with RAAN=0°. The results of the other two orbital planes can be found in *Annex D*.

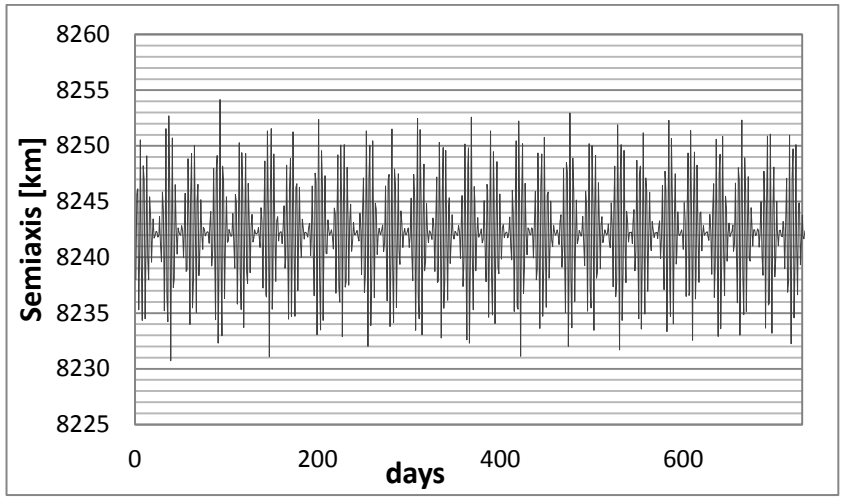

Figure 4.3 Semimajor axis evolution with all perturbation effects

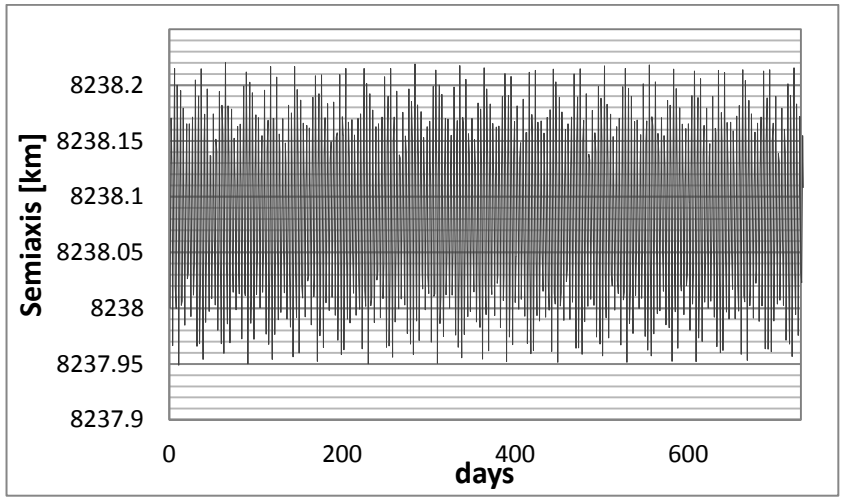

Figure 4.4 Semimajor axis evolution with only central body gravity perturbing effects

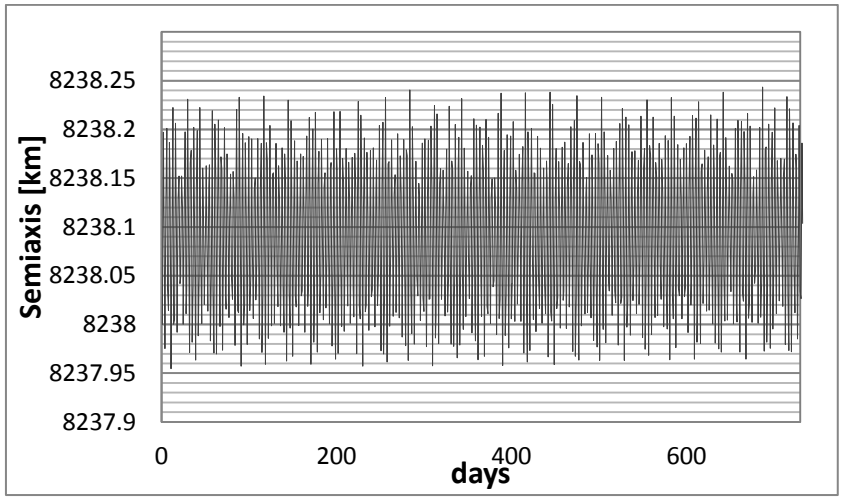

Figure 4.5 Semimajor axis evolution with only SRP perturbing effects

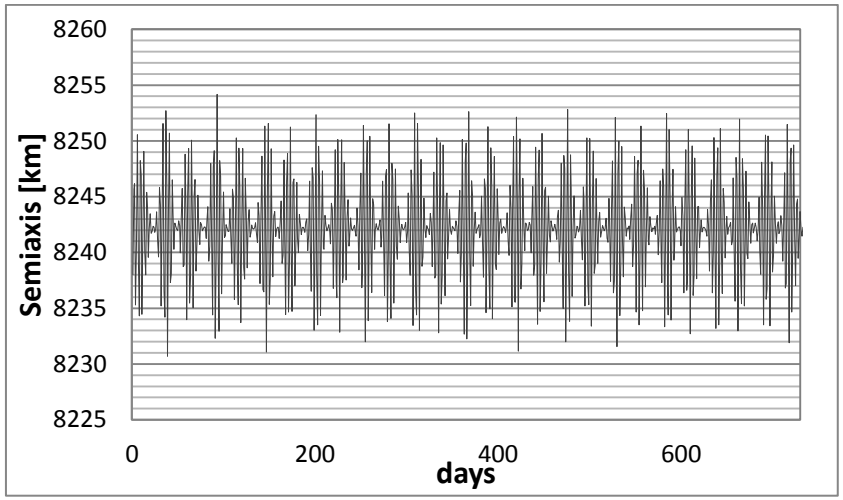

Figure 4.6 Semimajor axis evolution with only third body-perturbation effects

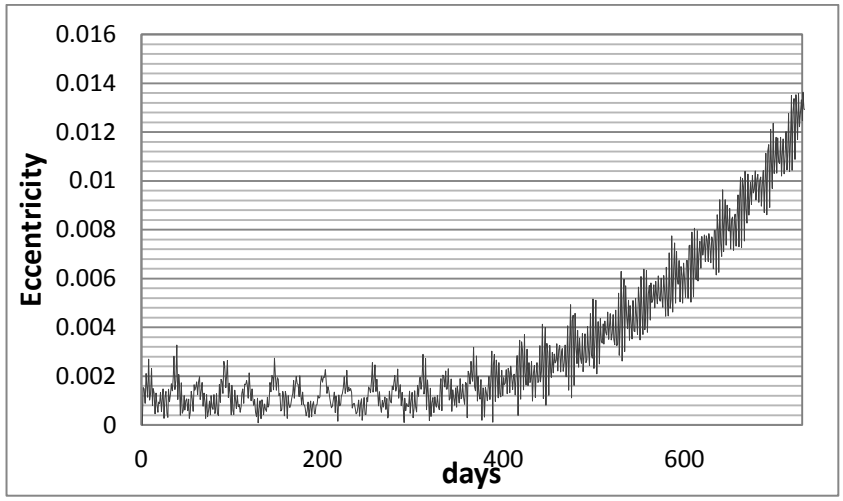

Figure 4.7 Eccentricity evolution with all perturbation effects

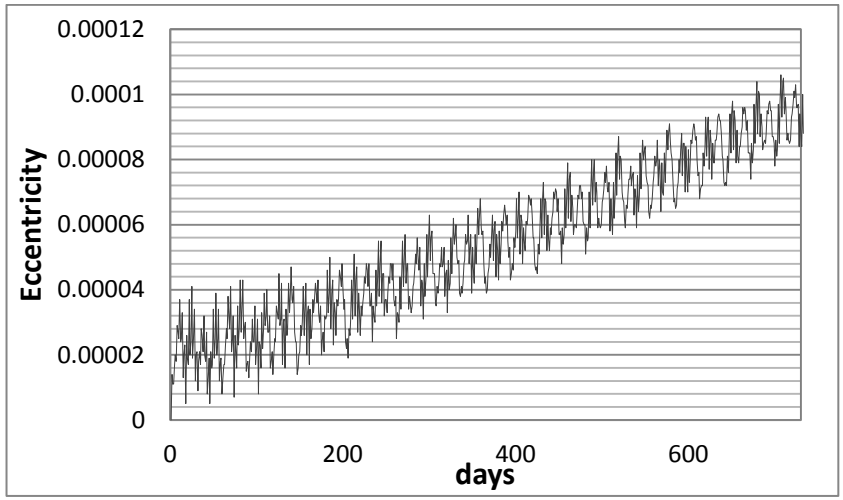

Figure 4.8 Eccentricity evolution with only central body gravity perturbing effects

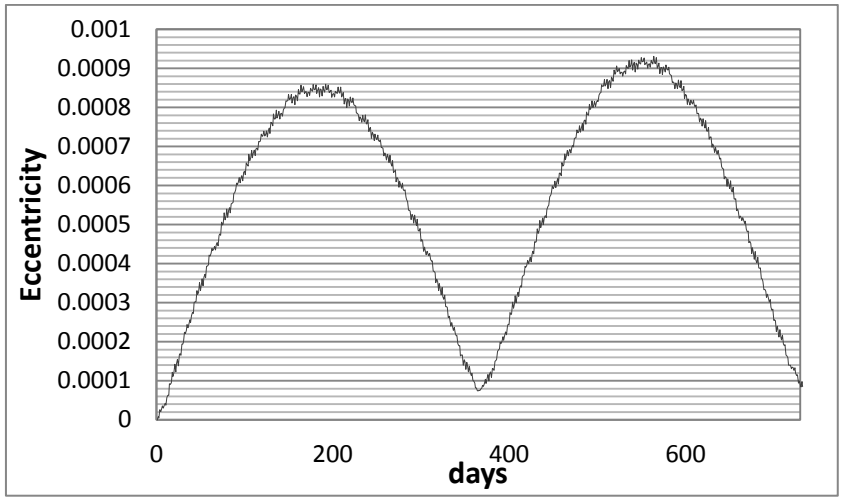

Figure 4.9 Eccentricity evolution with only SRP perturbing effects

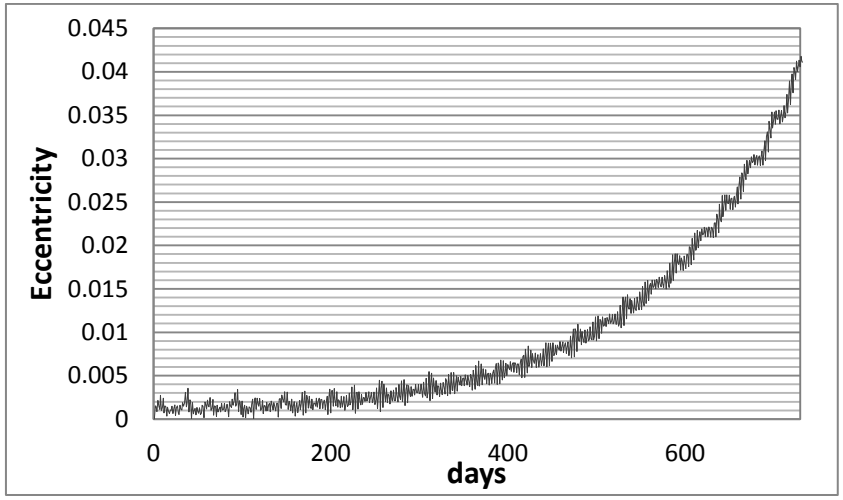

Figure 4.10 Eccentricity evolution with only third body-perturbation effects

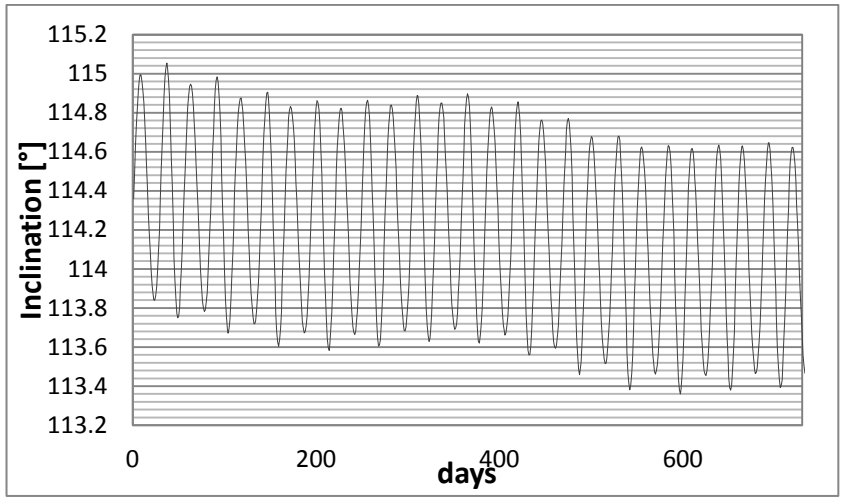

Figure 4.11 Inclination evolution with all perturbation effects

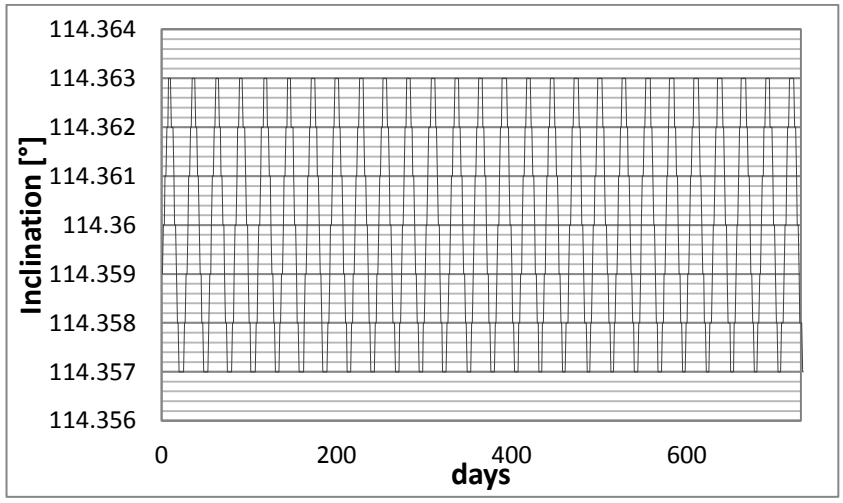

Figure 4.12 Inclination evolution with only central body gravity perturbing effects

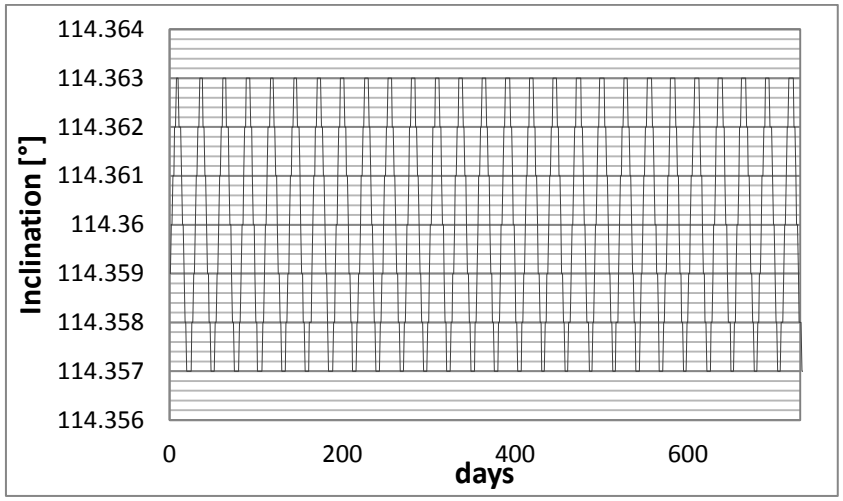

Figure 4.13 Inclination evolution with only SRP perturbing effects

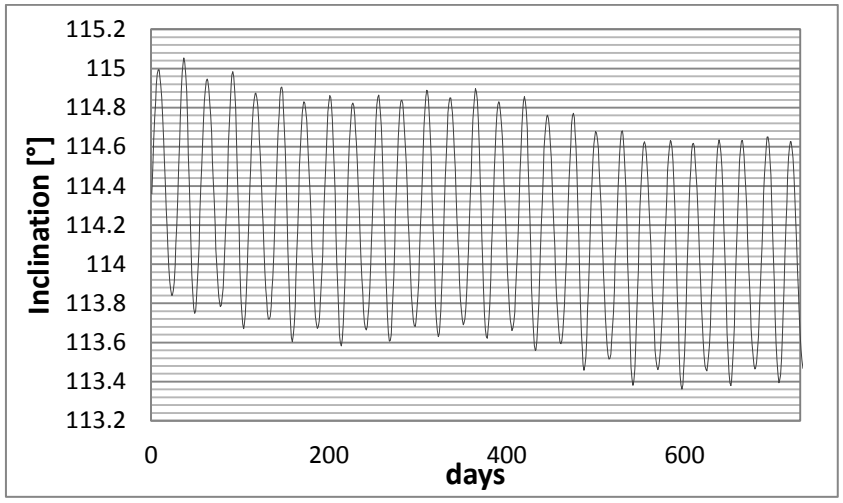

Figure 4.14 Inclination evolution with only third body-perturbation effects

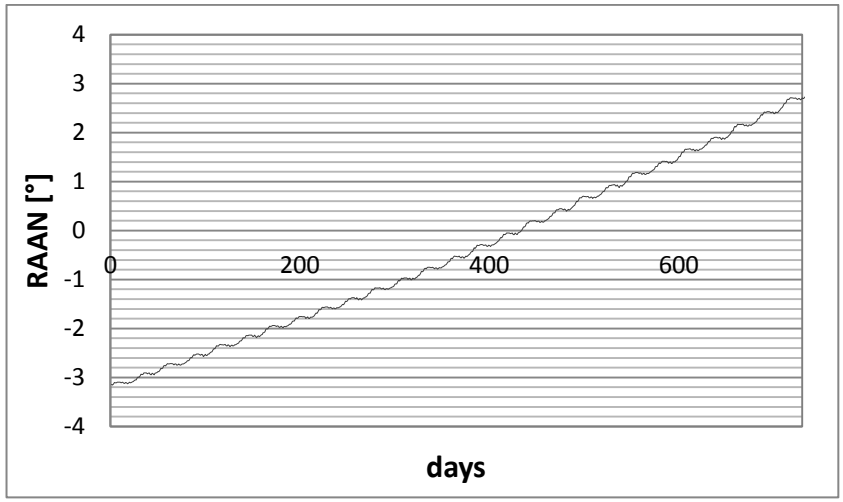

Figure 4.15 RAAN evolution with all perturbation effects

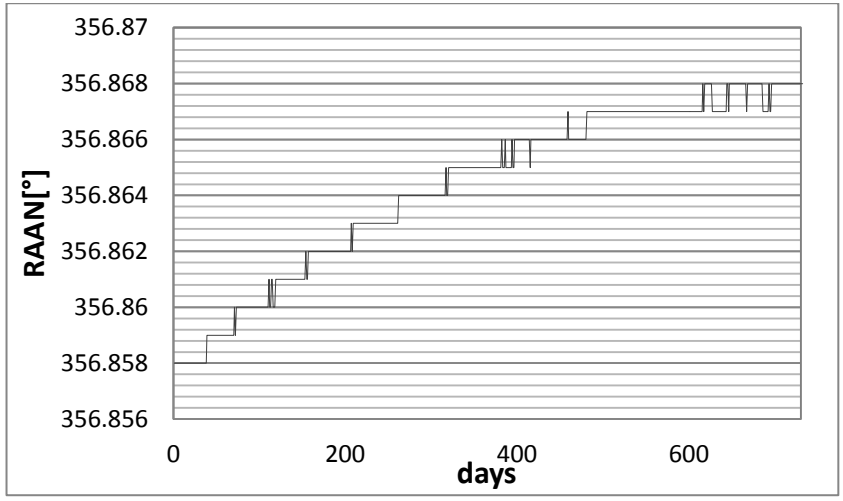

Figure 4.16 RAAN evolution with only central body gravity perturbing effects

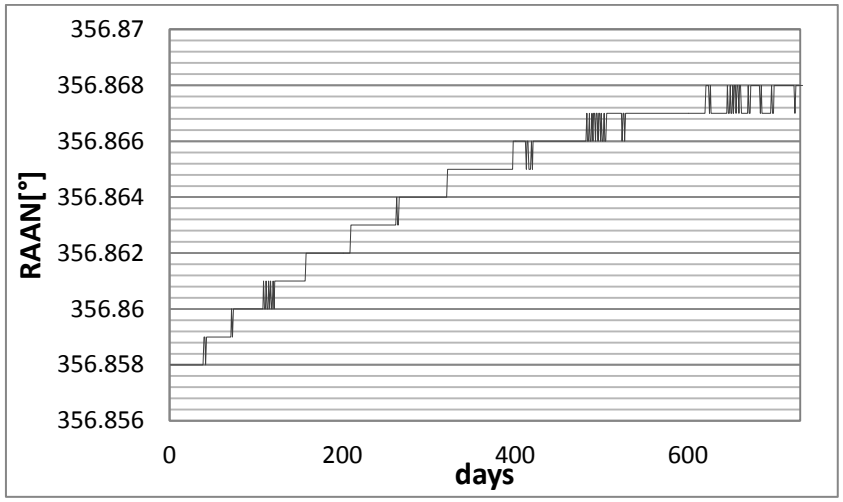

Figure 4.17 RAAN evolution with only SRP perturbing effects

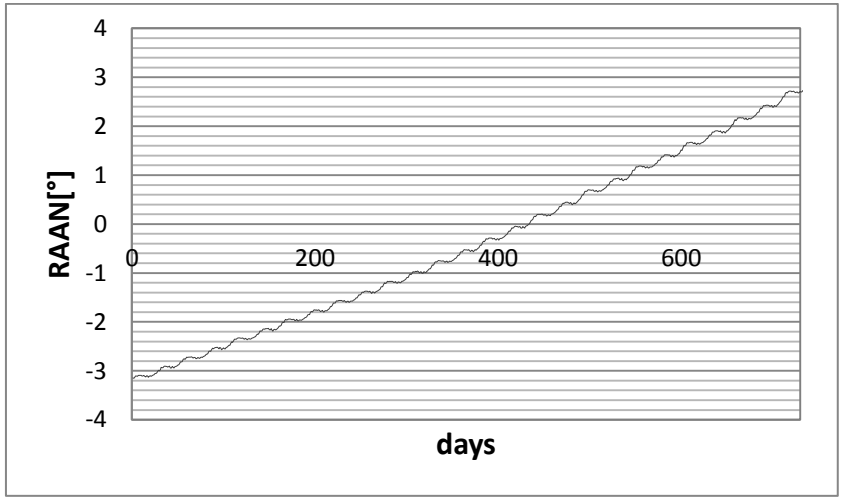

Figure 4.18 RAAN evolution with only third body-perturbation effects

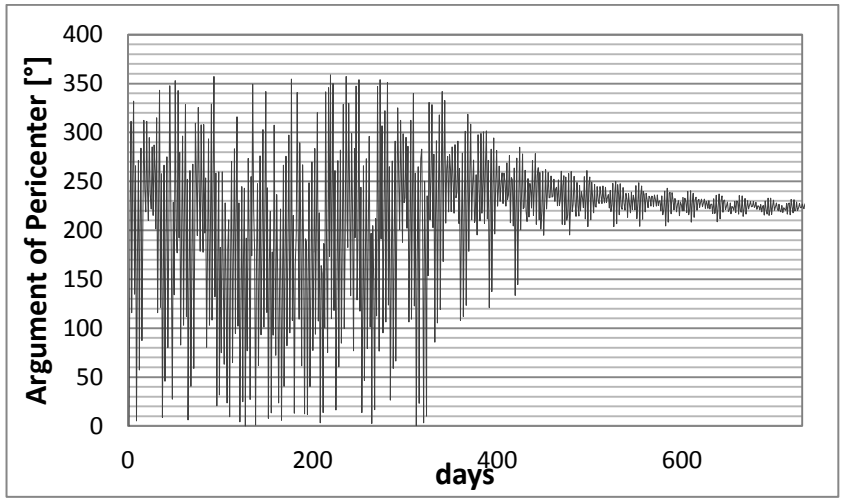

Figure 4.19 Argument of pericenter evolution with all perturbation effects

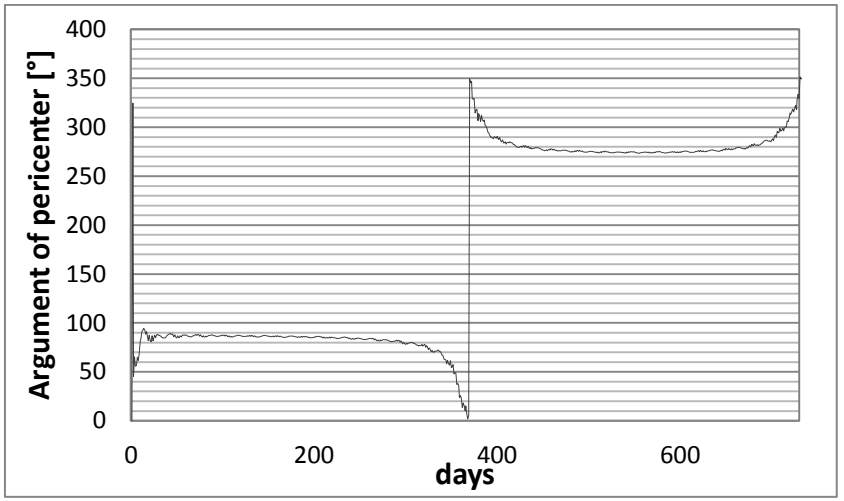

Figure 4.21 Argument of pericenter evolution with only SRP perturbing effects

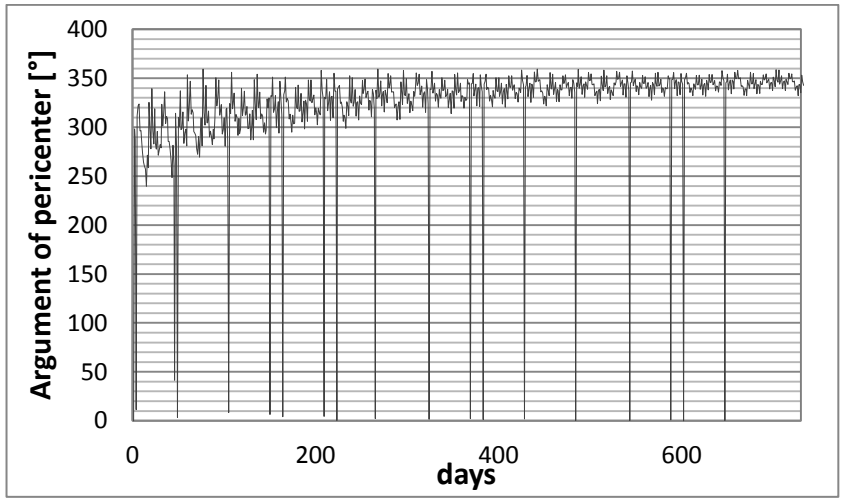

Figure 4.20 Argument of pericenter evolution with only central body gravity perturbing effects

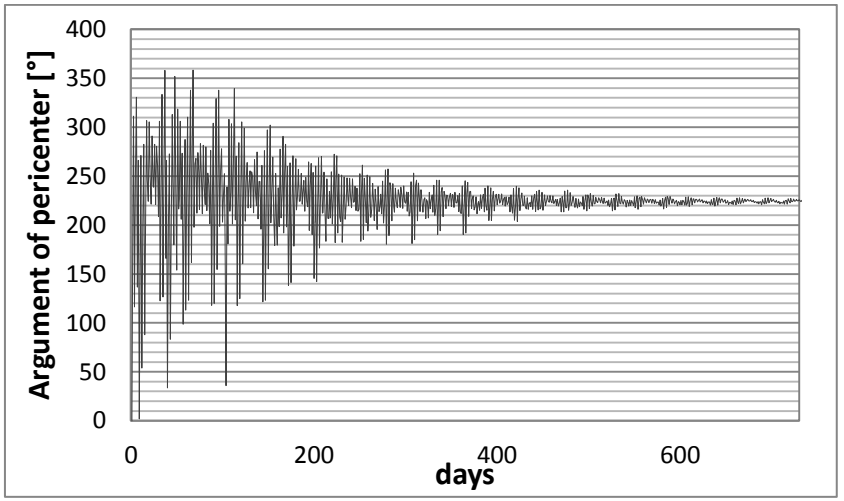

Figure 4.22 Argument of pericenter evolution with only third body-perturbation effects

The semimajor axis does not present a secular perturbation, it always maintains the same average value during the year. However, it does present a periodic fluctuation induced by the third body-perturbation, and its peak values oscillate between, approximately, 8230 km and 8250 km. Unlike the semimajor axis, the inclination and RAAN do present a secular behavior besides the periodic fluctuation. The degradation of the inclination during the year is less than one degree, whereas the RAAN varies by about six degrees. The eccentricity is the most affected orbital element; it remains stable for, approximately, half a year and then it increases quickly. Note that the argument of pericenter is only defined for elliptical orbits, therefore, in the figures it is meaningless when the eccentricity is zero or close to zero. In general, it can be observed that the main perturbing force is the third body-perturbation because it is the one that causes all the secular effects and whose variations are the highest.

Once the evolution of the orbital elements is known, a station-keeping strategy can be defined.

4.3. Station-keeping strategy

The moment when the satellite is inserted into orbit is very important for the achievement of the desired average semimajor axis value. In the case of the orbit plane with RAAN=0° (case represented above), it can be observed that the average value of the semimajor axis is not the desired one; instead of being 8238 km it is 8242 km. This deviation is caused by third body-perturbation. At the starting time of the propagation, the satellite is inserted in the orbit during third body-excitation which results in the deviation of the average value. In order to obtain an average value around 8238 km, it is necessary to correct the orbit in a point where the value of the satellite semimajor axis is equal or close enough to the average value. Once this is done, the average value of the semimajor axis will stay close to the design value (circular orbit).

This deviation also happens in the orbit plane with RAAN=120° but it does not happen in the orbit plane with RAAN=240°; in this case the average value of the semimajor axis is close to 8238 km.

The maneuver used to correct the semimajor axis is built on an impulsive velocity variation *Δv* given by

$$\Delta v^2 = v_1^2 + v_2^2 - 2v_1 v_2 \cos\varphi, \tag{4.24}$$

where v_1 is the velocity in the orbit point where the impulsive maneuver is applied and v_2 is the velocity of the design circular orbit. r_1 and r_2 represented in Eq. 4.25 and Eq. 4.26 are the position in the orbit point where the impulsive maneuver is applied and the circular radius value (8238 km), respectively. Velocity values are compute as

$$v_1 = \sqrt{2\left(\frac{\mu_{Moon}}{r_1} - \frac{\mu_{Moon}}{2a_1}\right)} \; with \; r_1 = \frac{a_1(1-e_1^2)}{1+e_1 cos\theta_1}, \tag{4.25}$$

$$v_2 = \sqrt{\frac{\mu_{Moon}}{r_2}}, \tag{4.26}$$

and

$$\varphi = \gamma_1 - \gamma_2, \tag{4.27}$$

$$\tan\gamma_i = \frac{e_i r_i \sin\theta_i}{a_i(1-e_i^2)} \; with \; i = 1,2. \tag{4.28}$$

φ is the angle between both velocities and γ_1 and γ_2 are represented in Figures 4.23 and 4.24.

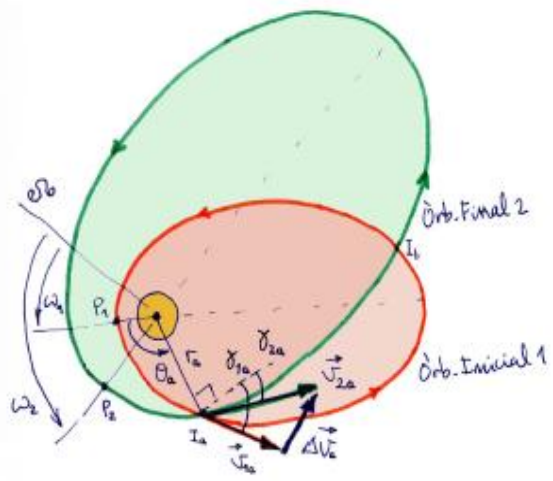

Figure 4.23 Orbit change maneuver diagram. Calaf, Jaume, "Astrodynamic's lecture notes", October 2011

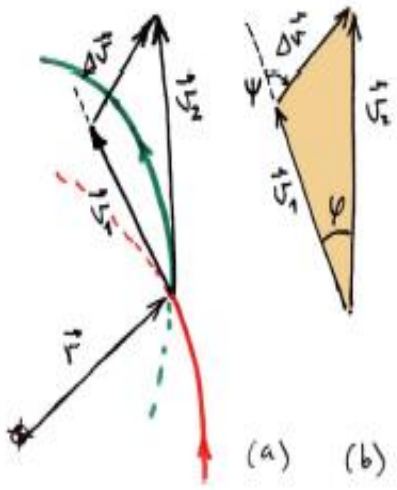

Figure 4.24 Representation of angle $\boldsymbol{\varphi}$**.** Calaf, Jaume, "Astrodynamic's lecture notes", October 2011

a_1, e_1 and $\theta_1$are the values of semimajor axis, the eccentricity and the true anomaly in the point of application of the maneuver.

Table 4.3 shows the values used during the maneuver and Table 4.4 shows the results of each maneuver.

Orbit plane *(Values in J2000 frame)*	**Date**	**a_1 [km]**	**e_1**	**θ_1 [°]**
RAAN=0°	29 March 2012	8242.2746	0.001485	338.667
RAAN=120°	24 March 2012	8232.6292	0.000995	143.794

Table 4.3 Orbit parameters during semimajor axis correction maneuver

Orbit plane	**Δv**
RAAN=0°	0.9720 m/s
RAAN=120°	0.5896 m/s

Table 4.4 Semimajor axis correction maneuver results

After correcting the semimajor axis average value, a station-keeping strategy has to be decided. The maneuver has to be applied when the satellites have a semimajor axis value near the average one (without third body-excitation) just as before. In order to maintain a circular and polar orbit a combined maneuver is selected. Furthermore, the maneuver is repeated every six months because this is the time interval over which the eccentricity does not increase appreciably, the variation in the RAAN is, at most, around three degrees and the inclination deviation is less than one degree.

By defining a new φ (see Figure 4.25) and using Eqs. 4.24, 4.25 and 4.26 it is possible to compute the impulse needed in each case. The new value of φ is:

$$\cos\varphi = \cos i_1 \cos i_2 + \sin i_1 \sin i_2 \cos\Delta\Omega. \tag{4.29}$$

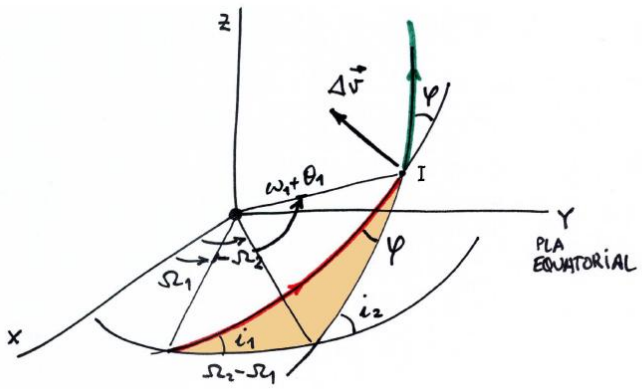

Figure 4.25 Representation of the new φ. Calaf, Jaume, "Astrodynamic's lecture notes", October 2011

Table 4.5 shows the orbital elements used in the computation of the maneuver and Table 4.6 show the resulting impulse needed in each case.

Orbit plane ***(J2000 frame)***	**Date**	**a_1 [km]**	**e_1**	**θ_1 [°]**	**i_1**	**i_2**	**$\Delta\Omega$**
RAAN=0°	20 Sep 2012	8238.1862	0.009727	275.832	114.359	114.367	3.041
RAAN=120°	18 Sep 2012	8237.9766	0.005563	292.205	78.099	77.593	1.476
RAAN=240°	10 Sep 2012	8238.04476	0.005248	200.692	78.099	77.133	3.560

Table 4.5 Orbit parameters during station-keeping maneuver

Orbit plane	**Δv**
RAAN=0°	37.6923 m/s
RAAN=120°	20.8788 m/s
RAAN=240°	49.3372 m/s

Table 4.6 Station-keeping maneuver results

By assuming a mission lifetime of 10 years and knowing that two maneuvers will be needed each year, we can find the total Δv budget of the mission (see Table 4.7).

Orbit plane	**Δv (Semimajor axis correction) [m/s]**	**Δv (Station-Keepting) [m/s]**	**$\Delta v_{per\ year}$ [m/s]**	**Δv_{TOTAL} [km/s]**
RAAN=0°	0.9720	37.6923	75.3845	0.754
RAAN=120°	0.5896	20.8788	41.7575	0.418
RAAN=240°	0	49.3372	98.6744	0.987

Table 4.7 Global **Δv** results

These results show that each orbital plane would need a different satellite design because of the difference in their Δv budget. However, designing three different satellites instead of a single one is very expensive so, in order to avoid it, the highest Δv value of the three orbital planes is chosen to design the single satellite. Oversizing is preferable to design three types of satellites. The final design Δv budget is 1 km/s. Figure 4.26 shows the final station-keeping process.

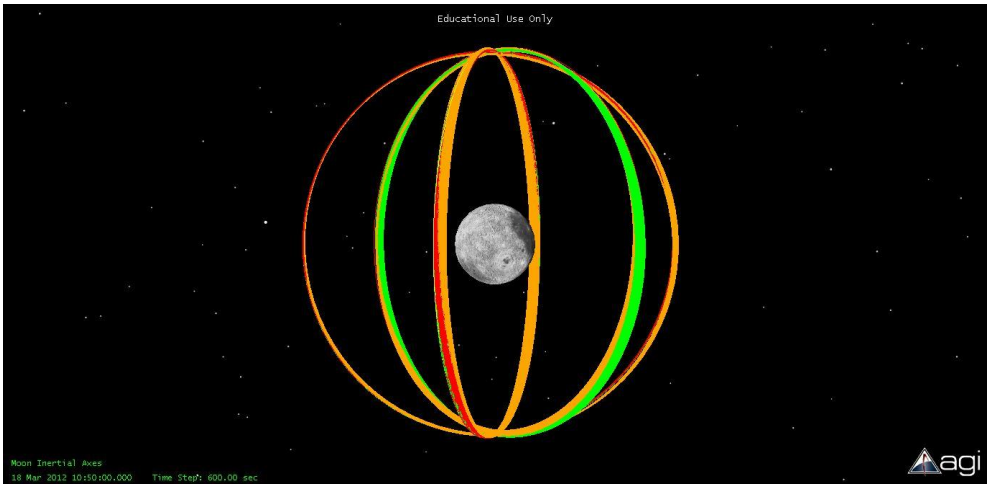

Figure 4.26 Final station-keeping representation

4.4. Space environment

Space systems design for lunar orbit requires analysis of potential system vulnerabilities to plasma and radiation environments to minimize anomalies and assure that environmental failures do not occur during the mission. In our case, the most important environmental hazards are galactic cosmic rays, solar energetic particles and plasma environment such as solar wind and Earth's magnetosheth and magnetotail interference.

Plasma and radiation environments that will be encountered during lunar missions begin with the outbound and inbound trajectories through the Earth's radiation belts. However, we are not going to deal with them, but we shall rather focus our attention on the relevant plasma and radiation environments that affect lunar orbit.

Reference for this section information and figures are [32], [33], [34], [35], [36] and [37].

4.4.1. Global Moon-plasma interaction

Contrary to the intuitive idea of the lunar environment as essentially static, the lunar surroundings are, in fact, very electrically active. The Moon has a minimal atmosphere and only localized weak crustal magnetic fields, leaving its surface essentially directly exposed to the impact of solar ultraviolet (UV) and X-rays as well as solar wind plasma and energetic particles. This creates a complex lunar electrodynamics' environment, with the surface typically charging positive in sunlight and negative in shadow to

potentials that vary over orders of magnitude in response to changing solar illumination and plasma conditions. Figure 4.27 represents the lunar environment and its three main plasma interactions: dayside interaction, lunar plasma wake and surface charging.

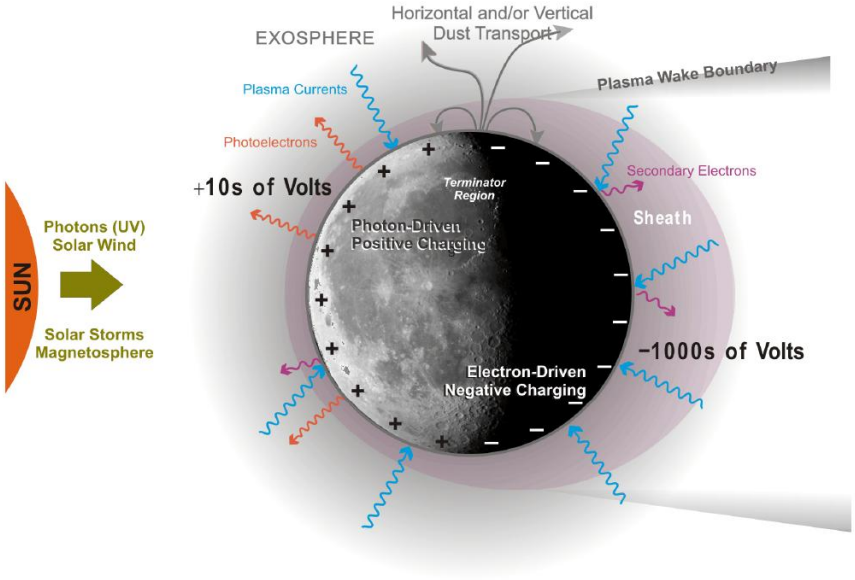

Figure 4.27 The Moon's electrodynamics' environment and its consequences: plasma wake, charged surface, etc.

4.4.1.1. Dayside interaction

Solar influences strongly drive the global Moon-plasma interaction, affecting the plasma environment directly and also influencing the surface and exosphere and their respective interfaces with plasma. To first order, solar wind interacts relatively weakly with the dayside lunar surface, with most ions impacting and implanting into the surface. However, between 10% and 20% of solar wind ions reflect from the surface with 0.1-1% of them remaining charged and the remainder gaining an electron to become energetic neutral atoms. Neutral hydrogen atoms have a long lifetime against photoionization and should not strongly interact with lunar environment, but the reflected protons may have interesting consequences, i.e., these reflected protons feel the force of the convective electric field and the interplanetary magnetic field and follow cycloidal pickup ion trajectories. In addition to the reflected solar wind protons, sputtering from the lunar surface and ionization of the neutral exosphere can produce heavier pickup ions. Therefore, the Moon provides not only a sink but also a source of plasma in the solar wind.

4.4.1.2. Lunar plasma wake

The Moon does not strongly affect the environment upstream from it. However, significant influences on the surrounding plasma unquestionably propagate to large distances downstream. The lunar wake forms because of the removal of solar wind ions and electrons at the dayside, through both absorption/implantation and scattering/reflection, resulting in a nearly complete plasma void immediately downstream from the nightside hemisphere of the Moon. However, as the supersonic solar wind flows past the Moon, solar wind plasma refills this void region.

4.4.1.3. Surface charging

Photoelectrons are generated when solar UV and extreme UV photons interact with the lunar surface. Since the photoelectron current is generally greater than the incident solar wind electron currents, the lunar surface will charge positively a few tens of volts in the dayside hemisphere. In contrast to the positive potential which the lunar surface charges in sunlight, the terminator and nightside regions of the Moon, which are not illuminated but still exposed to energetic electrons arriving from the distant tails and sunward flowing components of the solar wind, are charged to negative potentials between 10 to 100 V negative. Charging environments at night in lunar orbit may contain charging risks similar to geostationary orbit during extreme space weather events.

4.4.1.4. Earth's magnetotail interference

Plasma environments near the Moon are perturbed when the Moon passes through the Earth's magnetotail or a spacecraft passes behind the Moon. The effect of the Earth's magnetotail is demonstrated in Figure 4.28 where spin averaged electron flux records from the Lunar Prospector Electron Reflectometer instrument are shown. In Figure 4.28 (a) the complete month of April 1998 is shown including a depletion of low energy electrons by nearly two orders of magnitude near the middle of the month during the period the Moon is inside the Earth's magnetotail. Figure 4.28 (b) shows the detail of electron flux variations for 4 to 6 April 1998 while the Moon is in the solar wind showing plasma depletions in the lunar wake. In general, reductions in electron flux occur at all energies but are the greatest for the low energy electrons.

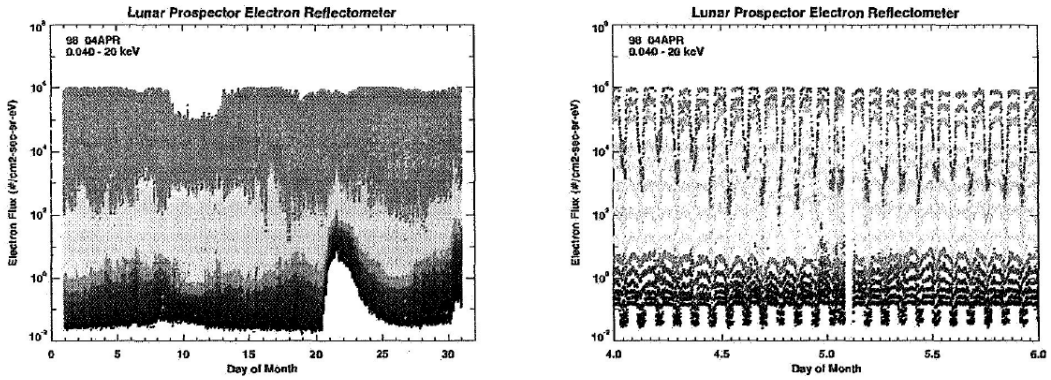

Figure 4.28 Lunar <20 keV Electron Environments

Charging environments in lunar orbit regularly produce negative potentials on the order of hundreds of volts suggesting that the most challenging charging environment for lunar exploration will be the dark side of the Moon. Spacecraft charging environment within the Earth's magnetosphere can be avoided using high inclination orbits, like in the LGSNS case, or mitigated with a good spacecraft design.

4.4.2. Lunar dusty exosphere

The lunar surface is composed of rocks and regolith, where regolith is a soil-like layer above the bedrock which has been generated by small meteoritic impacts. The regolith particles range in size from centimetre to submicron scales; the smaller particles are often referred to as lunar dust. The lunar surface, as described before, is electrostatically charged by the Moon's large-scale interaction with the local plasma environment and the photoemission of electrons due to solar UV light and X-rays. The charged surface and dust grains then act to repel each other and, under certain conditions, the dust grains are lifted above the surface. Figure 4.29 illustrates how dust is lifted from the lunar surface.

Nowadays, dust lifting is described by a dynamic "fountain" model which can explain how submicron dust is able to reach altitudes up to 100 km above the lunar surface. In this model, once the dust grain has attained sufficient charge (electrostatic force, F_q) to overcome lunar gravity (F_g) and any cohesive forces (F_c), it leaves the lunar surface. It is subsequently accelerated upward through a sheath region with a height of order the plasma Debye length, λ_D.

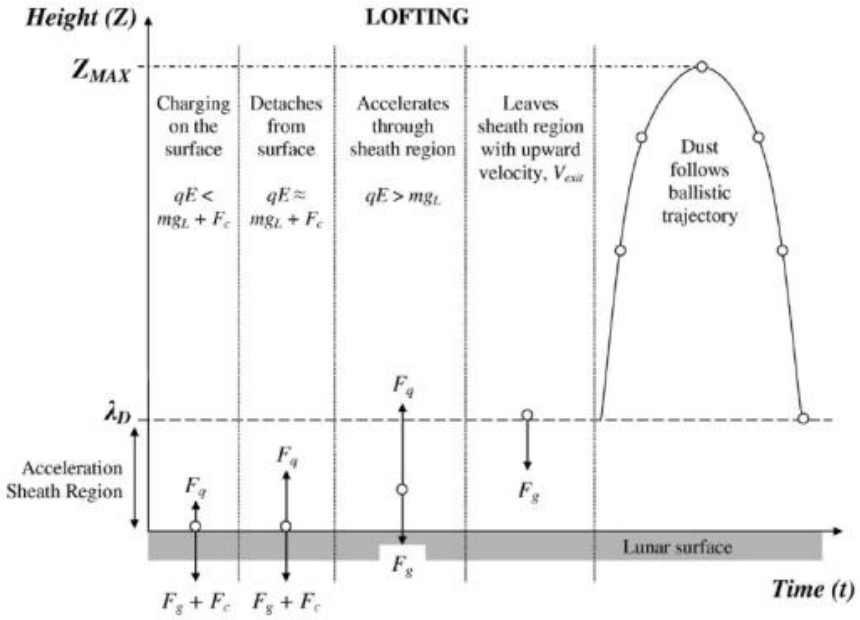

Figure 4.29 Evolution of a dust grain in a dynamic fountain model

As the dust grain is so small, the gravitational force acting on it is almost negligible in comparison with the initial electrostatic acceleration. The dust grain leaves the sheath region with an upward velocity and follows a near-parabolic trajectory back toward the lunar surface since the main force acting on it now is gravity. After leaving the sheath region, a dust grain follows a ballistic trajectory to a maximum height above the lunar surface, z_{max}.

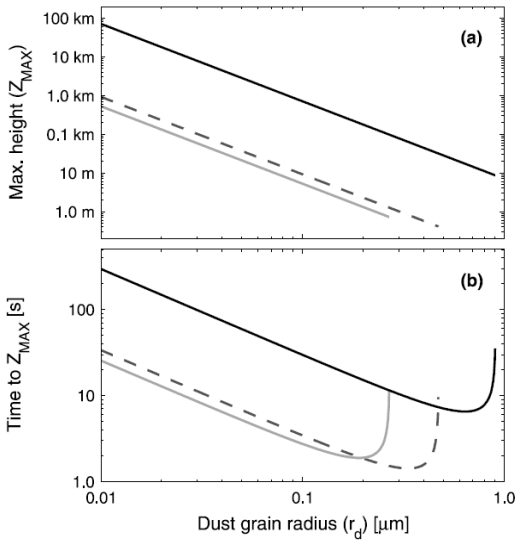

Figure 4.30 Predictions of (a) z_{max} and (b) the time taken to reach it as a function of r_d, as predicted at the subsolar point (dashed-lines), in an intermediate region (grey) and at the terminator (black)

Figure 4.30 shows the maximum height z_{max} and the time taken to reach it as a function of the grain radii, r_d. As it can be seen, the maximum height is 100 km which mean dust will not be a problem for the LGSNS.

If grain cohesion at the surface is neglected, then the criteria for grain lofting can be given in terms of a maximum grain radius that can be lofted, r_{max}. Dust grains with radii that exceed r_{max} will either be levitated (F_q=F_g, Figure 4.31) or will remain on the surface.

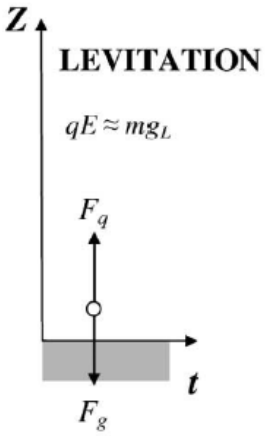

Figure 4.31 The static levitation concept, as suggested by Criswell (1973)

4.4.3. Radiation environment

Galactic cosmic rays (GCR) are electrons and ions accelerated to extremely high energies in astrophysical processes outside of the Solar System. The GCR energy spectrum, both in terms of intensity and particle energy, is reduced as the particles penetrate into the heliosphere due to scattering by irregularities in the interplanetary magnetic field. Because the magnetic field irregularities are solar cycle dependent with enhanced irregularities occurring during solar maximum, the GCR flux spectra exhibits a solar cycle modulation, GCR flux varies over a factor of approximately 2.5 from solar minimum to solar maximum with the greatest GCR flux observed at solar minimum. Flux variations are shown in Figure 4.32.

Because GCR are charged particles, their paths are affected by the magnetic fields along their trajectories. The Moon spends 15% of its orbit in the Earth's magnetosphere therefore it is relevant to consider whether GCR access to the Moon is influenced by the GCR's passage through the magnetotail as opposed to the interplanetary environment. When particles are going through regions of different magnetic strength and direction, their path will be bent and deflected due to the Lorentz force. However, simulation

proves that the Earth's magnetosphere does not substantially modify GCR at the lunar environment during typical solar wind conditions.

While cosmic ray fluence is not generally considered a significant source for ionizing dose in materials compared to the much larger particle fluence accumulated during solar energetic particle events, the GCR heavy ion component are a significant source of energetic ions producing single event effects in electronic systems due to the penetrating nature of the radiation.

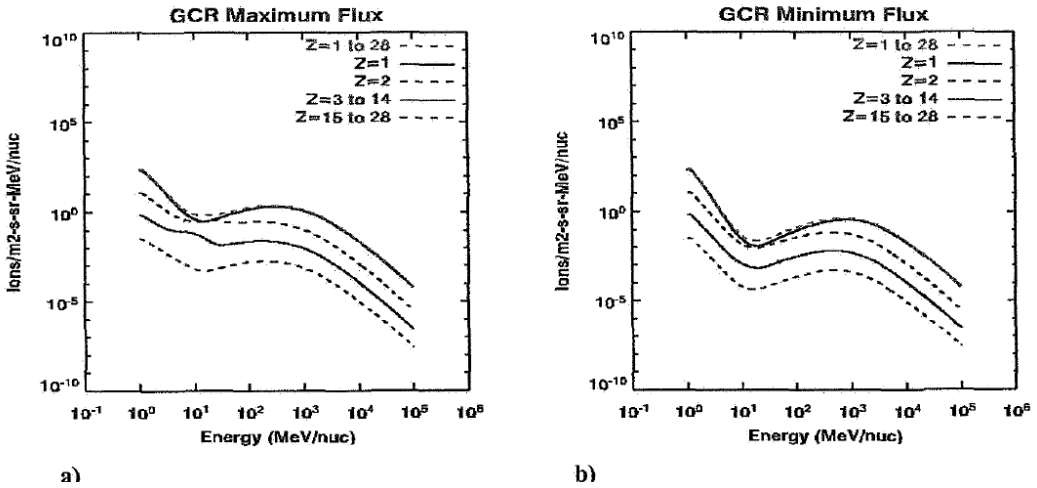

Figure 4.32 (a) Solar minimum conditions provide the maximum GCR flux while (b) solar maximum conditions yield a minimum GCR flux

The most intense solar energetic particle (SEP) events are produced by ion acceleration at the expanding shock front of coronal mass ejections and are the source of the most intense energetic radiation environments in interplanetary space. SEP events occur sporadically with the greatest probability in the years of solar maximum and for the first few years after the peak of solar activity. Individual events may last more than a week in extreme cases, but the effects typically last hours to days. Predicting individual SEP events is difficult, but it can be assumed that missions active over a solar cycle or longer will encounter a number of events during solar maximum and at least one large SEP per solar cycle. Engineering design for materials exposed to SEP radiation environments generally require qualifying material properties to remain within specified end of life values for at least one large SEP per solar cycle. Figure 4.33 shows the one year lunar surface radiation environment derived from the solar energetic ion fluence provided by the CREME96 Worst-Week Model flux over a 7.5 day period with a one year GCR fluence contribution (solar maximum).

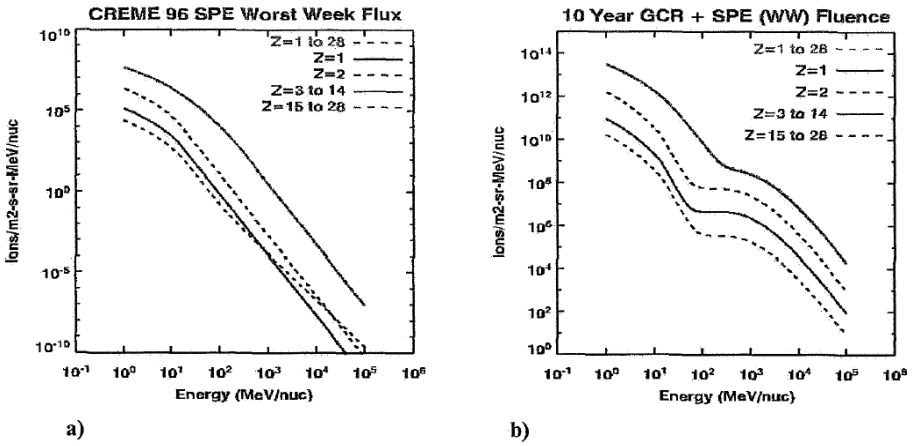

Figure 4.33 Solar energetic particles and 10 year fluence environment

The radiation environments in lunar orbits are not particularly challenging compared to those regularly encountered when designing spacecraft for long term use in geostationary orbit, geostationary transfer orbit, medium Earth orbit, or other orbits within the Earth's magnetosphere which regularly encounter the trapped flux within the Earth's magnetic field.

4.5. Eclipses

In this part of *Chapter four*, we report the results of the eclipse analysis carried out for a satellite on each plane of the final selected constellation for the LGSNS. The goal is to formulate a set of requirements for the power and thermal subsystems and to identify potential critical design issues.

As already said, the orbit has an altitude of 6500 km corresponding to a period of 67095 seconds (18.63 hours). The simulation begins on March 18th 2012 and ends on March 19th 2013, so day 1 on our simulation does not represent the 1st of January. Eclipses results are show in Figures 4.34, 4.35 and 4.36.

Figure 4.34 represent the daily duration and distribution of the eclipses during the simulation period. It has been obtained from the STK report data. The STK report data provides a lot of information: it indicates if the satellite is in penumbra or in umbra, it identifies the celestial body which is causing the eclipse (in our case the Moon or the Earth) and it contains the duration of each eclipse both under real condition and worst case condition. In the worst case condition the satellite is considered in umbra all its eclipse time, penumbra time is not distinguished which means that the umbra time is

higher than the real value. In real condition case, the software distinguish between penumbra and umbra and each one has its own duration. Figure 4.34 shows the eclipse duration for the worst case condition.

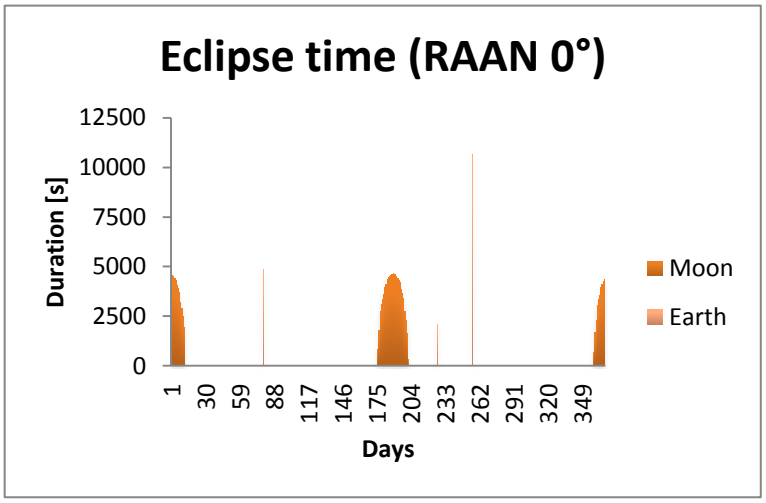

Figure 4.34 Eclipses results for orbit with RAAN=0°

Table 4.8 indicates the days when the lunar eclipses take place, their duration and the peak value of the eclipse period. Table 4.9 indicates the days when the Earth is between the satellite and the Sun and the duration of the corresponding eclipse.

Moon

Date	Duration [Days]	Peak value [s]
Mar 18th – Mar 29th (2012)	12	4597.693
Sep 9th – Oct 5th (2012)	26	4637.276
Mar 10th – Mar 19th (2013)	10	4335.76

Table 4.8 Lunar eclipses data for RAAN=0°

Earth

Date	Duration [s]
Jun 1st (2012)	4854.26
Oct 29th (2012)	2106.232
Nov 28th (2012)	10639.691

Table 4.9 Earth eclipses data for RAAN=0°

Equivalent figures (Figure 4.35 and 4.36) and tables (Tables 4.10, 4.11, 4.12 and 4.13) have been obtained for the other two planes.

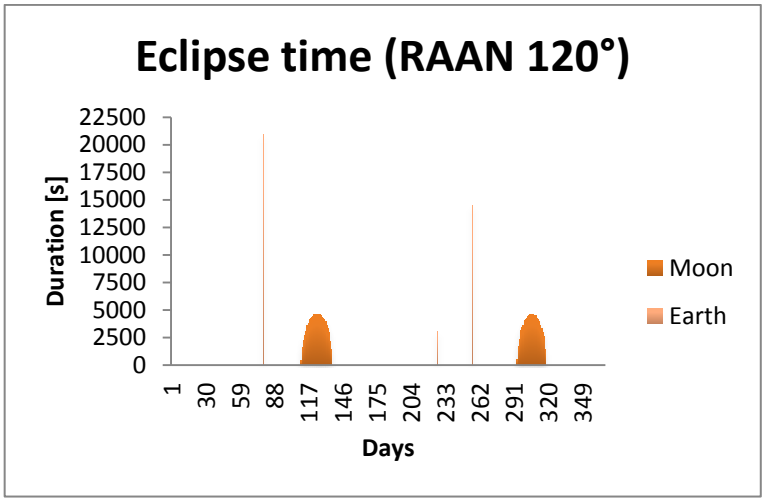

Figure 4.35 Eclipses results for orbit with RAAN=120°

Moon

Date	Duration [Days]	Peak value [s]
Jul 6th – Aug 1st (2012)	26	4630.177
Jan 5th – Jan 29th (2013)	24	4561.872

Table 4.10 Lunar eclipses data for RAAN=120°

Earth

Date	Duration [s]
Jun 4th (2012)	20907.991
Oct 29th (2012)	3059.81
Nov 28th (2012)	14482.947

Table 4.11 Earth eclipses data for RAAN=120°

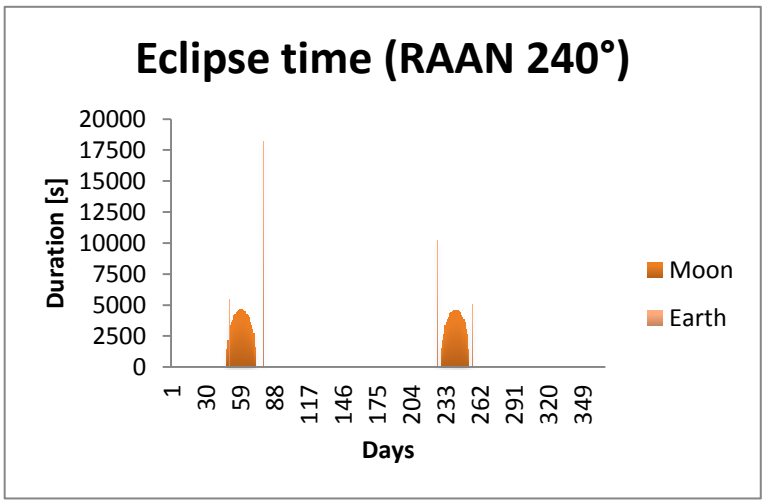

Figure 4.36 Eclipses results for orbit with RAAN=240°

Moon

Date	Duration [Days]	Peak value [s]
May 4th – May 28th (2012)	24	4632.926
Nov 2nd – Nov 25th (2012)	23	4594.836

Table 4.12 Lunar eclipses data for RAAN=240°

Earth

Date	Duration [s]
May 6th (2012)	5480.448
Jun 4th (2012)	18179.877
Oct 29th (2012)	10198.741
Nov 28th (2012)	5061.869

Table 4.13 Earth eclipses data for RAAN=240°

After observing all the data from the eclipses we can state some conclusions. The Moon and the Earth orbits around the Sun are both almost on the ecliptic plane (there is a different of approximately 5° between Moon's orbit and the ecliptic plane) with make eclipse periods for a satellite orbiting around the Moon or around the Earth very similar. In this case, our results are similar to the GPS eclipse periods. It is similar because there is a geometric similarity between both planet-orbit configuration; as the GPS is in a MEO orbit, our constellation is in a MMO.

The peak duration of the eclipses is approximately 1.3 hours. The orbit period is 18.63 hours so there is only one eclipse per day during the eclipse epoch but the exact time of occurrence varies from day to day.

There are two different eclipse epochs because the Sun lies in the orbital plane twice a year. This is easily understood when the Sun motion along the ecliptic is observed. The Sun aligns progressively and begins generating shadows zones over the orbit, until the alignment is maximum and the eclipses reach their maximum duration. Figure 4.37 shows the varying position of the Sun relative to the orbital plane.

Batteries will have to be able to provide the power needed in this period during both lunar eclipse epochs. These have the same peak value because the orbit is circular but, as it can be seen in the figures, eclipse epochs change dates depending on the RAAN.

As it happens with Earth orbits, the orbit's RAAN on a lunar orbit will be the main design driver in the eclipse epochs because it fixes the orbital plane which determines when the solar rays are aligned with it. Depending on the Sun's positions, durations and season periods can be affected.

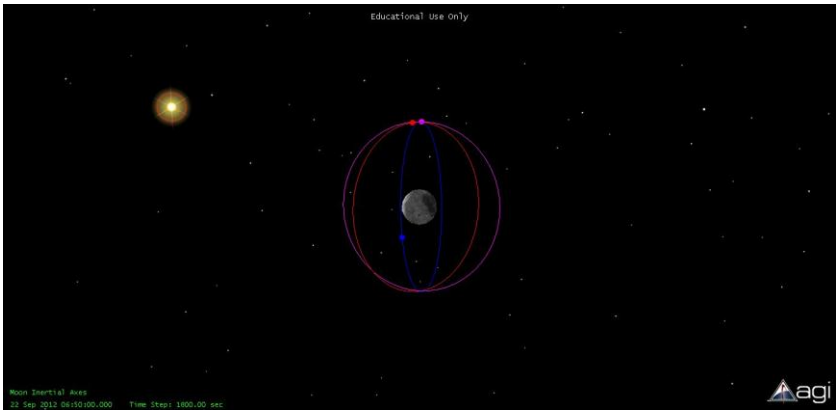

Figure 4.37 Relative position between orbital plane and the Sun: Lunar eclipse

Earth eclipses will need to be treated separately because they represent a peak on the batteries operation and their power. Earth eclipses are longer because of the Earth is bigger. They last between 5000 and 20000 seconds and they happen on separated days during the year. The periods of time when these eclipses happen are approximately the same in the three different orbital planes (beginning of June, end of October and end of November). It is this way because the eclipses happen when the Earth goes between the Moon and the Sun which has nothing to do with the relative position of every orbital plane. Figure 4.38 shows the position of the three bodies involved in the eclipses (Moon, Earth and Sun).

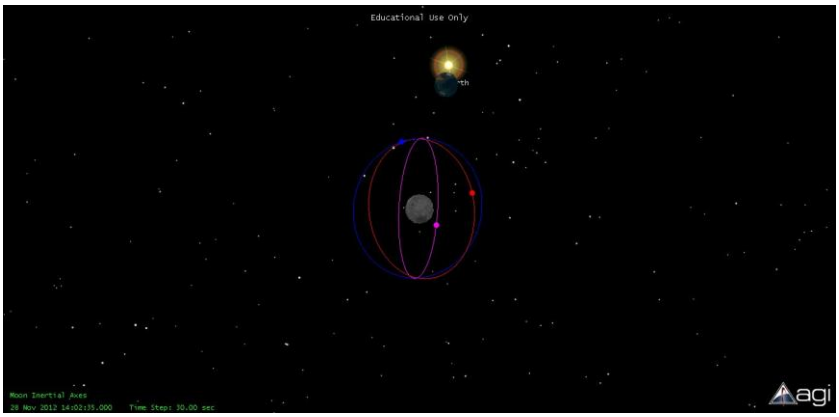

Figure 4.38 Relative position between orbital plane, the Earth and the Sun: Earth eclipse

Chapter five.

Payload design

In this chapter we are going to deal with the payload characterization. Its mass, required power and thermal limits are going to be discussed. Because the main component of a navigation payload is its atomic clocks a study about the relativistic effects on time is mandatory hence, it also is going to be held.

5.1. Payload characterization

Payload characteristics and needs are, along with the orbit, the main source of requirements and constraints during the design of a spacecraft. After all, the payload is the reason why the whole mission is being designed; the goal of every space mission is that its payload completes the task for which it was built. The rest of subsystems (structure, thermal control, power supply, etc.) must allocate, protect from the space environment and maintain the payload within the operational values of all the relevant parameters (among which power and temperature). So, predicting the payload mass, the power needed to make it work and its thermal tolerance, along with its general shape, is mandatory to begin any speculations on the spacecraft.

In our case, we are dealing with a GNSS so historical data from past and current similar satellite constellations is going to be used to estimate the specifications of our payload.

5.1.1. Payload's mass

Although we are not going to deal with launches, an estimated mass from the navigation payload is required. Table 5.1 shows a comparison between current different GNSS spacecraft in terms of mass.

Our spacecraft is assumed to have a mass of 1000 kg. Payload's mass ranges between 10% and 30% of the dry satellite mass[1]. For our purposes, we choose 25%.

Spacecraft	Satellite mass [kg]	Payload mass [kg]	% of payload mass
Glonass	1415	180	12.7
Glonass M	1570	250	25.9
Glonass K	935	260	27.8
Galileo	680	130	19.1
GPS block I	509	104	20.4
GPS block II	918	185	20.2

Table 5.1 Historical mass data from current GNSS

5.1.2. Payload's power

As in the case of the mass, a comparison between current GNSS satellites power characteristics is presented in Table 5.2.

Spacecraft	Onboard power supply [W]	Payload consumption [W]	% of payload consumption
Glonass	1000	600	60.0
Glonass M	1450	580	40.0
Glonass K	1270	750	59.1
Galileo	1600	900	56.3
GPS	1100	-	-

Table 5.2 Historical power data from current GNSS

Once the satellite is in its operational orbit, the order of magnitude of the onboard power for a GNSS satellite is, at least, 1000 W. Any power supply capable of providing more power than this will fulfil the mission objectives. A typical navigation payload consumes between 600 to 900 W; the highest values of power consumption are those of Galileo and Glonass K satellites, which are the newest GNSS systems and, therefore, the more complex. Besides, the use of inter-satellite link (ISL) payload increases, even more, the complexity of the spacecraft (mass, power consumption) and thus, its cost.

ILS consists of a radio signal travelling from one satellite to another. With this radio signal, the distance between the two spacecraft can be derived and, their state vectors found. These measurements cannot be used alone, they need a ground reference. The ISL provides an observation with a completely different geometry from those of the ground referenced links, which is an advantage, especially for satellites in higher orbits. An ISL between satellites results in a much better observability of the tangential orbit

errors and hence, the decorrelation of the clock error and the radial orbit error is enhanced and shortened. Another benefit from ISL is the improvement in satellite tracking capability for satellites in low orbit[38]. The ISL also allows to perform an AutoNav function. AutoNav synchronizes constellations clocks by processing inter-satellite pseudoranges and exchanged state vectors in their Kalman filters[39].

In the LGSNS, an ISL payload can be possibly necessary, so power needs should range between about 700 and 900 W. However, a trade-off between the benefits in accuracy and observability and the overall system complexity must be done in a further stage of the design. In this preliminary approach, we assume a payload power consumption of 60% of the total supply.

5.1.3. Payload's thermal limits

Spacecraft equipment is generally devised to operate within the thermal limits presented in Table 5.3.

Component	Typical Temperature Ranges (°C)	
	Operational	Survival
Batteries	0 to 15	-10 to 25
Power box baseplates	-10 to 50	-20 to 60
Reaction wheels	-10 to 40	-20 to 50
Gyros/IMUs	0 to 40	-10 to 50
Star Trackers	0 to 30	-10 to 40
C&DH box baseplates	-20 to 60	-40 to 75
Hydrazine tank and lines	15 to 40	5 to 50
Antenna gimbals	-40 to 80	-50 to 90
Antennas	-100 to 100	-120 to 120
Solar panels	-150 to 110	-200 to 130

Table 5.3 Thermal limits from different spacecraft components[1]

Besides, the payload for navigation involves precise atomic clocks. It is interesting to know their operating temperature ranges, since they are essential for the mission and, at the same time, they are relatively uncommon components.

These data are available in their specifications sheets[40], [41], [42], [44]:

- Active hydrogen masers operate from 5 to 35 °C.

- Passive hydrogen masers operate from 5 to 40 °C.
- Rubidium clocks work in the -25-65 °C range.
- Cesium clocks work in the 0-50 °C range.

5.1.4. Payload's components

A navigation payload is composed of different units:

- a clock unit which is composed of atomic clocks,
- a signal generation unit which generates the navigation signal,
- a frequency generation unit which permits to upconvert the signal to the L-band, and
- an amplifier unit

The overall performance of the navigation payload is dependent on the performance of the onboard clocks. Better stability leads directly to improved space segment autonomy and simplified ground segment operation. Figures 5.1 and 5.2 are two examples of a navigation payload's configuration.

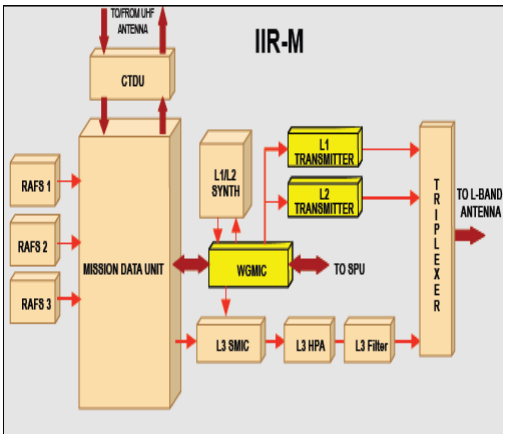

Figure 5.1 GPS payload's diagram[39]

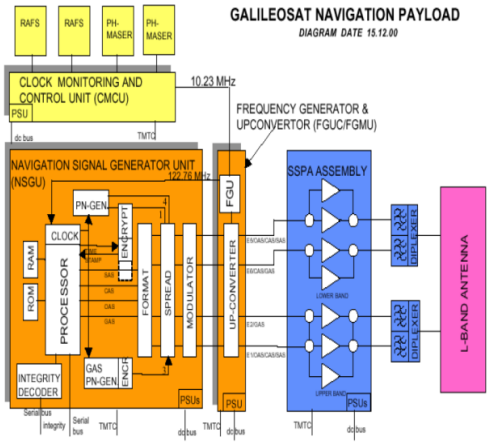

Figure 5.2 Galileo payload's diagram[45]

The navigation payload functions are[45]:

- reception and storage of up-linked Navigation Data,
- reception and decoding of integrity data,
- generation of PRN code and carrier frequencies,
- provision of precise timing data,
- prediction of ephemeris and clock parameters,
- error correction coding of messages,

- assembly of navigation messages to be transmitted and,
- broadcast of modulated navigation signals.

The atomic clocks are the heart of the navigation service. GPS relies on rubidium and cesium clocks whereas Galileo uses a combination of rubidium clocks and passive hydrogen masers. These clocks usually work in combination to feed a central computing unit, named Navigation Signal Generator Unit (NGSU in Galileo) or Mission Data Unit (MDU in GPS). This hardware is in charge of the payload operation.

The original candidate of the onboard master clock for Galileo was an active hydrogen maser (AHM). However, in the Galileo definition phase it became evident that the accomodation of an AHM on board was too penalizing in terms of mass and volume. Moreover, it was recognized that the excellent stability performances of the AHM were not required[46]. The difference between active and passive hydrogen masers is that in the AHM the microwave oscillation in the hydrogen filled cavity is self-sustained whereas in the passive ones, a microwave signal is injected into the cavity[43].

The rubidium clocks (Figure 5.3) are the most common “inexpensive” atomic clocks. They work by lighting a cell of dilute rubidium gas. The vapour is excited by a 6.8 GHz frequency microwaves which minimize the light transmission, and a photodetector senses the light out the cell and feedbacks the excitation frequency to maintain the minimal light transmission. The microwaves frequency is then used as clock stable reference. Its inaccuracy is 3 seconds per million years and they present short term stability but long-term drifts.

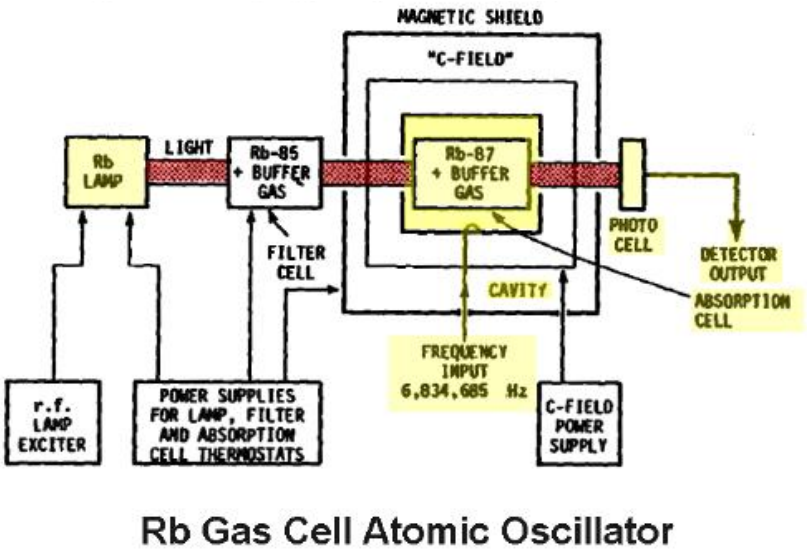

Figure 5.3 Rubidium clock diagram[43]

A better type of atomic clock is the cesium clock (Figure 5.4). The Cesium atom (Cs-133) is now used to define the second. The second is 9129631 periods of the radiation corresponding to the transition between two specific hyperfine levels of the ground energy state. They work by sending a cesium atoms beam into a cavity where these are irradiated at a certain microwave frequency (9.2 GHz). If the frequency is the correct one, the internal atom state changes and then, the atoms move through a strong magnet and are deflected by a precise quantity. This allows to precisely control the frequency of the irradiation and use it as time step. They present short term oscillations but a better long-term behaviour compared with the rubidium clocks. Cesium clocks lifetime is limited by its tube (where the atoms beam passed through). These limits are caused by contamination of Cesium atom detectors inside the tube.

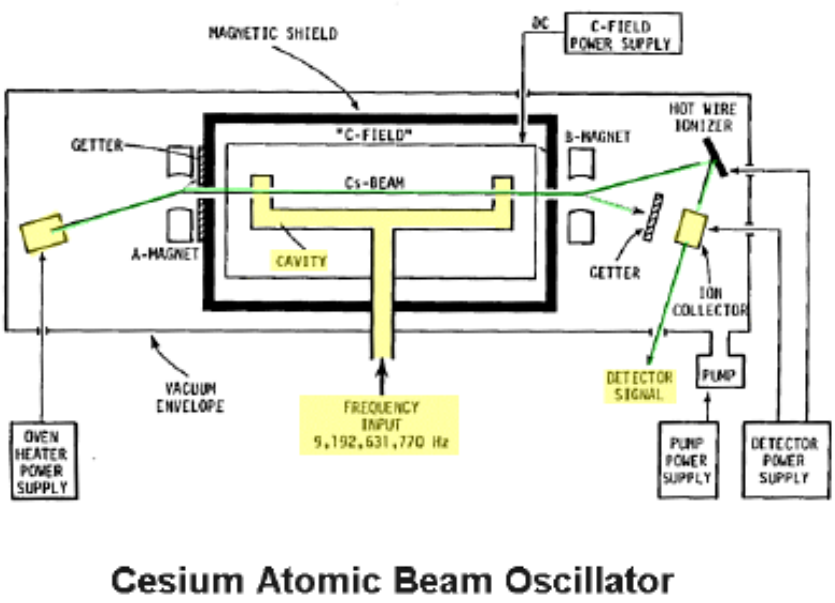

Figure 5.4 Cesium clock diagram[43]

Hydrogen masers are substantially more precise (1 second loss in a million years) and have the best short term stability of the three types of clocks. Their principles of operation are similar to those of Cesium, which means that a beam of selected hydrogen atoms is sent to a cavity where a 1410 Hz radiation changes the energy states of the atoms. This kind of clocks is affected by frequency drift caused by the ageing of the inner coating of the maser's storage bulb. They are more sensitive to the environment because of the impact on the mechanically defined resonance frequency of the maser's microwave cavity and their main physical limitation is the consumption of the fuel (hydrogen)[43], [47], [48].

5.2. Relativistic effects on time

In a GNSS, the measurement of a distance is obtained by measuring the time interval taken by the light to cover it. These time intervals are extremely short, and a poor clock data processing could make the concept of a GNSS practically useless; a small difference in times between clocks could result in a deviation of meters in position.

Nowadays, current GNSS include several corrections to clock predictions from a variety of sources; most of them are done in the Control Centre instead of in-orbit. The importance of relativity theory in real engineering has grown with the improvement of GNSS. The case of GPS gives us an example of how relativistic effects can affect this kind of systems. However, although the GPS case has been widely analysed, it is well known that the relativistic effects are time-varying and dependent on the orbital elements. For this reason, we must analyse the effect on the LGSNS and compare them with the results of the GPS.

The formulation used in this section follows [49], [50] and [51].

5.2.1. Simplified equations: introductory estimations

A detailed presentation of the theory of special and general relativity can be found in [52]. We refer to those basic principles to discuss the relativistic effects on time in navigation.

There are two main relativistic influences upon the time measured between different clocks. The first one is a special relativity correction and has to do with the relative movement between clocks. The second source of clock de-synchronization is gravitational field difference. There exist other error sources, such as the rotation of the central body and the perturbations on the gravity field.

5.2.1.1. The velocity effect (Lorentz contraction)

This effect is based upon the difference between the velocity of the transmitter's and receiver's clocks. A clock in a spaceship travelling at a speed *v* runs slow compared to a stationary clock on the surface of the central body by a factor γ. In other words, the time t_2 measured by the moving clock relates to the time t_1 measured by the stationary clock as

$$t_2 = \gamma \cdot t_1 = \frac{1}{\sqrt{1 - \frac{v^2}{c^2}}} \cdot t_1 \approx \left(1 - \frac{v^2}{2c^2}\right) \cdot t_1. \tag{5.1}$$

In our case, 2 is the orbiting clock and 1 is the receiver or ground station clock. The time will beat slower for the orbiting clock because of its speed. Although the orbital speed is much slower than the speed of light, the difference in time Δt is small but sufficient to cause error. This effect is called "time dilation" and is defined as

$$\Delta t = -\frac{v^2}{2c^2} t_1 = -\frac{g_{cb} R_{cb}^2}{2rc^2} t_1, \tag{5.2}$$

where g_{cb} is the gravity of the central body, R_{cb} is the central body radius, r is the orbital radius, c is the speed of light (300000 km/s) and t_1 is time measured by the receiver's clock. Table 5.4 shows the parameters used during the computation and Table 5.5 compares the effect on the GPS with the effect on the LGSNS.

	$\mathbf{g_{cb}}$ $[\mathbf{km/s^2}]$	$\mathbf{R_{cb}}$ $[\mathbf{km}]$	$\mathbf{r}$ $[\boldsymbol{km}]$
Moon (LGSNS)	0.001624	1738	8238
Earth (GPS)	0.0098	6380	26580

Table 5.4 Orbital parameters to be used in the computations

	$\boldsymbol{\Delta t}$ $[\boldsymbol{\mu s/day}]$	**Position error [m/day]**
Moon (LGSNS)	-0.286	85.8
Earth (GPS)	-7.2	2160

Table 5.5 Time dilation computations results

As reported in Table 5.5, at the end of the day the difference between GPS clocks is 7.2 μs which cannot be neglected because light travels more than 2 km in such time. In the Moon's case, the time dilation is smaller, only 0.286 μs. That means that the accumulated position error is significantly lower: 85.8 m.

5.2.1.2. Gravitational effect

A clock in a higher orbit runs faster than a clock on the surface because the gravitational potential decays with height. To understand it let us make an analogy with a photon. The quantum of light acts like a material particle gaining kinetic energy as it falls through

the gravity field. The energy of the photon is $h \cdot f$, where h is Planck's constant and f is the frequency. So if a photon falls into a potential well, it is shifted to a higher frequency; climbing up, it loses frequency. If it were a material particle, from special relativity its total energy would be $m \cdot c^2$. These two energy expressions are equivalent so, the mass m of a particle must correspond to $(h \cdot f)/c^2$ of the photon. Then, since the potential change is the energy change of the particle per unit mass, such equivalence requires that

$$\Delta(hf) = m\Delta\Phi = -\frac{hf}{c^2}\Delta\Phi \tag{5.3}$$

or

$$\frac{\Delta f}{f} = -\frac{\Delta\Phi}{c^2}. \tag{5.4}$$

In general relativity this effect is called "gravitational frequency shift". Its practical effect is opposite to time dilatation because clocks in a stronger gravitational field (near the surface) appear to "beat slower" whereas they "beat faster" compared with the orbiting clocks due to their velocity difference.

By replacing $\Delta\Phi$ with the gravitational field caused by a central mass, we obtain:

$$\frac{\Delta\Phi}{c^2} = \frac{1}{c^2}\big(\Phi(r) - \Phi(R_{cb})\big) = \frac{1}{c^2}\left(-\frac{Gm_{cb}}{r} + \frac{Gm_{cb}}{R_{cb}}\right) = \frac{g_{cb}R_{cb}}{c^2}\left(1 - \frac{R_{cb}}{r}\right). \tag{5.5}$$

By using the same parameters presented in Table 5.4 and Eq. 5.6

$$\Delta t = \frac{g_{cb}R_{cb}}{c^2}\left(1 - \frac{R_{cb}}{r}\right)t_1, \tag{5.6}$$

we can obtain the values of this effect for the GPS case and the LGSNS case.

	$\boldsymbol{\Delta t}$ $[\boldsymbol{\mu s/day}]$	**Position error [m/day]**
Moon (LGSNS)	2.14	642
Earth (GPS)	45.6	13680

Table 5.6 Gravitational shift computations results

From Table 5.6 we deduce that the error produced by this effect is about ten times more disturbing than the pure special relativity effect.

There is also an acceleration effect. It can be absorbed in the gravitational potential. The formal justification for doing so is the Principle of Equivalence in Einstein's general theory of relativity. By this principle we find

$$\frac{\Delta f}{f} = -\frac{v}{c} = -\frac{gt}{c} = -\frac{gr}{c^2}. \tag{5.7}$$

The product *gr* in Eq. 5.7 corresponds to a potential difference so we can include the observer's acceleration by modifying the gravity term. However, there is no need to do so because this correction is simply a Doppler shift adjustment due to the change in the receiver's velocity during signal propagation. The Dopple's effect is already computed as part of the special relativity correction; by using the relative velocity between clocks at the time of reception of the signal, we include the acceleration effects automatically.

Table 5.7 shows the results of the total Δt, obtained by adding both effects (time dilation and gravitational shift).

	Δt_{TOTAL} $[\mu s/day]$
Moon (LGSNS)	1.854
Earth (GPS)	38.4

Table 5.7 Global relativistic effect results

5.2.2. Complete formulation: eccentricity effects

By taking into account the rotation of the central body, a new effect appears: the Sagnac effect. By ignoring the gravitational potential and considering the simplest transformation from a system at rest (inertial system) to a uniformly rotating system with an angular velocity of ω, we obtain:

$$\int_{path} dt' = \int_{path} d\tau + \frac{2\omega}{c^2}\int_{path} dA. \tag{5.8}$$

The time transformation (t=t') is simple: it means that the coordinate time in the rotating frame is determined in the underlying inertial frame. dA is the infinitesimal area in the rotating frame swept out by a vector from the rotation axis of the orbiting clock.

The last term in Eq. 5.8 is the Sagnac term and only appears in rotating frames. However, in our computation of the relativistic effects on clock onboard a satellite we are going to use a centred inertial frame so the Sagnac effect becomes irrelevant.

For a slowly moving clock (slow compared with the speed of light) in a centred inertial frame, the final equation to be solved is:

$$\int_{path} dt = \int_{path} \left(1 - \left(\frac{(\mathrm{V} - \Phi_0)}{c^2} - \frac{v^2}{2c^2}\right)\right) d\tau. \tag{5.9}$$

By assuming that the satellite orbits are Keplerian, we can rewrite the potential *V* and the velocity *v* with orbital mechanics and obtain the following final expression:

$$\Delta t = \int_{path} \left(1 + \frac{3GM_{cb}}{2ac^2} + \frac{\Phi_0}{c^2} - \frac{2GM_{cb}}{c^2}\left(\frac{1}{a} - \frac{1}{r}\right)\right) d\tau, \tag{5.10}$$

where Φ_0 is the gravitational potential. In our computation, only the central gravity potential ($\frac{Gm_{cb}}{R_{cb}}$) is to be used, since the perturbations are demonstrated to have a slight impact (of the order of centimetres). From the first term in the integral without further corrections, the time measured by the orbiting clock and the surface clock are the same ($\Delta t = \Delta \tau$). The next two terms of the integral are a constant correction coefficient that for the LGSNS would be:

$$\frac{3GM_{cb}}{2ac^2} + \frac{\Phi_0}{c^2} = 9.9495 \cdot 10^{-12} - 3.1440 \cdot 10^{-11} = -2.149 \cdot 10^{-11} s/s = -1.86\ \mu s/day$$

where *a*=*r*. This value matches the value found in the previous section. That is because in our case the orbit is circular and the semimajor axis is equal to the orbital radius. However, if the orbit was not circular, there would be a slight difference induced by the mismatch between the orbital radius and the semimajor axis. Besides, if the eccentricity is not zero, the last term of the integral becomes important. It is called the "eccentricity correction" and to solve the equation we need to find a r(τ) expression.

$$\Delta t_{ecc} = \int \frac{2GM_{cb}}{c^2}\left(\frac{1}{a} - \frac{1}{r}\right) d\tau. \tag{5.11}$$

From orbital mechanics we know that

$$r = a(1 - e\cos E), \tag{5.12}$$

hence

$$\Delta t_{ecc} = \frac{2GM_{cb}}{c^2} \int \left(\frac{e\cos E}{1 - e\cos E}\right) d\tau. \tag{5.13}$$

Deriving Kepler's equation

$$M = \sqrt{\frac{\mu_{Moon}}{a^3}}\, t = E - e\sin E \tag{5.14}$$

provides

$$\frac{dE}{dt} = \frac{\sqrt{\frac{\mu_{Moon}}{a^3}}}{1 - e\cos E}. \tag{5.15}$$

Rearranging the integral and assuming *dt=dτ* gives

$$\Delta t_{ecc} = \frac{2e\sqrt{\mu_{Moon} \cdot a}}{c^2} \int_{orbit} \cos E \, dE = \frac{2e\sqrt{\mu_{Moon} \cdot a}}{c^2} (\sin(E_t) - \sin(E_0)). \tag{5.16}$$

By selecting the E_0 eccentric anomaly equal to zero, we obtain a compact expression for the cyclic Δt_{ecc}:

$$\Delta t_{ecc} = \frac{2e\sqrt{\mu_{Moon} \cdot a}}{c^2} \sin(E_t). \tag{5.17}$$

This expression is useful to determine the eccentricity correction of any elliptical orbit. It allows to derive the eccentric anomaly from Kepler's equation for a certain time and then to calculate the value of Δt_{ecc}.

In order to see the effects of the eccentricity, we plotted Δt_{ecc} for the GPS and for the LGSNS (see parameters in Table 5.4). The residual eccentricity used in each case can be found in Table 5.8. Figures 5.5 and 5.6 are the results of these computations.

	e
Moon (LGSNS)	0.010
Earth (GPS)	0.013

Table 5.8 Residual eccentricity for a LGSNS and a GPS

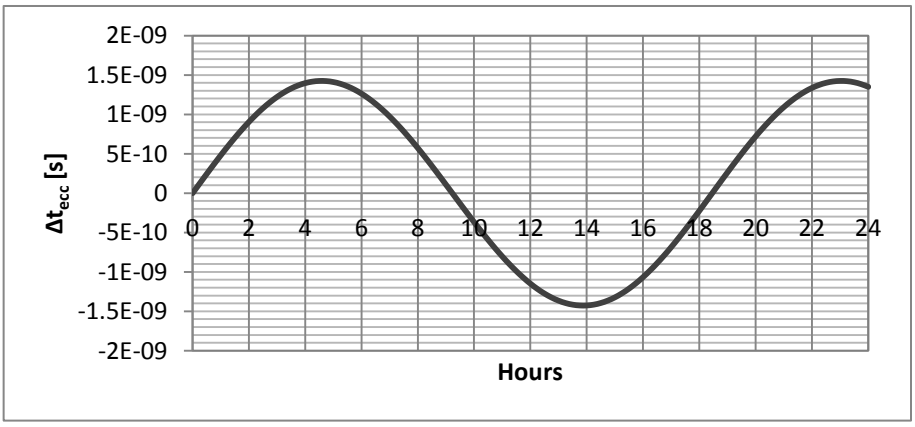

Figure 5.5 LGSNS results for the "eccentricity correction"

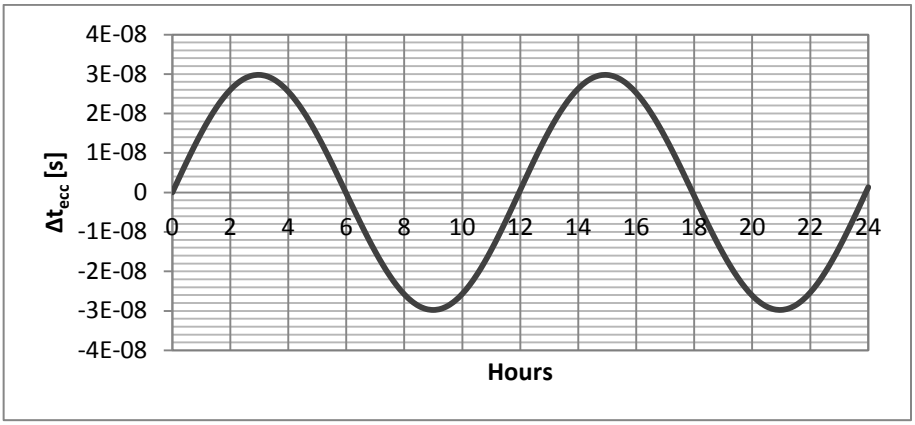

Figure 5.6 GPS results for the "eccentricity correction"

The amplitude for the GPS oscillation is 60 ns with a twelve-hour period. For the LGSNS, the effect is less important, about 3 ns, and the period of the oscillation is, approximately, 18 hours instead of twelve as in the GPS case. Note that the computation begins at the pericenter in both cases.

Now, a computation of all the effects together (equivalent of solving the integral expression) can be done for a better understanding of the overall relativistic effect on time.

Figures 5.7 and 5.8 show that at the end of the day the drift in the GPS case is about 40 μs. In this time lights travels 12 kilometres, thus correcting this would be mandatory in a system like that in order to obtain any navigation performance. However, in the LGSNS case, the effect is considerably smaller; in a 24-hour period the drift is about 2 μs, which means that the light only travels 560 meters.

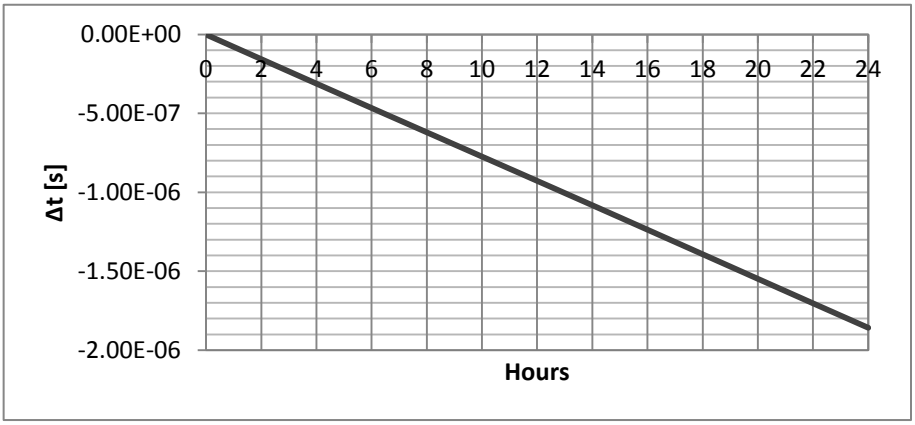

Figure 5.7 Global relativistic effects on a LGSNS for a 24h period

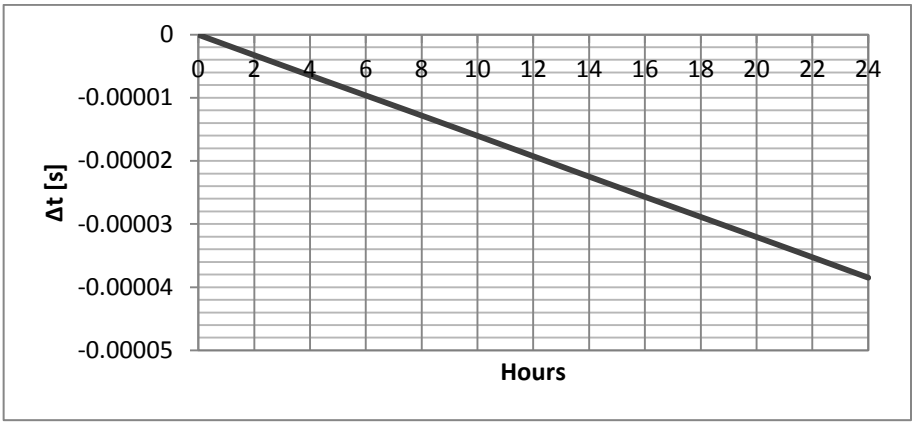

Figure 5.8 Global relativistic effects on a GPS for a 24h period

5.2.3. Conclusions

In this chapter's section we have obtained the basic corrections applicable to our LGSNS onboard clock, related to relativistic time effects. This section essentially replicates the corrections currently in use by GPS processors and adapts them to the LGSNS orbit. The results are that for a LGSNS the daily drift is about ten times smaller than in the GPS case. This difference is possibly caused by the difference in size and mass between Earth and the Moon. However, in order to be able to offer accurate satellite navigation data, a proper management of clock data is fundamental.

Chapter six.

Preliminary subsystems design

In this chapter, the preliminary power and mass budgets of project are addressed. It also holds a preliminary study of the propulsion, thermal and communications subsystems in order to have an overview of the main characteristics that the final spacecraft design will present.

6.1. Power subsystem

In this chapter's section, the power budget is addressed. This preliminary budget does not take into account Earth eclipses. As it will be seen in following sections of this chapter, Earth eclipses increase significantly the power demands of the thermal control subsystem and its implications must be analysed with great detail in further design stages. The computations follow the approach illustrated in [1].

6.1.1. Power requirements

The input parameter for this estimation is the payload power consumption. Navigation payload usually consumes between 600 and 900 W of electrical power. For our purposes, an intermediate value of 800 W has been chosen. By knowing the fraction of power consumed by the payload to the total required by the spacecraft and its value, we can estimate the power consumed by the rest of the spacecraft subsystems. Table 6.1 shows the results of these estimations. All the different subsystem power fractions have been chosen following historical data of similar missions.

This preliminary budget holds for a chemical propulsion system. If the propulsion system was electric, such as Hall or Ion thrusters, the power consumed would be much higher than the specifications given in Table 6.1. The normal range of power values for Hall engines is 500-10000 W, depending on the I_{sp}. For Ion thrusters the power range is 300-5000 W.

Power Budget		
	% of the total power	Power [W]
Payload (Estimation)	60	800
Propulsion Subsystem	4	54
Attitude Control Subsystem	5	67
Communication Subsystem	7	94
Command and Data Handling	7	94
Thermal Subsystem	4	54
Power Subsystem	12	160
Structure Subsystem	1	14
TOTAL	**100**	**1337**

Table 6.1 Power consumption estimation of the spacecraft's subsystems

Once the total average power P_{TOTAL} requirement is estimated, a security margin is applied. In this case we adopted a 10% margin, thus the final requirement is

$$P_{sun} = 1.1 \cdot P_{TOTAL} = 1471\ W. \tag{6.1}$$

P_{sun} is the power that the spacecraft needs in order to operate properly during the mission lifetime. Although solar array will be the main source to obtain this power, during eclipses batteries will be needed. To calculate the solar array area and the mass of the secondary batteries, we need to know P_{array} which is the sum of P_{sun} and P_{charge}. P_{charge} is the power required to charge the secondary batteries during sunlight by the solar array. We also need to know the fraction of power needed during eclipses, $P_{eclipse}$.

In order to estimate $P_{eclipse}$, we need to know the time that the satellite is in shadow so, we need lunar eclipse data. Table 6.2 shows data extracted from *Chapter four* which includes the maximum eclipse period and the difference between the orbital period (T) and the eclipse duration ($T_{eclipse}$), T_{sun}:

$$T_{sun} = T - T_{eclipse}. \tag{6.2}$$

Eclipse data		
Orbital period [h]	**T_{eclip} [h]**	**T_{sun} [h]**
18.46	1.29	17.17

Table 6.2 Eclipse data extracted from *Chapter four*

Once, the eclipse period is known, the estimation of the power needed during eclipses is obtained. It is estimated that during eclipses the satellite will only use 90% of P_{sun}. The

reason why $P_{eclipse}$ is not equal to P_{sun} is that, during lunar eclipses communication with the Earth is not possible so, the power consumed by Earth-Moon communication and its data handling will not be spent.

$$P_{eclipse} = 0.9 \cdot P_{sun} = 1324\, W. \tag{6.3}$$

The difference between P_{array} and P_{sun} is P_{charge}. In our case,

$$P_{charge} = \frac{T_{eclip} P_{eclip}}{T_{sun} \eta_{batteries}} = 118\, W \tag{6.4}$$

where an efficiency of 0.85 is chosen since it is the average value for this parameter.

Now,

$$P_{array} = P_{sun} + P_{charge} = 1589\, W\ (\text{EOL}) \tag{6.5}$$

Eq. 6.5 defines the final End Of Life (EOL) power needed to be produced by the solar array. With this power estimation, the solar array can be sized.

6.1.2. Solar array sizing

Depending to the solar cell chosen, the area of the solar array will vary. Silicon (Si), Gallium Arsenide (GaAs) and Multijuntion, which is not a material but a combination of them (Gallium Indium Phosphide (GaInP) and GaAs), are the most common materials for solar cells, each of them have different values of efficiency and degradation.

To find the solar array area we need to know the EOL power P_{EOL} produced by a single cell for each type of solar cell,

$$P_{EOL} = P_{BOL} \cdot (1 - \gamma)^{years} \tag{6.6}$$

where *years* is 10, the lifetime of the mission, degradation γ can be found in Table 6.3 and P_{BOL} is,

$$P_{BOL} = P_{cell} \cos\theta\, \eta_{st} = S \cdot \eta \cdot \cos\theta \cdot \eta_{st}. \tag{6.7}$$

S is the solar constant (1371 W/m^2), η is the cell efficiency, η_{st} is the inherent degradation of the cell (as before, the average value 0.85 is chosen) and θ is the incident angle which is assumed to be zero.

Finally, the area of the solar array is,

$$Area = \frac{P_{array}}{P_{EOL}}. \tag{6.8}$$

Table 6.3 shows different sizing values for three kinds of solar cells.

Solar array parameters						
	Efficiency (η)	**Degradation per year (γ)**	**P_{cell} [W/m²]**	**P_{BOL} [W]**	**P_{EOL} [W]**	**Area [m²]**
Si	0.148	0.0375	202.908	172.472	117.686	14
GaAs	0.185	0.0275	253.635	215.590	163.126	10
Multijuntion	0.295	0.06	404.445	343.778	185.164	9

Table 6.3 Solar array parameters and final needed area for different type of materials

6.1.3. Sizing of the batteries

To complete the preliminary sizing of the power subsystem, we need to estimate the weight of the secondary batteries in order to be able to estimate a mass budget for the complete spacecraft. As in the case of the solar array, the battery weight depends on the battery type. Our computations are going to be done for three types of batteries: Nickel-Cadmium (NiCd), Nickel-Metal hydride (NiMH) and Lithium-Ion (Li-Ion).

The battery mass is,

$$m_{battery} = \frac{E}{e} \tag{6.9}$$

where *e* is a parameter of each kind of battery and can be found in Table 6.4, and *E* is energy produced by the battery and is obtained as

$$E = V_{av} Chg. \tag{6.10}$$

V_{av} is the total voltage provided ($n^{\underline{o}}\ of\ cell \cdot V_{cell}$) and *Chg* is calculated as

$$Chg = \frac{P_{eclip} T_{load}}{V_{av} \%DOD_{max}}. \tag{6.11}$$

where $\%DOD_{max}$=0.7 and $T_{load} = 1.2\ h$.

The final mass can also be found in Table 6.4.

Battery characteristics						
	V_{cell} [V]	e [Wh/kg]	V_{av} [V]	Chg [Ah]	E [Wh]	Mass [kg]
NiCd	1.2	39	27.6	82.24	2269.71	59
NiMH	1.2	57	27.6	82.24	2269.71	40
Li-Ion	3.6	83	28.8	78.81	2269.71	28

Table 6.4 Battery parameters and final mass for different types of batteries

6.2. Propulsion budget

Following what has been done in this chapter, the propulsion budget presented here is for a chemical propulsion system with an I_{sp} of 320s, typical value for a bipropellant thruster. However, a comparison between electric and chemical thrusters will be made in order to obtain a better understanding of their advantages and disadvantages. This information will be important in further stages of the design, when the final propulsion system for station-keeping will be chosen.

The study of the satellites positioning into orbit is beyond the scope of this report, therefore only the station-keeping propulsion budget is considered.

6.2.1. Comparison between electric and chemical thrusters

The value ranges of specific impulse I_{sp}, thrust and input power of electric and chemical thrusters are very different. Chemical thrusters have a specific impulse range of 200-350 seconds whereas electric thrusters can achieve an I_{sp} of more than 4000 seconds. Their thrust supply is reversed; for chemical propulsion systems it goes from a few to hundreds of Newtons, and for Hall and ion thrusters it is around one Newton. I_{sp} and power input are highly related; the more I_{sp} you want, the more power you will need. Table 6.5 shows different values of I_{sp}, thrust F, and input power for different types of engines.

	I_{sp} [s]	F [N]	Input power [W]
Solid	240 - 300	50	-
Monopropellant	220 - 240	0.5 - 22	< 50
Bipropellant	305 - 325	4 - 500	< 50
Dual Mode	313 - 322	10 - 22	< 50

Hybrid	250 - 340	4 - 500	< 50
Hall thruster	1600 - 2500	< 1	500 – 10000
Ion Engine	2500 - 4000	< 5	300 – 5000

Table 6.5 Values of I_{sp}, thrust and input power for different types of propulsion systems[1], [53]

Another important difference between the two families of propulsion systems is the propellant mass M_p that they need. For the same velocity impulse, a greater I_{sp} results in a lower propellant mass and the other way around. Table 6.6 shows the propellant mass needed for the mission under study ($\Delta v = 1 km/s$) calculated using Eq. 6.12,

$$M_p = M_0 \left(1 - e^{-\frac{\Delta v}{I_{sp} g_0}}\right). \tag{6.12}$$

for different kinds of thrusters. Eq. 6.12 is the well-known rocket equation due to Tsiolkovsky[54]. It gives the propellant mass for a given velocity variation Δv. M_0 is the dry mass of the satellite, g_0 a conversion factor to express I_{sp} in units of time; it was found convenient to use the gravitational acceleration of the Earth's surface (9.81 m/s^2). Finally, I_{sp} is the specific impulse of the propulsion system.

	I_{sp} [s]	Propellant mass [kg]
Monopropellant	240	259.50
Bipropellant	320	204.60
Hall thruster	2200	33.96
Ion Engine	3600	20.94

Table 6.6 Computation of the propellant mass needed in the LGSNS mission for different types of propulsion systems

The derivation of the thrust equation in vacuum is as follows,

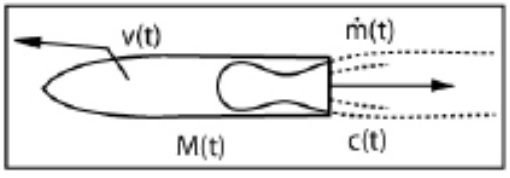

Figure 6.1 Representation of a space propulsion system[55]

$$p(t) = M(t)v(t) + \int_0^t \dot{m}(\tau)[v(\tau) - c(\tau)]d\tau = constant \tag{6.13}$$

where $p(t)$ is the momentum of the spacecraft, $M(t)$ is the total spacecraft mass, $v(t)$ is the velocity of the spacecraft, $\dot{m}(\tau)$ is the mass variation per unit of time which can be

defined as $\dot{m} = -\frac{dM}{dt}$ and, finally, $c(\tau)$ is the velocity of the ejected mass. Eq. 6.13 represents the conservation of momentum of the system.

By differentiating Eq. 6.13, we obtain:

$$\frac{dp}{dt} = 0 = M\frac{dv}{dt} + v\frac{dM}{dt} + \dot{m}(v - c) = M\frac{dv}{dt} + v\frac{dM}{dt} - \frac{dM}{dt}v + \frac{dM}{dt}c, \tag{6.14}$$

$$M\frac{dv}{dt} + \frac{dM}{dt}c = 0, \tag{6.15}$$

$$M\frac{dv}{dt} = -\frac{dM}{dt}c = \dot{m}c. \tag{6.16}$$

The velocity of the ejected mass or c is also defined as $c = I_{sp}g_0$. With this new definition of *c,* the spacecraft thrust F (Eq. 6.16) can be rewritten as

$$F = -I_{sp}g_0\frac{dM}{dt}, \tag{6.17}$$

$$|F| = I_{sp}g_0\frac{\Delta M}{\Delta t} = I_{sp}g_0\frac{M_p}{\Delta t}. \tag{6.18}$$

Where Δt is the duration of the maneuver[55]. In order to make a rough estimate, we change $\frac{dM}{dt}$ into $\frac{\Delta M}{\Delta t}$. By doing this, we introduce some error in the calculation, however, we know the value of ΔM which is the mass that the spacecraft loses or, equivalently, the propellant mass. The only unknown is the impulse duration Δt. By making this approximation we can use Δt as the independent variable and then estimate different thrust values. In the case of the LGSNS, the Δv needed per maneuver is 50 m/s which represent a propellant mass of around 12 kg.

Table 6.7 shows the results of this estimation for a bipropellant propulsion system.

	F [N] approx.
$\boldsymbol{\Delta t = 1\ min}$	620
$\boldsymbol{\Delta t = 5\ min}$	124
$\boldsymbol{\Delta t = 15\ min}$	42
$\boldsymbol{\Delta t = 20\ min}$	31
$\boldsymbol{\Delta t = 30\ min}$	21
$\boldsymbol{\Delta t = 1\ h}$	11

Table 6.7 Thrust values depending on the impulse duration

As reported in Table 6.7, the longer Δt is, the lower thrust will be need. However, our Δv budget estimations have been done with the hypothesis of impulsive maneuvers. An impulsive maneuver is an instantaneous change in the spacecraft's velocity. In reality an instantaneous change in velocity would require an "infinite force" applied during an "infinitely short time". In other words, the equations used to estimate the Δv budget for station-keeping (see *Chapter four*) are an approximation. This means that we cannot increase Δt as much as we want because then the maneuvers would not be impulsive and the equations used would entail too much error.

In non-impulsive maneuvers the thrust acts over a significant time interval and must be included in the equations of motion. Adding an external force **F** to the spacecraft yields the following equation of relative motion

$$\ddot{\boldsymbol{r}} = -\mu \frac{\boldsymbol{r}}{r^3} + \frac{\boldsymbol{F}}{m} \tag{6.19}$$

where *m* is the mass of the spacecraft. If the external force is a thrust *T* in the direction of the velocity vector ***v***, then ***F****=T(**v**/v)*. This equation may not have a straightforward analytical solution, so numeric methods are needed[56].

With a chemical propulsion system a thrust of 42 N can be easily achieved ($\Delta t = 15\ min$). Nowadays there are commercial 10 N bipropellant thrusters[57] which are a good solution. By having four of these thrusters, the propulsion requirements for station-keeping will be fulfilled and the maneuver could be made with a single thrust which is the ideal configuration. However, in order to achieve the thrust range available with electrical thrusters (1 N), the impulse should last 10 hours which is completely out of the impulsive maneuver hypothesis. There are two possible solutions: either executing the station-keeping with many shorter impulses or carrying out the complete correction maneuver with a continuous impulse (non-impulsive option) instead of a single impulse. Both these solutions would need to be deeply studied because, as it has been said in *Chapter four*, in order to maintain the average value of the semimajor axis, the correction maneuver needs to be done when the spacecraft does not feel third body-perturbations. The effect of the continuous impulse in the semimajor axis or the study of when each small impulse should be applied becomes mandatory for the election of an electric propulsion system.

6.2.2. Propellant budget

As has already been said at the beginning of this section, the propulsion budget will be held for a chemical thruster with a specific impulse of 320 seconds. From *Chapter four*, we know that the impulse needed in order to maintain the orbit circular, polar and within its range of permitted RAAN is

$$\Delta v = 1000 \frac{m}{s}.$$

We also know that the dry mass M_{dry} is 750 kg so, the nominal propellant mass $M_{p_{nominal}}$ can be found using Eq. 6.12.

$$M_{p_{nominal}} = 750 \left(1 - e^{-\frac{1000}{320 \cdot 9.81}}\right) = 204.60\ kg$$

By adding a 10% margin, the final propellant mass value can be found,

$$M_p = 1.1 \cdot M_{p_{nominal}} = 225\ kg. \tag{6.20}$$

6.3. Mass budget

The final budget to conclude the preliminary sizing of the spacecraft is the mass budget. In order to estimate the mass of each subsystem we need a value of dry mass. In *Chapter four* the loaded and dry mass of the satellite have already been predicted: the dry mass is set at 750 kg and the loaded mass at, approximately 1000 kg. Definitions of the different masses presented can be found in [58].

Now, with this preliminary mass values we can estimate the weight of the power, propulsion and attitude subsystem. Tables 6.8, 6.9 and 6.10 show the results. All the different subsystems and components percentages of mass have been chosen by following historical data from similar missions. The process followed can be found in [1].

6.3.1. Power Subsystem mass budget

Battery mass estimation follows the process presented in this same chapter. Since we have estimated the mass of three different types of batteries, an average value of 44 kg is used in the final power subsystem mass budget. Table 6.8 shows the mass results for the power subsystem.

		Weight [kg]
Solar Array	$0.04 \cdot P_{EOL}$	63.56
Battery		44
Power Control Unit	$0.02 \cdot P_{EOL}$	31.78
Regulators	$0.025 \cdot P_{EOL}$	39.725
Wiring	$0.025 \cdot M_{dry}$	18.75
TOTAL		**198**

Table 6.8 Power subsystem mass budget results

6.3.2. Propulsion Subsystem mass budget

Propellant mass estimation follows the process presented in section *Propellant Budget* . In Table 6.9 there is the estimation of a chemical bipropellant propulsion system components with hydrazine as the propellant (I_{sp}=320 s). For an electrical engine (Hall or Ion) the estimation would be different; propellant weight would be much lower (40-60 kg, depending on the I_{sp}) and the engine weight itself would be between 2 and 6 kg/kW, making the overall mass of the subsystem lower[53]. However, as already said, the power needed by electrical engines is much higher than for a chemical propulsion system which means that the power subsystem weight would be also higher. Besides what has been mentioned in the previous section, in order to take the final decision of which propulsion system is the best for the mission, a trade-off study between the difference in mass and power of each system will be also mandatory in future design stages.

		Weight [kg]
• **Propellant**		225
• **Engine**		39
○ **Tank**	$0.125 \cdot M_p$	28.125
○ **Thrusters**	5 thrusters, 0.65 kg each	3.25
○ **Limes, Valves & Fittings**	Historical data	7.5
TOTAL (Propellant + Engine)		**264**

Table 6.9 Propulsion subsystem mass budget results

Figure 6.2 represents the subsystem mass fraction against the Δv needed for the maneuver.

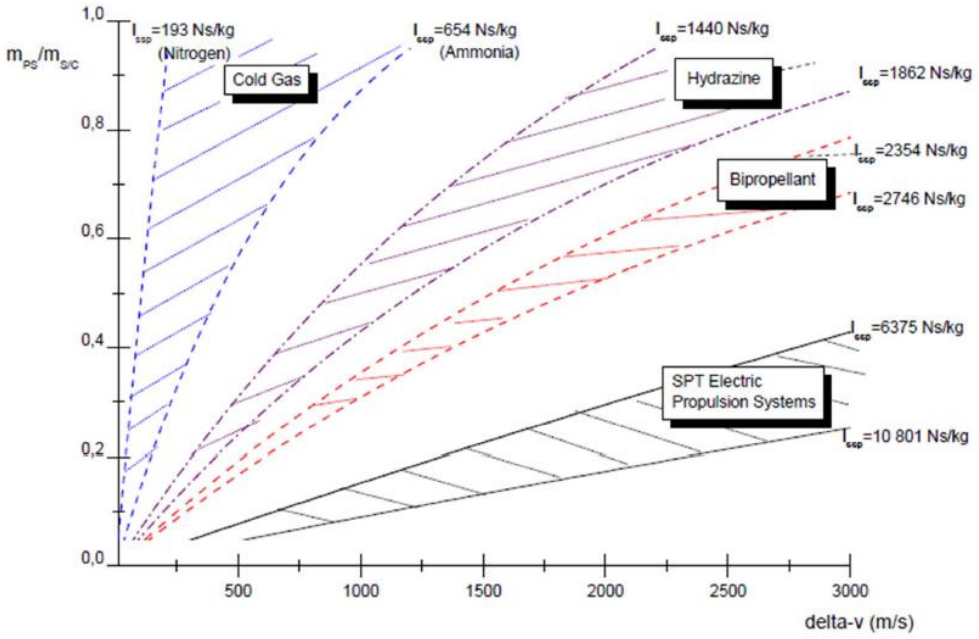

Figure 6.2 Subsystem mass fraction against delta-v budget

6.3.3. Attitude control subsystem mass budget

The selection of the attitude subsystem component is a generalization for this kind of spacecraft; zero momentum, three-axis stabilization. A part of the elements of Table 6.10, thrusters will be needed to desaturate the reaction wheels.

		Quantity	Weight [kg]
Star Tracker	*8 kg/unit*	*1*	8
Sun sensor	*1 kg/unit*	*1*	1
Reaction wheels	*6 kg/unit*	*4*	24
TOTAL			**33**

Table 6.10 Attitude mass budget results

6.3.4. Global mass budget

From *Chapter five* we know the range of the payload weight. In order to close the preliminary mass budget, a mass of 187.5 kg has been estimated for the payload. By knowing that the dry mass must be 750 kg, we can estimate the loaded mass and see if it matches the first estimation of 1000 kg. Table 6.11 shows the final results of each subsystem estimated mass.

Mass budget [kg]		
	% of M_{dry}	Weight [kg]
M_{PL}	25	187.5
M_{prop} (Only engine)		39
M_{att}		33
M_{Com}	6	45
$M_{C\&DL}$	8	60
M_{ther}	5	37.5
M_{pow}		198
M_{struc}	20	150
TOTAL (M_{dry})		**750**

Table 6.11 Final mass budget results

M_{att}, M_{prop} and M_{pow} are the values found in Tables 6.8, 6.9 and 6.10. The remaining estimations are done with historical data.

Finally, M_{loaded} can be estimated:

$$M_{bus} = M_{prop} + M_{att} + M_{Com} + M_{C\&DL} + M_{ther} + M_{pow} + M_{struc} = 562.5\ kg, \quad (6.21)$$

$$M_{dry_{margin}} = M_{dry} + 0.1M_{dry} = 825\ kg, \quad (6.22)$$

$$M_{loaded} = M_{dry_{margin}} + M_p = 1050\ kg, \quad (6.23)$$

where M_p is the propellant mass (225 kg). Injected weight and adapter mass have not been taken into consideration.

As it can be seen, the loaded mass estimated matches the expected 1000 kg mass.

6.3.5. Spacecraft general parameters

Finally, Table 6.12 shows a few more parameters estimations of the spacecraft.

Volume	$0.01 \cdot M_{loaded}$	11 m^3
Linear dimension	$0.25 \cdot M_{loaded}^{1/3}$	3 m
Body Area	s^2	9 m^2
Density	M_{loaded}/V	97 kg/m^3

Table 6.12 General spacecraft parameters such as volume and density

6.4. Thermal control feasibility

How does the LGSNS orbit affect the thermal environment of the spacecraft? On this section we are going to predict the worst-case thermal margins of a satellite in a LGSNS orbit and evaluate the options of passive and active thermal control techniques.

6.4.1. Hot case

The analytic estimation called "hot case" corresponds to the worst, fully illuminated conditions. The estimation considers the spacecraft as isothermal and it is an energy balance between absorbed and emitted power. Its formulation can be found in [1].

$$Q_{absorbed} = Q_{Emitted}, \tag{6.24}$$

$$(J_s A_s + J_a A_a)\alpha + J_p A_p \epsilon + Q = A_{emission}\epsilon\sigma T^4 \tag{6.25}$$

where σ is the Stefan-Boltzmann constant and α and ϵ are the absorptivity and the emissivity, respectively. *Q* is the internal power dissipation in form of heat by the spacecraft systems operation. J_s is considered constant and its value is 1371 W/m^2, J_a is approximated as $a \cdot J_s$ (F and $\cos\alpha$ are equal to 1, see Eq. 4.17) and J_p is computed assuming that the Moon radiates an IR flux equal to the average value measured at some given phase on the illuminated side. Moreover, its thermal radiation emanates uniformly and the intensity of this radiation decreases with altitude as[25]

$$J_p = 997\left(\frac{R_{Moon}}{r_{orbit}}\right)^2. \tag{6.26}$$

The areas A_a and A_p correspond to the cross section area exposed to the Moon and are therefore equal. However, A_s and $A_{emission}$ are generally different. A_s is the area offered to direct solar radiation and during the STK simulation (*Chapter four*) was considered to be 20 m^2. A_a and A_p are estimated in 12.5 m^2 because from the 20 m^2 offered to the direct solar radiation, approximately 10 were allocated to the solar arrays, so 10 m^2 represent the spacecraft body's cross sectional area. Solar arrays are continuously pointing to the Sun, but not necessarily completely perpendicular to the Moon; this explains the additional 2.5 m^2 in the final estimated area. Finally, $A_{emission}$ is the area which emits radiation. This includes all the external surfaces of the spacecraft and it is estimated in 50 m^2[15].

By these assumptions, the final expression of the spacecraft temperature *T* is

$$T^4 = \frac{(J_s A_s + J_a A_a)}{A_{emission}\sigma}\frac{\alpha}{\epsilon} + \frac{J_p A_p}{A_{emission}\epsilon\sigma} + \frac{Q}{A_{emission}\epsilon\sigma}. \quad (6.27)$$

By assuming an albedo factor an equal to 0.07[25] and ignoring internal power dissipation, it is possible to plot the equilibrium temperature against the α/ϵ ratio. Figure 6.3 shows the results.

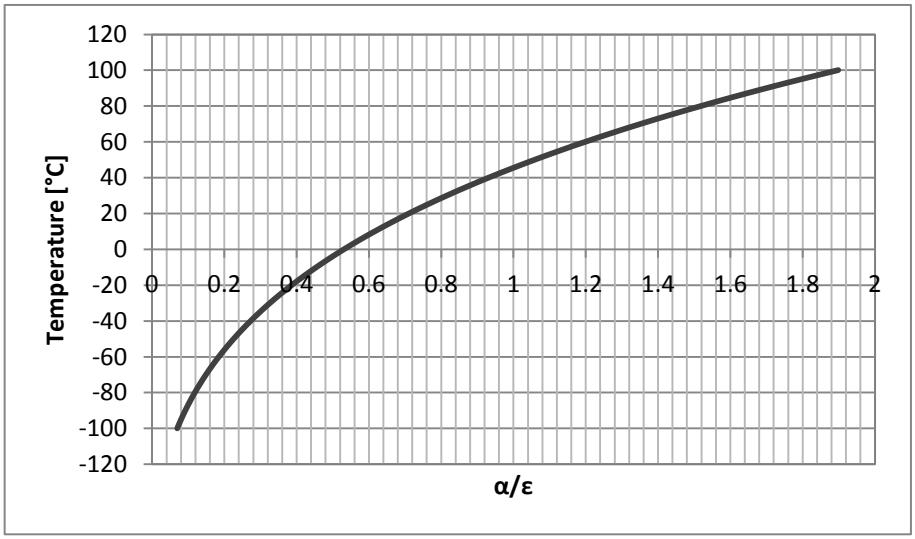

Figure 6.3 Temperature against α/ϵ "Hot case" computation

The target temperature should be within the thermal limits of the most restricting component of the spacecraft. Batteries normally have the narrowest thermal limits as it can be seen in Table 5.3. The ideal spacecraft temperature should be near 15°C so we conclude that regarding the hot case, an external surface finish characterized by an absorptivity to emissivity ratio α/ϵ between 0.6 and 0.8 is recommended. Aluminized kapton (kapton outside) allows to achieve this α/ϵ value[59].

Moreover, if we take the α/ϵ characteristics of aluminized kapton ($\frac{\alpha}{\epsilon} = 0.63$)[59], it is possible to plot the equilibrium temperature against internal power dissipation by treating the internal power dissipation as an independent variable. The effect of the internal power dissipation in the hot case is moderate because even 1000 W of dissipated power would only increase the isothermal temperature by 6°C. For this reason, the influence of the internal power dissipation can be ignored in a preliminary thermal estimation. As it can be seen in Figure 6.4, the effect appears linear because the influence of the internal power dissipation (independent term) is much less significant than the constant solar contribution. In the cold case, as it will be seen in the next section, the relation between temperature and internal power dissipation is not linear for the same value of α/ϵ (there is no solar direct flux contribution). However, depending on the target temperature, the surface layer design would have to be slightly

adjusted, but it can be stated that α/ϵ should be in the 0.6-0.8 range despite the internal power dissipation.

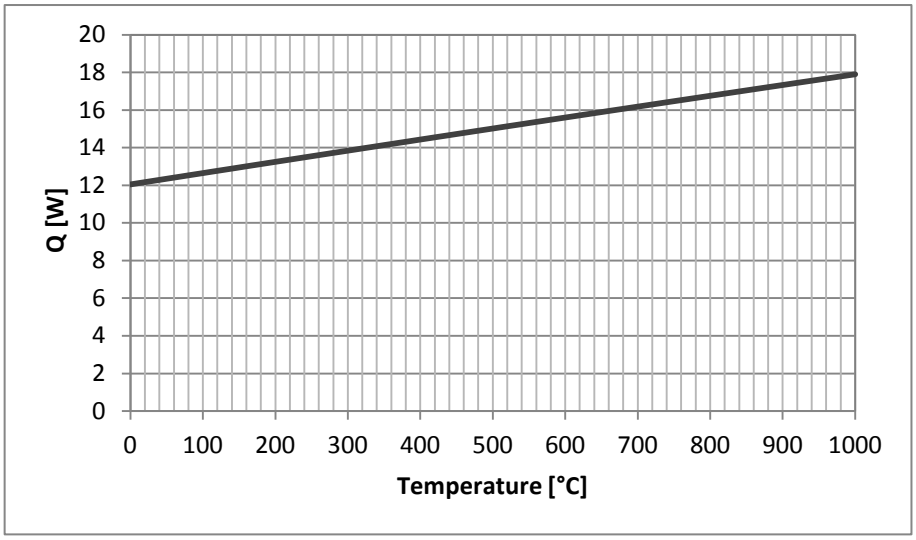

Figure 6.4 Internal power dissipation variation effects on temperature during the "Hot case"

6.4.2. Cold case

In the "cold case" scenario the external heat at the spacecraft is considerably lower than during the "hot case". Because the satellite is under the shadow of the Moon, only the thermal infrared flux of the Moon is able to reach the satellite which, obviously, leads to an important temperature drop. From *Chapter four* we know that the longest lunar eclipse lasts 77 minutes and the average eclipse lasts around 59 minutes. However, the main unknown is represented by the thermal inertial of the spacecraft. Thermal inertia is important because it will help maintain a constant temperature in the spacecraft[15] relative to thermal variations.

This is a fundamental issue because an approach without taking into account the spacecraft's thermal inertia penalizes strongly the design. If the albedo and the direct solar flux contributions are deleted, we can recalculate the equilibrium temperature with kapton layer and ignoring internal power dissipation. The result is as low as -155°C.

By dealing with the transient interval that takes place when the satellite reaches the shadow of the Moon, a better estimation of what happens in reality can be found. As it has been done before, to solve the new equation the spacecraft will be considered isothermal. Things are kept as simple as possible in order to avoid developing a TMM; that is why we are only doing a single-node analysis. Consider the heat power Q_{net} equilibrium of the spacecraft as

$$Q_{net} = Q_{IN} - Q_{OUT} = Q_{planetary} - Q_{emitted}. \quad (6.28)$$

As it has been said, the only active contributions in darkness are the IR radiation of the Moon and the loss of power emitted to deep space. The transient would be calculated as follows[60]

$$\frac{mC(T_f - T_i)}{\delta t} = Q_{net}, \quad (6.29)$$

where m is the body mass, C is the specific heat, δt is the time interval for the calculation and T_f and T_i are the final and initial temperatures, respectively. Expressions for $Q_{planetary}$ and $Q_{emitted}$ are known so Eq. 6.30 can be developed as

$$\frac{mC(T_f - T_i)}{\delta t} = J_p A_p \epsilon - \sigma \epsilon A_{emission} T^4. \quad (6.30)$$

It is important to recall that, in order to solve Eq. 6.29, some assumptions are necessary: the spacecraft is an isothermal node, the thermal emission takes place through the entire surface (the view factor is 1), the spacecraft is a solid body and a finite numerical approach is adopted. The values used in the computation are summarized in Table 6.13.

$\boldsymbol{\epsilon}$	0.63 (aluminized kapton)[59]
$\boldsymbol{m}$	1000 kg
$\boldsymbol{A_p}$	12.5 m^2
$\boldsymbol{A_{emission}}$	50 m^2
$\boldsymbol{C}$	897 $Jkg^{-1}K^{-1}$ (aluminium)
$\boldsymbol{T}$	$\frac{(T_f + T_i)}{2}$
$\boldsymbol{\delta t}$	60 seconds

Table 6.13 Estimation parameters

Figure 6.5 shows the evolution of the temperature during the eclipse. The spacecraft temperature after 77 minutes in complete darkness would be -30°C and, although it is out of the allowed range, it is much more solvable than the first value found of -155°C.

So, in the real "cold case", ignoring internal power dissipation, we can expect for the longest eclipse to drop the spacecraft temperature to -30°C. How can we increase this temperature? A good strategy could be to reduce the spacecraft's average emissivity to avoid losing heat through the surfaces. This strategy is a passive one. However, an active

thermal control solution would probably be needed in some of the spacecraft's components with the narrowest thermal limits such as batteries.

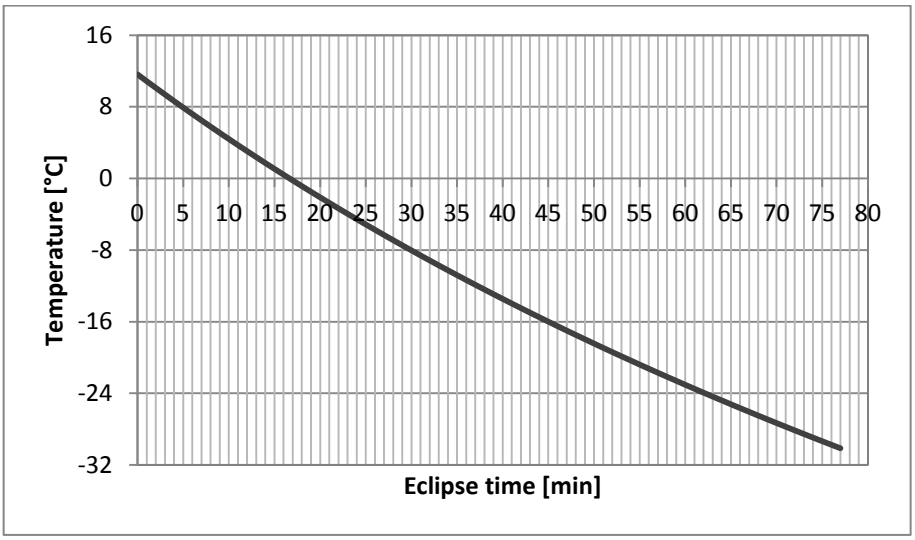

Figure 6.5 Temperature evolution during the "Cold case" transient computation, ϵ=0.63

A different global emissivity may be provided by a louvre system with two different values of emissivity, one for its blades (the same as the satellite's surface) and other for its radiator (in this case, in order to avoid heat dissipation, lower). If we lower the global emissivity to 0.2, a value possible to achieve by current technology, we can replot Figure 6.5 and see how the temperature develops (Figure 6.6).

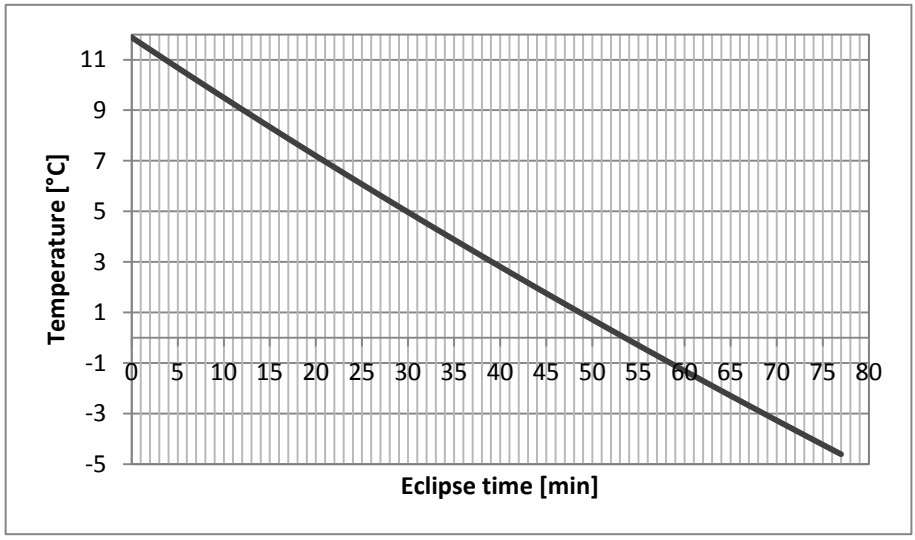

Figure 6.6 Temperature evolution during the "Cold case" transient computation, ϵ=0.2

Now, the temperature drops only approximately to -5°C instead of -30°C. But, how does it affect the internal power dissipation? With this new configuration we can build a plot

with the final temperature after the eclipse depending on the internal power dissipation *Q* produced. Figure 6.7 is the result.

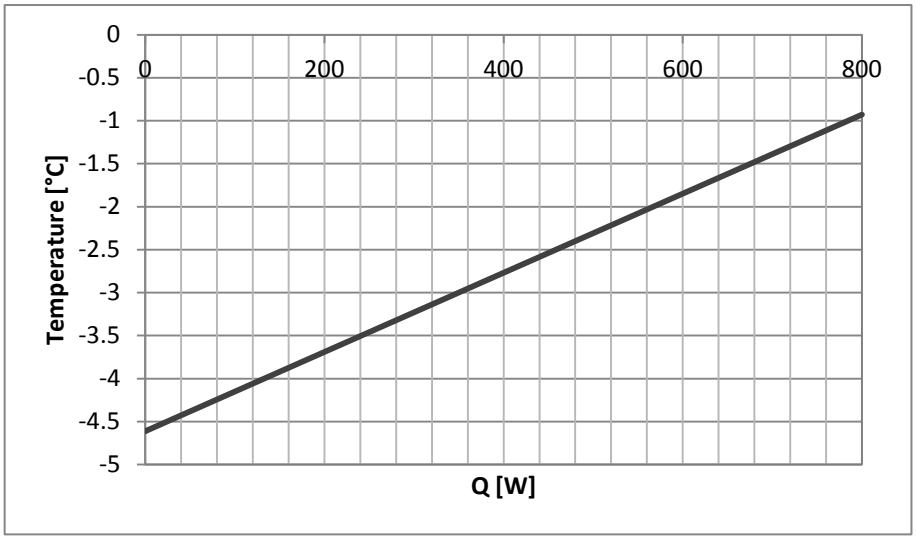

Figure 6.7 Internal power dissipation variation effects on temperature during the "Cold case"

Under normal operation, the spacecraft's components could be assumed to dissipate between 300 W and 400 W. If we assume an internal power dissipation of 350 W, the spacecraft can always be maintained over -3°C.

This temperature is consistent with most of the components thermal limits. However, batteries, star trackers and the payload have their lower thermal limit at or above 0°C. The first two needs to be over 0°C and the payload needs to be over 5°C, this means that active thermal control will be need. The easiest solution is to attach next to each of these components heaters which would increase the few degrees up to its operational temperature range. Heaters consume power so it would be important, in further design stages, to do a detailed study of how much power would be needed by them.

The design of the louvre, its blades, its mechanism and its radiator also needs to be faced in further design stages in order to obtain the required emissivity.

After all these observations, it can be stated that thermal requirements during lunar eclipses can be managed without serious difficulties. However, Earth eclipses are also an important issue to take into consideration because of their duration. Earth eclipses can last more than 5 hours (see *Chapter four*) so the spacecraft will reach a lower temperature than during lunar eclipses. Figure 6.8 shows the temperature evolution during an Earth eclipse. Internal power dissipation has been maintained in 350 W and the emissivity in 0.2.

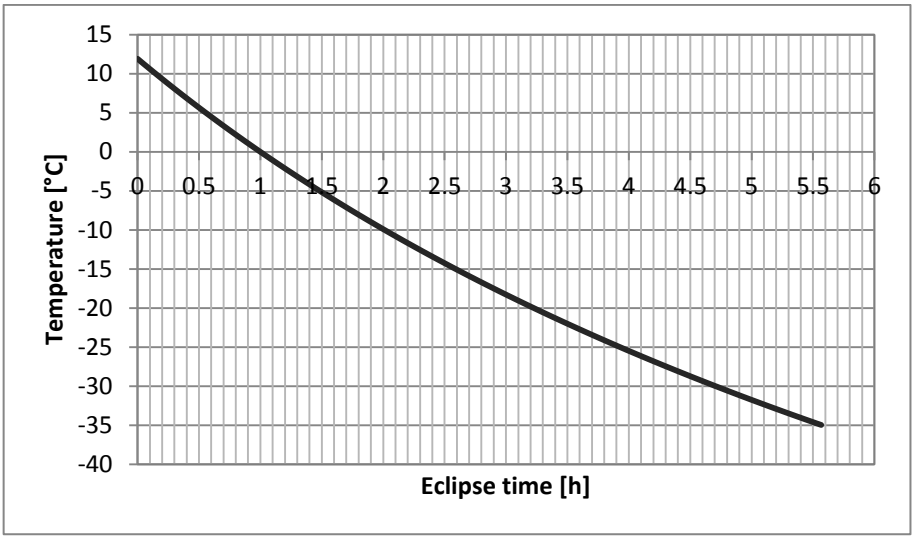

Figure 6.8 Temperature evolution during Earth eclipse

As it can be seen, the temperature drops to -35°C. This case needs further study but we can do a few observations. MLI blankets cannot be used because they have an absortivity-emissivity ratio ($^{\alpha}/_{\epsilon}$) of 4-5 which would lead to an average spacecraft temperature during the "hot case" of 200°C. That means that heaters or other kind of active control devices will be needed and their power consumption would probably be very high so a new set of batteries will be essential to provide exclusively this extra power. A good action to reduce the power required during Earth eclipses could be to shut down all spacecraft subsystems except for the thermal control. This does not mean a complete shutdown of the positioning system but a partial one since each orbital plane suffers Earth eclipses in different epochs of the year.

6.5. Communications

In this section we present a preliminary design of the communication link budgets of the mission. An option for the navigation message is offered and we also present a possible configuration for a possible ground station architecture on the lunar surface. The theory adopted in this section is explained in [1].

6.5.1. Communications with the lunar surface

Since the purpose of this study is to provide navigation services in the lunar surface, it is essential to characterise the radio-link between the satellite and the ground, obtain the transmission power and estimate the antenna dimensions.

In order to size the emitting part of the system, a set of requirements and constraints should be applied. These requirements are mainly extracted from GPS features[61].

- The transmission frequency (*f*) shall be 1575.42 MHz, the same as in GPS L1.
- The transmission bandwidth shall be 20 MHz (similar to the GPS bandwidth).
- The minimum power guaranteed in reception (P_r) shall be -160 dBW, which is L1 GPS standard. A 4.5 dBW margin is added to cover the uncertainty. The final power in reception shall be -155.5 dBW.
- The satellite range (*r*) is 6500 km.
- The transmission and reception losses (L_t and L_r) are set both at 3 dB.

In order to reach the lunar surface with sufficient intensity, the navigation signal has to be prepared. From the signal generation units up converters, the signal to be transmitted is forwarded to high power amplifiers. There exist two types of amplifiers: travelling wave tube amplifiers (TWTA) and solid state power amplifiers (SSPA). TWTA amplifiers are the most common and proven, have an output up to hundreds of Watts and their efficiency is up to 60%. SSPA are based on transistors, they are cheaper, lighter and reliable but their efficiency is around 15%. After the amplification some filtering with low noise units may be necessary. Then, the signal goes to a multiplexer because the antenna is usually required to emit different signals. Once the signal is prepared for broadcast, it arrives to the antenna and is sent to the receiver antenna on the surface. For our purposes the receiver antenna will be ignored; the required power of the receiver must be reached with independence of the receiver antenna gain ($G_r = 0\ dB$)[15].

By knowing P_r and the other parameters of the link, we can determine the EIRP (effective isotropic radiated power) value:

$$P_r = EIRP + G_r - L_{FS} - L_r, \tag{6.31}$$

where

$$L_{FS} = 20\log(f[GHz]) + 20\log(r[km]) + 92.44. \tag{6.32}$$

The EIRP is built only from the output power and the antenna gain:

$$EIRP = P_t + G_t. \tag{6.33}$$

So, if we plot the transmitting power versus the transmission gain we can observe their evolution for a defined EIRP value which fulfils the requirements of the mission. Figure 6.9 is the resulting plot.

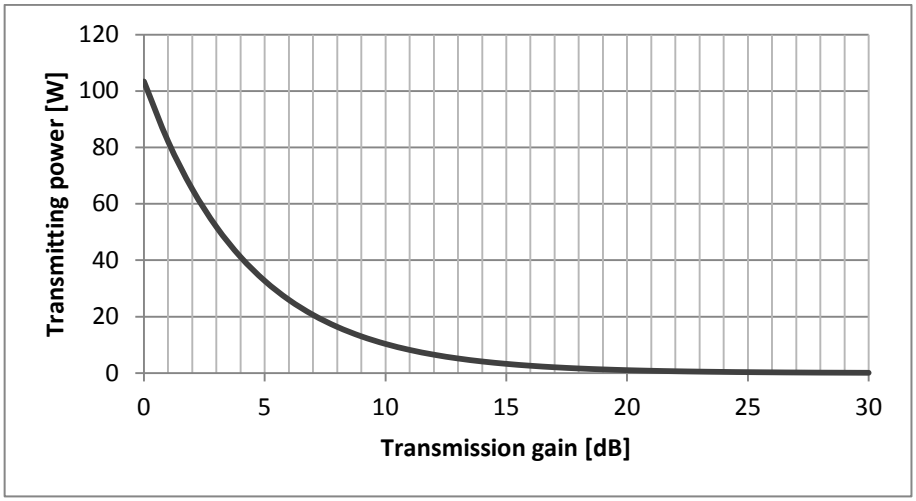

Figure 6.9 Values of transmitting power and gain for a defined EIRP value (Link Satellite-lunar surface)

The power and gain required are comfortably achievable so constraints can be allocated on one to free the other. The amplifier choice could constrain the design but, since neither the gain nor the power required are excessively high, both SSPA and TWTA are a possible choice but neither of them is completely satisfactory. On the one hand, TWTAs normally deliver higher power (an average TWTA delivers 150 W) than SSPAs, though nowadays there are commercial TWTAs capable of delivering only 20 W[62]. On the other hand, the SSPA's low efficiency and unproven components do not meet the expectation of a reliable mission such as the LGSNS.

Another way to constrain the design is by sizing the transmitting antenna. For current navigation satellites, helix antennas are the most widespread solution. These antennas can work either omnidirectionally or axially. When operating in omnidirectional mode, they can manage wavelengths much higher than the actual antenna dimensions. This allows operating with relatively small antennas at different attitudes. When working axially their behaviour resembles that of a directional antenna. Helix antennas are relatively lightweight and compact for 10-20 dB gains at L1 and they work with circular polarization[15].

For our purposes we decided that each satellite will only have one transmitting helix antenna with a longitude of 33 cm. In order to size the antenna we need to know the wavelength which, commonly, matches the perimeter of the coil *C*,

$$\lambda = \frac{c}{f} = D\pi \approx C, \tag{6.34}$$

where *D* is the antenna diameter.

By knowing the transmission frequency, we find the value of the wavelength: 0.190 m. The following represents the helix gain equation[63]:

$$G_t = 10.8 + 10\log\left[N\left(\frac{S}{\lambda}\right)\left(\frac{C}{\lambda}\right)^2\right] = 10.8 + 10\log\left[N\left(\frac{S}{\lambda}\right)\right] \tag{6.35}$$

where,

$$S = \frac{\lambda}{4} \tag{6.36}$$

and

$$BW = \frac{115}{\frac{C}{\lambda}\sqrt{N \cdot \frac{S}{\lambda}}} = \frac{115}{\sqrt{N \cdot \frac{S}{\lambda}}}. \tag{6.37}$$

Finally, the longitude depends of the number of turns (*N*) and the spacing between the coils (*S*).

$$L = (N-1) \cdot S. \tag{6.38}$$

Table 6.14 summarizes the resulting antenna parameters.

Antenna design parameters	
$\boldsymbol{D}$	0.061 m
$\boldsymbol{S}$	0.048 m
$\boldsymbol{G_t}$	13.810 dB
$\boldsymbol{BW}$	36.770°
$\boldsymbol{N}$	8
$\boldsymbol{L}$	0.333 m

Table 6.14 Antenna design parameters

From Table 6.14 we observe that the antenna can deliver a gain of almost 14 dB. The final gain selected is 13 dB and the corresponding (Figure 6.9) output power is 7.146 dBW. The final power required needs to be adjusted with the transmission losses and the efficiency of the amplifier:

$$P_{t_{final}} = P_t + L_t = 10.146\ dBW = 10.342\ W. \tag{6.39}$$

Finally, the input power P_{input} is:

$$P_{input} = \frac{P_{t_{final}}}{\eta}. \tag{6.40}$$

Table 6.15 shows the difference of input power required with a TWTA and a SSPA.

	$\boldsymbol{\eta}$	$\boldsymbol{P_{input}\ [W]}$
TWTA	0.6	17.24
SSPA	0.15	68.95

Table 6.15 Input power depending on the amplifier used for a link satellite-lunar surface

6.5.2. Communication with the Earth

The control station of the constellation is thought to be set in the Earth so, a Telemetry and Command communication budget needs to be dimensioned. Since this link is interplanetary, an X-band frequency is chosen: 8.4 GHz[64]. The sizing process will be the same as before. However, because of the distance, the antenna selected is parabolic. The new set of requirements is:

- The transmission frequency (*f*) will be 8.4 GHz.
- The transmission beamwidth (*BW*) will be 20°.
- The energy per bit to noise rate (E_b/N_0) will be 24.6 dB which is high enough to assure a good link quality.
- Satellite range (*r*) is 384400 km.
- Transmission and reception losses (L_t and L_r) are both set in 3 dB.
- The download data rate (*R*) will be 50 bps (the same as GPS).
- The noise equivalent temperature (T_s) is set in 311 K[65].

As before, we can find an EIRP value that fulfils the requirements following Eq. 6.41:

$$\frac{E_b}{N_0} = EIRP + G_r - (L_{FS} + L_r) - 10\log T_s - 10\log R + 228.6, \tag{6.41}$$

where G_r is the receiver antenna gain and is defined as

$$G_r = -159.59 + 20\log D_r + 20\log f + 10\log \eta. \tag{6.42}$$

The receiver antenna diameter D_r is set in 1 m, this antenna is going to be in the control centre in the Earth so a diameter of one meter does not represent any problem. The efficiency η is set in 0.55 which is the average value for parabolic antennas.

Once the EIRP value is found, we can plot the output power against the transmission gain following Eq. 6.41. Figure 6.10 shows the result.

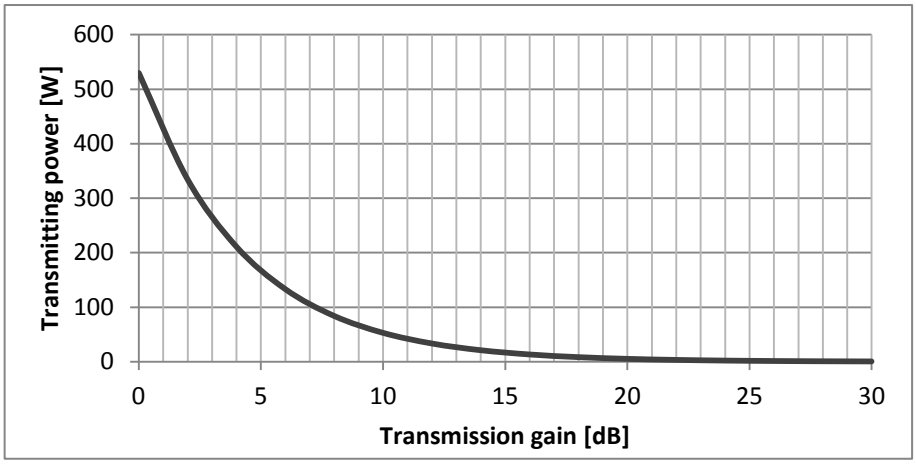

Figure 6.10 Values of transmitting power and gain for a defined EIRP value (Link Earth-Moon)

Now, in order to select the design values of output power and gain we are going to dimension the transmitting antenna. The transmitting antenna diameter is found as

$$D_t = \frac{21}{f[GHz] \cdot BW_t[°]} = 0.125\ m. \tag{6.43}$$

By using Eq. 6.42 and the same value of efficiency (0.55), we find the gain of the transmitting antenna:

$$G_t = 18.237\ dB.$$

For a gain value of 18 dB, the output power required is 9.239 dB (Figure 6.10). By following Eqs. 6.39 and 6.40 we find $P_{t_{final}}$ and the values of P_{input} of Table 6.16:

$$P_{t_{final}} = 12.239\ dBW = 16.747\ W$$

	$\boldsymbol{\eta}$	$\boldsymbol{P_{input}\ [W]}$
TWTA	0.6	27.912
SSPA	0.15	111.646

Table 6.16 Input power depending on the amplifier used a link with the Earth

6.5.3. Ground stations architecture

A possible ground segment for the LGSNS can consist of 4 major components: a Master Control Station (MCS) on Earth, a Lunar Control Station (LCS) on the lunar surface, monitoring stations around the Moon and ground antennas also on the Moon.

The Earth's MCS would be the central control node for the LGSNS satellite constellation. It would be responsible for all aspects of constellation command and control, to include: routine satellite bus and payload status monitoring, satellite maintenance and anomaly resolution and station-keeping operations.

The LCS would be the ground station responsible to generate the navigation message and to offer the SPS (Standard Positioning Service). Some of its tasks would be: monitoring and management of SPS performance in support of all performance standards, navigation data upload operations as required to sustain performance in accordance with accuracy performance standards, and prompt detection and response to service failures.

The monitoring stations would be distributed around the Moon's surface and equipped with atomic clocks standards and LGSNS receivers to continuously collect LGSNS data for all the satellites in view from their locations. The collected data would be sent to the LCS where it would be processed to estimate satellite orbits (ephemerides) and clock errors, among other parameters and to generate the navigation message.

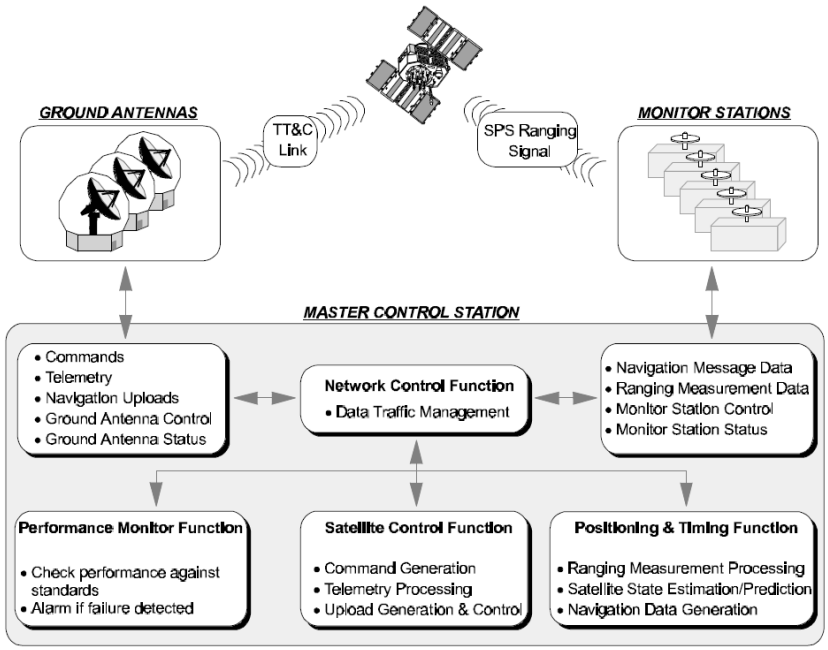

Figure 6.11 Overview of the GPS ground segment[61]

Finally, the ground antennas would uplink data to the satellites. These data includes ephemerides and clock correction information transmitted within the navigation message. Figure 6.11 shows an overview of the GPS ground segment which could represent the lunar part of the LGSNS ground segment: LCS, monitoring stations and ground antennas[66].

6.5.4. Navigation message

Since the LGSNS orbit is circular like the GPS orbit, the same kind of navigation message as in the GPS system can be used in the LGSNS. The GPS navigation message has a total duration of 12.5 minutes and it is constituted by 25 frames lasting 30 seconds each. The frames are the essential information unit, and are further divided in 5 subframes with the architecture shown in Figure 6.12.

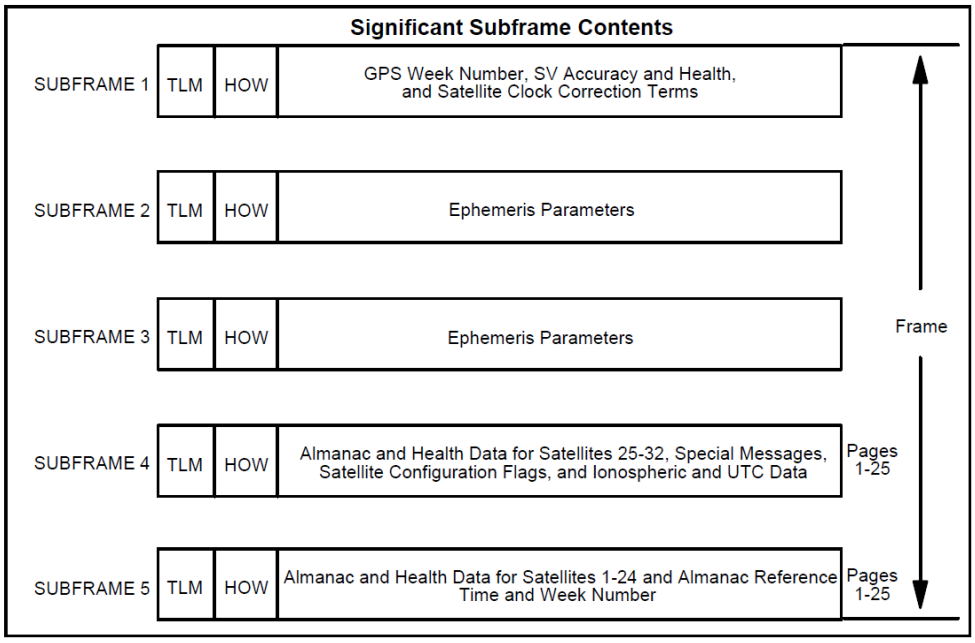

Figure 6.12 Navigation message content and format overview[61]

Each GPS satellite provides the data required to support the position determination process. The data includes information required to determine the following[61]:

- Satellite time of transmission
- Satellite position
- Satellite house-keeping
- Satellite clock correction
- Propagation delay effects

- Time transfer to UTC (Universal Time Coordinate)
- Constellation status

All this is transmitted at 50 bps. Every subframe lasts 6 seconds and is made of 10 words of 30 bits each. The ephemeris is updated every 2 hours and the almanac every 24 hours. The first three subframes repeat the same content over all the navigation message and store the essential information to calculate the receiver's position. The receiver also needs a relatively updated content on networks' almanac. This is transmitted on the last two subframes but each frame of the message carries a different piece of information, so when the receiver has no guess on the possible almanac it needs the complete 12.5 minutes message to get the full picture[15].

Chapter seven.

Conclusions and future work

The aim of the present study was to carry out a preliminary analysis and design of a lunar global satellite navigation system. Such a system would be able to provide accurate positional information to operators on the lunar surface or in low lunar orbits, making possible to set an enduring lunar scientific base. The mission analysis has been carried out with a Systems Engineering approach which means that the outcome has been a set of objectives, requirements and constraints concerning the implications inherent in such a system.

The chosen constellation has a performance accurate enough to fulfil the mission objectives. However, more detailed DOP studies should be made in order to completely define the real DOP of the constellation and to identify the surface locations where there is a DOP gap (the constellation performance deteriorates). Station-keeping needs to be held every six moth to ensure the correct performance of the constellation. The total delta-v budget of the LGSNS station-keeping is 1 km/s per year which is very similar to that of the GPS.

Concerning the payload, some atomic clock options have been presented: rubidium and cesium clocks, and passive and active hydrogen masers. A combination of two of these types of clocks would be the optimal solution for the navigation payload. Relativistic effects on time have to be handled with care in order to ensure the accuracy of the system. In our case there is a drift between clocks of approximately 2 μs, which means a position error of 560 meters. The relativistic effects on the lunar orbit are considerably smaller than in the GPS orbit which presents a time drift of 40 μs (12 km of position error). However a proper management of clock data is still fundamental.

The final spacecraft would weigh around 1000 kg and would consume around 1600 W of power. However, the power and mass budgets have been designed only by taking into account lunar eclipses so their results need to be adjusted with the final thermal power requirements induced by Earth eclipses.

Communication link budgets, navigation message and ground segment architecture have only been outlined in this study so, a thorough analysis need to be done. The same holds for the propulsion subsystem. The preliminary results suggest that the selection of

a bipropellant thruster for station-keeping is the optimal solution. However, electrical propulsion is a very interesting option so, it may be a interesting to continue its analysis and see if the smaller amount of propellant needed by electrical propulsion is a bigger advantage in front of the power that it would require.

Futures studies should include a better analysis of the performance of the incomplete constellation and the receiver that would be needed to make it works. Another important issue that must be approached in further detail is the thermal analysis and the mission design option concerning Earth eclipses. It needs to be made in order to choose the best solution to maintain the spacecraft temperature in the Earth shadow within the operational limits.

Appendix A.

Technology Readiness Levels

Technology Readiness Levels (TRLs) are a systematic metric system that supports assessments of the maturity of a particular technology and the consistent comparison of maturity between different types of technology. Figure A.1 provides a synthetic view of the technology maturation process model for NASA space activities for which the TRL's were originally conceived. The general model must include: "basic" research in new technologies and concepts, focused technology development addressing specific technologies for one or more potential identified applications, technology development and demonstration for each specific application before the beginning of full system development of the application, system development and system "launch" and operations[67].

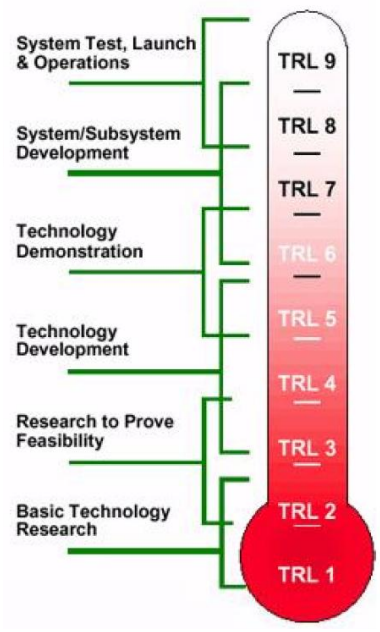

Figure A.1 Technology Readiness Levels

In the case of the LGSNS mission, almost all the technology used on the spacecraft is already flight proven or flight qualified which would lead to a global mission TRL of 9 if the mission was set in Earth orbit. However, some components such as hydrogen masers or the possible choice of an Ion or Hall thruster have a lower TRL. Passive hydrogen masers have been validated by ESA with the GIOVE (Galileo In-Orbit Validation Elements) mission. Therefore they have a TRL of 8. Electric propulsion TRL is between 4

and 6. As a result, the global mission TRL will depend on the final choice of the propulsion system.

While the mission uses almost exclusively existing flight proven components, the operation of the mission is set in a lunar orbit. This fact lowers the mission TRL; even though lunar space environment is known, long exposure effects on a spacecraft have not been tested. For this reason, the final global mission TRL is 7 which means that the LGSNS mission is a system prototype demonstration in a space environment which has not been implemented in the past.

Appendix B.

Cost analysis

Cost is an engineering parameter that varies with physical parameters, technology and management methods. A system's cost depends on its size, complexity, technological innovation, design life, etc. Analyzing and predicting program cost is becoming increasingly important to determine whether a program is feasible.

The costs of a space mission architecture can be divided in three main categories: Research, Development, Test and Evaluation (RDT&E), production and Operations and Maintenance (O&M). RDT&E includes design, analysis and test, prototypes and qualification units. The production phase, also called Theoretical First Unit (TFU), incorporates the cost of producing flight units and launching them. For multiples units, production cost is estimated using a learning curve factor applied to the TFU cost. The O&M phase consists of ongoing operations and maintenance costs, including spacecraft unit replacements and software maintenance.

In this chapter we are not going to deal with O&M costs and launch segment (information of the cost of launching anything to the Moon can be found in [68]) and ground segment costs are not going to be estimated. Only the space segment costs will be made. Space segment RDT&E and production costs are going to be estimated with a parametric approach. Parametric estimation uses sets of mathematical relationships that relate cost to physical, technical and performance parameters that are known to strongly influence costs. An equation called the Cost Estimating Relationship, or CER, expresses the cost as a function of the parameters. Cost drivers and function forms are selected based on a combination of engineering judgment and statistical quality of regression results.

The CERs for the payload and spacecraft bus subsystems are primarily based on parameters available during the concept and mission design phase. In our case, the basic parameter used as an input for the CERs has been the mass.

The process and all the equations used in the elaboration of this cost estimation can be found in [1].

Since our project is the creation of a constellation, a learning curve is needed. The learning curve is a mathematical technique to account for productivity improvements as a larger number of units are produced. This includes cost reductions due to economies of scale, set up time and human learning as the number of units increase. The total production cost for N (15 satellites) units is modelled as:

$$Production\ cost = TFU \cdot L \tag{B.1}$$

where

$$L = N^B, \tag{B.2}$$

$$B = 1 - \frac{\ln\left(\frac{100\%}{S}\right)}{\ln 2}. \tag{B.3}$$

L is the learning curve factor and S is the learning curve slope in percentage. For a number of units between 10 and 50, a 90% learning curve slope is recommended.

Heritage factors are also important in the RDT&E cost estimation. These are multiplicative factors to be applied to the RDT&E CER for design maturity of a given subsystem. Heritage is defined as the percentage of a subsystem that is identical to one or more previous spacecraft, by mass. In our case, since the spacecraft's design is based on historical information of current GNSS, a heritage factor of 0.6 is selected.

Table B.1 shows the cost estimation results. SE represents the standard error of the estimation and FY00M$ indicates that the estimation has been in millions of dollars of the fiscal year 2000. The cost estimation presented in Table B.1 is the very first estimation of the mission's cost. Hence, it would be wise to understand its results as the minimum expected cost for the mission.

Cost component	RDT&E CER (FY00M$)	TFU CER (FY00M$)	Production final cost (FY00M$)	TOTAL cost (FY00M$)	SE (FY00M$)
1. Payload	39.75	26.25	260.89	300.64	124.34
2. Spacecraft					
2.1 Structure	6.03	1.97	19.58	25.61	9.73
2.2 Thermal	2.36	0.66	6.56	8.92	4.64
2.3 EPS	15.91	2.26	22.46	38.37	13.51
2.4 TT&C/DH	7.37	7.05	70.07	77.44	31.25
2.5 ADCS	6.19	0.09	0.89	7.08	2.09
2.6 Propulsion	0.70	0.49	4.87	5.57	1.08
3. Integration, Assembly & Test	17.43	7.80	77.52	94.95	38.92
4. Program Level	23.62	0.10	0.99	24.61	5.77
5. Ground Support Equipment	10.69	-	-	10.69	2.18
6. Launch & Orbital Operations Support	-	3.68	36.57	36.57	15.36
TOTAL (M$)	**130.05**	**50.34**	**500.40**	**630.45**	**248.88**

Table B.1 RDT&E and production costs

Bibliography

[1] Larson, W.J., Wertz, J.R., "Space Mission Analysis and Design"; Space Technology Library, Microcosm Press (1992).

[2] Handwerk, Brian, "After Space Shuttle, Does U.S have a future in space?"; National Geographic, Daily News; date of access: February 2012; available at: http://news.nationalgeographic.com/news/2011/07/110708-space-shuttle-launch-atlantis-nasa-future-science/#.

[3] Bodkin, David K.; Escalera, Paul; Bocam, Kenneth J., "A Human Lunar Surface Base and Infrastructure Solution"; Orbital Sciences Corporation, Dulles, VA, 20166.

[4] Lunar and Planetary Institute, "Lunar base concepts"; NASA Astrophysics Data System.

[5] "Sustained Moon Surface Operations", Automated Surface Infrastructure Elements, ESA-ESRIN, 16 January 2009.

[6] Mintz, Toby; Maslowski, Edward A.; Colozza, Anthony; McFarland, Willard; Prokopius, Kevin P., "Simulation of a Lunar Surface Base Power Distribution Network for the Constellation Lunar Surface Systems"; Glenn Research Center, Cleveland, Ohio, February 2010.

[7] Li, Ron; He, Shaojun; Jiang, Jinwei; Tang, Pingbo; Yilmaz, Alper; Banks, Martin; Oman, Charles, "Development of a lunar astronaut spatial orientation and information system (LASOIS)", ASPRS Annual Conference, San Diego, California, 2010.

[8] NASA, "Systems engineering handbook", NASA Headquarters, Washington, D.C., December 2007.

[9] Lainez Samper, María Dolores, Romay Merino, Miguel. M., "Seminario Navegación por Satélite: Introducción a la Navegación por Satélite, descripción de los sistemas actuales"; 2009, GMV.

[10] Guier, William H., Weiffenbach, George C., "Genesis of Satellite Navigation", Johns Hopkins APL Technical Digest, Volume 19, 1998.

[11] Department of Defense, "Global positioning system standard positioning service performance standard", USA, September 2008.

[12] Benedicto, J., Dinwiddy, S. E., Gatti, G., Lucas, R., Lugert, M., " GALILEO: Satellite System Design and Technology Developments", ESA, November 2000.

[13] Langley, Richcard, B., "GLONASS Overview", Geodetic Research Laboratory, University of New Brunswick, Canada

[14] Lu, Mingquan, "Simulation and Measurements on BeiDou-2 Positioning Performance", Department of Electronic Engineering, Tsinghua University, November 2011.

[15] Lluch i Cruz, Ignasi, "Study of design challenges for LCNSS satellites (Low cost navigation satellite systems) on inclined and eccentric geosynchronous orbits"; Universitat politècnica de Catalunya, Barcelona, June 2011.

[16] Positim, "GNSS Principles", date of access: March 2012; available at http://www.positim.com/gnss_principles.html.

[17] Kumar, Arun, "GNSS Princliples Tutorial: Determining the Accuracy of a GPS Device", BRIGHT HUB, date of access: March 2012; available at http://www.brighthub.com/electronics/gps/articles/42314.aspx.

[18] Spirent, "Inside GNSS", date of access: March 2012; available at http://www.insidegnss.com/node/2512.

[19] Ahn , Yong-Won, "GPS Error Sources and Mitigation"; University of New Brunswick, Canada.

[20] Hugentobler, Urs, Van der Marel, Hans & Springer, Tim, "Identification and Mitigation of GNSS Errors"; IGS Workshop, Mai 6-11, 2006, ESOC, Darmstadt, Germany.

[21] Kowoma, "Sources of erors in GPS", date of access: March 2012; available at http://www.kowoma.de/en/gps/errors.htm.

[22] Langley, Richard B., "Dilution of Precision"; University of New Brunswick; GPS WORLD, May 1999.

[23] AGI, "STK 9.2.4 Desktop Application Help", date of access: March, May, June and July 2012; available at http://www.agi.com/resources/help/online/stk/index.html?page=source%2Fmanuals%2Fmanuals.htm.

[24] Bate, R.R., Mueller, D.D., White, J.E., "Fundamentals of Astrodynamics"; Dover Publications, New York (1971).

[25] Cardoso, Vilana, Edgar, "Study of spacecraft orbits in the gravity field of the Moon"; Universitat politècnica de Catalunya, Barcelona, January 2012.

[26] Kaula, W.M., "Theory of Satellite Geodesy"; Dover (2000).

[27] Bos, M. S., Baker, T. F., Lyard, F. H., Zürn, W. E., Rydelek, P. A., "Long-period lunar Earth tides at the geographic South Pole and recent models of ocean tides", Geophys. J. Int. (2000).

[28] Vallado, D.A., "Fundamentals of Astrodynamics and Applications"; Space Technology Library, Microcosm Press (2007).

[29] Chobotov, V.A., "Orbital Mechanics"; 3rd Edition, AIAA, Reston, Virginia (2002).

[30] NASA, "Lunar Prospector", date of access: July 2012; available at http://pds-geosciences.wustl.edu/missions/lunarp/index.htm.

[31] Milbert, Dennis, "Solid Earth Tide", date of access: July 2012; available at http://home.comcast.net/~dmilbert/softs/solid.htm#link4.

[32] Minow, Joseph I., Edwards, David L., Altstatt, Richard L., Diekmann, Anne M., Blackwell, William C. Jr., Harine, Katherine J., "Radiation and plasma environments for lunar missions", NASA, Marshall Space Flight Center, Huntsville, Alabama.

[33] Halekas, J. S., Delory, G. T., Brain, D. A., Lin, R. P., Fillingim, M. O., Lee, C. O., Mewaldt, R. A., Stubbs, T. J., Farrell, W. M., Hudson, M. K., "Extreme lunar surface charging during solar energetic particle events", Geophysical Research Letters, Vol. 34, January 2007.

[34] Halekas, J. S., Saito, Y, Delory, G. T., Farrell, W. M., "New views of the lunar plasma environment", Planetary and Space Science, Elsevier, 2011.

[35] Huang, Chia-Lin, Spence, Harlan E., Kress, Brian T., "Assessing access of galactic cosmic rays at Moon's orbit", Geophysical Research Letters, Vol. 36, May 2009.

[36] Delory, Gregory T, "Electrical Phenomena on the Moon and Mars", Space Sciences Laboratory, University of California, Berkeley.

[37] Stubbs, Timothy J., Vondrak, Richard R., Farrell, William M., “A dynamic fountain model for lunar dust”, Laboratory for Extraterrestial Physics, NASA Goddard Space Flight Center, Greenbelt, 2005.

[38] Wolf, Robert, “Satellite Orbit and Ephemeris Determination using inter Satellite Links”, Universität der Bundeswehr München, 2000.

[39] “Evolution of the GPS Navigation Payload – A Historical Journey”. Division, IT Space Systems, SCPNT, 2009.

[40] Precise Time and Frequency, Inc., “CHI-75 Active Hydrogen Maser”; date of access: July 2012; available at http://www.ptfinc.com/.

[41] Oscilloquartz, “OSA 3705 Passive Hydrogen Maser”; date of access: July 2012; available at http://www.oscilloquartz.com/.

[42] AccuBeat Ltd., “GPS-Rubidium Clock, AR-51A Series”; date of access: July 2012; available at http://www.accubeat.com/.

[43] OscilloQuartz, ”Cesium Clock and Hydrogen Maser Compared”, 2005.

[45] Hein, Guenter W., Eissfeller, Bernd, “Galileo – Design options for the European GNSS 2”; Institue of Geosdesy an Navigation (FAF Munich), Neubiberg, Germany, 2010.

[46] Mattioni, L., Berthoud, P., Rochat, P. , “The Development of a Passive Hydrogen Maser Clock for the Galileo Navigation System”; Galileo Avionica, Temex Neuchâtel, 2004.

[47] Clynch, James R., “Precise Time and Time Interval Clocks, Time Frames and Frequency”, 2002.

[48] Jeanmaire, A., Rochat, P., Emma, F., “Rubidium Atomic clock for the Galileo”; Temex Neuchâtel, ESA ESTEC.

[49] Gulklett, Mikkjal, “Relativistic effects in GPS and LEO”; University of Copenhagen, October 2003.

[50] Fliegel, Henry F., Diesposti, Raymond S., “GPS and relativity: an Engineering overview”; GPS Joint Program Office, The Aerospace Corporation, California.

[51] Mugan, Carl E., “Relativistic Effects on Clocks aboard GPS satellites”, U.S. Naval Academy, Annapolis, October 2006.

[52] Landau, L.D., Lifshitz, E.M, "The Classical Theory of Fields", Reed Educational and Professional Publishing Ltd, 1975.

[53] Martinez-Sanchez, M., Pollard, J.E., "Spacecraft Electric Propulsion-An Overview"; Journal of propulsion and power, Vol. 14, No. 5, September-October 1998.

[54] Turner, Martin J. L., "Rocket and spacecraft propulsion: Principles, practice and new developments", Springer-Praxis Books in astronautical engineering, UK, 2009.

[55] Martinez-Sanchez, Manuel, "Lecture 1b: Review of Rocket Propulsion"; 16.522, Space Propulsion, MIT.

[56] Curtis, Howard D., "Orbit Mechanics for Engineering Students"; Elsevier Ltd, 2010.

[57] Astrium, "10 N Bi-Propellant Thuster"; available at http://cs.astrium.eads.net/sp/.

[58] Brown, Charles D., "Elements of spacecraft design", American Institute of Aeronautics and Astronautics, Inc., 2002.

[59] Fortescue, Peter, Stark, John, Swinerd, Graham, "Spacecraft Systems Engineering", Third edition, John Wiley & Sons Ltd., The Atrium, Southern Gate, Chichester, February 2004.

[60] Thirumaleshwar, M., "Fundamentals of heat & mass transfer", Dorling Kindersley, 2006.

[61] GPS NAVSTAR, "Global Positioning System, Standard positioning service, signal specification", 2n edition, June 2, 1995.

[62] Satcom division, "6900K4 Series 20 Watt TWT Amplifier"; date of access: August 2012; available at http://www.cpii.com/division.cfm/7.

[63] Daycounter, Inc: Engineering Services, date of access: August 2012; available at http://www.daycounter.com/Calculators/Helical-Antenna-Design-Calculator.phtml.

[64] Vagberg, Daniel, "Deep Space Communication"; Space Physics C 5p, Umea University, October 2005..

[65] Morabito, D. D., "Lunar Noise-Temperature Increase Measurements at S-Band, X-Band and Ka-Band Using a 34-Meter-Diameter Beam-Waveguide Antena"; IPN Progess Report 42-166, Augusr 15, 2006.

[66] ESA Navipedia, “GPS Ground Segment”; date of access: August 2012; available at http://www.navipedia.net/index.php/GPS_Ground_Segment.

[67] Mankins, John C., “Tecnology Readiness Levels”; Office of Space Access and Technology, NASA, April 6, 1995.

[68] NASA, “Lunar Reconnaissance Orbiter (LRO): Leading NASA’s way back to the Moon & Lunar Crater Observation and Sensing Satellite (LCROSS): NASA’s mission to search for water on the Moon”, Press kit, June 2009.